2003

Remote sensing of crop biophysical parameters for site-specific agriculture

Rabe, Nicole J.

Lethbridge, Alta. : University of Lethbridge, Faculty of Arts and Science, 2003

Remote Sensing of Crop Biophysical Parameters for Site-Specific Agriculture

Nicole J. Rabe
B.A., University of Western Ontario, 1996

A Thesis

Submitted to the School of Graduate Studies

of The University of Lethbridge

In Partial Fulfillment of the

Requirements for the Degree

MASTER OF SCIENCE

Department of Geography
University of Lethbridge
LETHBRIDGE, ALBERTA, CANADA

Dedication

First and foremost this research is dedicated to my husband Greg, who left his job and moved across the country with his wife so that she could pursue her graduate studies. Without your emotional support and your continuous motivation I could not have completed this journey.

I also dedicate this to both of our parents (Harvey Rabe and Donna Brown) who have continued to "grin-and-bear" the distance and who have consistently stood behind this decision. Also to my brother Brennan, and sister-in-laws Tanya and Melissa, as well as to our extended families, without your love and support this would have been very difficult to finish.

Much appreciation and love to all of you.

Abstract

Support for sustainable agriculture by farmers and consumers is increasing as environmental and socio-economic issues rise due to more intensive farm practices. Site-specific crop management is an important component of sustainable agriculture, within which remote sensing can play an integral role. Field and image data were acquired over a farm in Saskatchewan as part of a national research project to demonstrate the advantages of site-specific agriculture for farmers. This research involved the estimation of crop biophysical parameters from airborne hyperspectral imagery using Spectral Mixture Analysis (SMA), a relatively new sub-pixel scale image processing method that derives the fraction of sunlit canopy, soil and shadow that is contributing to a pixel's reflectance. SMA of three crop types (peas, wheat and canola) performed slightly better than conventional vegetation indices in predicting leaf area index (LAI) and biomass using Probe-1 imagery acquired early in the growing season. Other potential advantages for SMA were also identified, and it was concluded that future research is warranted to assess the full potential of SMA in a multi-temporal sense throughout the growing season.

Acknowledgements

There are many I need to acknowledge without which this research would not have been possible. First I would like to express my deepest gratitude to Dr. Derek Peddle, my thesis supervisor. Derek provided me the encouragement to pursue my graduate studies across the country and an optimal environment to make this work possible. Derek you also helped me to develop more advanced skills in remote sensing analysis, and provided me with the mentoring I required to develop my academic writing ability. I also acknowledge the valuable contributions of my other thesis committee members, Dr. Anne Smith and Dr. Wei Xu. Dr. Anne Smith of Agriculture and Agri-Food Canada - Lethbridge Research Centre provided the data, extensive in-field knowledge, and a great deal of the agronomic insight required to keep a realistic footing in this project. Anne without your background and resources this project would not have been so successful. I would also like to thank Dr. Wei Xu who gave me some of the best advice in terms of managing my thesis program, and his GIS / spatial statistics expertise was invaluable. A special thank-you to Dr. Dave Major as well.

I gratefully acknowledge financial support for this research provided through a Natural Science and Engineering Research Council of Canada (NSERC) PGS-A scholarship and additional student funding from the University of Lethbridge. This research was supported by the following faculty grants awarded to Dr. Derek Peddle: NSERC Research and Equipment Grants, Alberta Research Excellence Grants, Natural Resources Canada grants, and University Faculty Research Grants, as well as support from the Water Institute for Semi-arid Ecosystems (WISE).

I also gratefully acknowledge the Canada Centre for Remote Sensing (CCRS) who initiated the Indian Head research project. I could not have completed this research without the expertise of several research scientists at CCRS including Dr. Heather McNairn, Jean-Claude Deguise, and Anna Pacheco. Many thanks to Dr. Guy Lafond and Yann Pelcat of the Indian Head Agricultural Research Foundation (IHARF) who provided the background data and knowledge on the experimental farm.

Table of Contents

DEDICATION III
ABSTRACT IV
ACKNOWLEDGEMENTS V
TABLE OF CONTENTS VI
LIST OF FIGURES IX
LIST OF EQUATIONS XII
LIST OF TABLES XIII
CHAPTER I 1
1.0 INTRODUCTION 1
1.1 INTRODUCTION 1
1.2 RESEARCH OBJECTIVES 4
1.3 ORGANIZATION OF THESIS 6
CHAPTER II 8
2.0 LITERATURE REVIEW 8
2.1 INTRODUCTION 8
2.2 SUSTAINABILITY AND SITE-SPECIFIC AGRICULTURE 8
2.2.1 Sustainable Agriculture 8
2.2.2 Site-Specific Agriculture 12
2.3 REMOTE SENSING OF CROP INFORMATION 15
2.3.1 Factors Affecting the Spectral Properties of Crops 17
2.3.1.1 Leaf Spectral Properties 17
2.3.1.2 Canopy Spectral Properties 20
2.4 BIOPHYSICAL PARAMETERS 21
2.4.1 Ground Based Biophysical Parameters 21
2.4.1.1 Percent Crop Cover 21
2.4.1.2 Leaf Area Index (LAI) 22
2.4.1.2.1 Direct Measurements of LAI 22
2.4.1.2.2 Indirect Measurements of LAI 24
2.4.1.3 Biomass 26
2.4.1.4 Yield 26
2.4.2 Conventional Remote Sensing Methods for Biophysical Information Extraction 28
2.4.2.1 Band Ratios and Vegetation Indices 28
2.5 CHAPTER SUMMARY 33
CHAPTER III 35
3.0 SPECTRAL MIXTURE ANALYSIS 35
3.1 INTRODUCTION 35

3.2 ENDMEMBERS 36
3.3 SPECTRAL MIXTURE ANALYSIS THEORY 38
3.3.1 Unconstrained SMA *39*
3.3.2 Constrained SMA *41*
3.4 SMA INPUTS 42
3.4.1 Reference Endmembers *42*
3.4.1.1 Non-Destructive *In Situ* Endmember Acquisition 43
3.4.1.2 Destructive Endmember Acquisition 45
3.4.2 Image Endmembers *47*
3.4.3 Integrated Endmember Selection Method *52*
3.5 AGRICULTURE APPLICATIONS OF SMA 54
3.5.1 SMA for Crop Area Estimation *55*
3.5.2 SMA for Ground Cover Estimation *55*
3.5.3 SMA for the Prediction of Crop Biophysical Parameters *56*
3.5.4 SMA for the Detection of Weeds in Crops *59*
3.5.5 SMA in Comparison to Conventional Vegetation Indices *61*
3.6 CHAPTER SUMMARY 63

CHAPTER IV 64

4.0 METHODS 64

4.1 INTRODUCTION 64
4.2 STUDY AREA AND FIELD DATA SET 64
4.2.1 Indian Head Study Area *64*
4.2.1.1 Soil and Climate 67
4.2.1.2 Cropping Practices 70
4.2.2 Field Data Collection *73*
4.2.2.1 Selection of Sample Sites 73
4.2.2.2 Crop Biophysical Measurements 75
4.3 REMOTE SENSING IMAGERY 78
4.3.1 Airborne Imagery *78*
4.3.2 Satellite Imagery *79*
4.3.3 Image Pre-Processing *80*
4.3.3.1 Ground-based Spectral Measurements 80
4.3.3.2 Radiometric Correction 84
4.3.3.3 Image Rectification 87
4.3.3.4 Co-Registration of Imagery and Sample Site Locations 88
4.3.3.5 Band Selection 90
4.4 EXPERIMENTAL DESIGN 93
4.4.1 Vegetation Indices *93*
4.4.2 Spectral Mixture Analysis *95*
4.4.2.1 Reference Endmembers 97
4.4.2.2 Image Endmembers 102
4.4.2.3 Integrated Endmembers 104
4.4.2.4 SMA Software 105
4.4.3 Statistical Methods *107*
4.5 CHAPTER SUMMARY 107

CHAPTER V 109

5.0 RESULTS AND DISCUSSION 109

5.1 INTRODUCTION 109
5.2 BIOPHYSICAL DATA 109
5.3 LAI AND BIOMASS PREDICTION USING VEGETATION INDICES 111
5.4 LAI AND BIOMASS PREDICTION USING SMA 117
5.4.1 Reference Endmembers 117
5.4.2 Image Endmembers 123
5.4.3 Integrated Endmembers 127
5.5 DISCUSSION 140
5.5.1 Biomass Prediction by Crop Type 142
5.5.2 LAI Prediction by Crop Type 144
5.5.3 Summary of Results for All Crop Types 148
5.6 CHAPTER SUMMARY 149

CHAPTER VI 152

6.0 SUMMARY AND CONCLUSIONS 152

6.1 INTRODUCTION 152
6.2 SUMMARY OF THE COMPARISON BETWEEN VIS AND SMA FOR PREDICTING CROP BIOMASS AND LAI 153
6.3 CONCLUSIONS 155
6.4 CONTRIBUTIONS TO RESEARCH 156
6.5 FUTURE RESEARCH 158

REFERENCES CITED 162

APPENDIX A - PROBE-1 BANDS AND GAINS 178

APPENDIX B - COMPARISON OF SMA PROGRAMS 181

APPENDIX C: LINEAR REGRESSION ANALYSIS FOR THE PREDICTION OF BIOMASS AND LAI USING VEGETATION INDICES 183

APPENDIX D: LINEAR REGRESSION ANALYSIS FOR THE PREDICTION OF BIOMASS AND LAI USING SMA 187

APPENDIX E: LINEAR REGRESSION ANALYSIS OF GROUND-BASED BIOMASS AND LAI DATA FOR EACH CROP TYPE. 193

List of Figures

Figure 2-1 Reflectance, absorptance, and transmittance spectra of a plant leaf (from Knipling, 1970). 18
Figure 2-2 The effect of leaf dehydration on the spectral reflectance of bean leaves. The numbers on the curves (10% and 100%) refer to the water content of the leaves at the time of sampling as a percentage of their water content when fully hydrated (from Knipling, 1970). 19
Figure 2-3 LI-3100 instrument. Leaves are measured by a camera with cumulative area reported in cm^2 on the LED display (LI-COR, 2003a). 24
Figure 2-4 LAI-2000 instrument performs all calculations on-site and results are available for immediate inspection (LI-COR, 2003b) 25
Figure 2-5 Yield map for the IHARF farm in 2000. Data were collected using an AgLeader PF300 yield mapping system and Trimble GPS (top right) 28
Figure 3-1Convex hull approach to image endmember selection. Above shows 2D spectral space for three components with feasible mixtures located inside the 2D simplex (triangle) (Boardman, 1995) 48
Figure 3-2 Image endmember selection in 2D spectral space where the x-axis is the red band, and y-axis is the NIR band (units in % reflectance) 49
Figure 4-1 Study Area (a) provincial map showing Indian Head study site (star) east of Regina; and (b) false colour multispectral IKONOS satellite image, June 28, 2000. IHARF experimental farm shown in yellow box 65
Figure 4-2 Crop types (clockwise from top left: wheat, canola, and field peas) at the IHARF study area (a) oblique photograph of each crop type, and (b) close-up view of each crop type taken from SMA endmember samples. 66
Figure 4-3 3D illustration of IHARF precision farm, created as TIN digital elevation model from 1998 elevation data. False colour 1999 aerial image was draped over the DEM and illustrates the drainage area running south central to northeast (IHARF, 2003) 67
Figure 4-4 Site-specific map of IHARF study area showing soil type relative to slope (Kozac and Padbury, 1999) 68
Figure 4-5 Nitrogen fertilizer application strategy for wheat and canola, seeding rates shown for peas. Units in imperial gallons per acres unless otherwise specified (from IHARF, 2003). 73
Figure 4-6 Location of 98 sample sites selected to capture the extent of within-field variability. The sample sites were mapped using GPS with an accuracy of +/-1 metre. 74
Figure 4-7 The above diagram is a profile of the LAI-2000 instrument pointed away from the field technician. 77
Figure 4-8 Ground based LAI-2000 sampling method 78
Figure 4-9 The aircraft and Probe-1 sensor that were used in the 2000 campaign. Services provided by Earth Search Systems Inc. 79

Figure 4-10 (a) ASD FieldSpec® Pro spectroradiometer FOV and video camera mount (b) ASD FieldSpec® Pro stationary field set-up, target shown is the Spectralon™ panel. 83
Figure 4-11 GER3700™ Spectroradiometer used by CCRS to measure the radiometric calibration target for radiometric correction. 84
Figure 4-12 Flow diagram illustrating the pre-processing steps applied to the airborne hyperspectral data (Secker et al., 2001). 86
Figure 4-13 False colour multispectral IKONOS imagery showing the location of the 12 GCPs (yellow asterisk). 87
Figure 4-14 Natural colour composite of Probe-1 flightline one showing the co-registered sample site locations (yellow crosses). 89
Figure 4-15 Natural colour composite of Probe-1 flightline 2 showing the co-registered sample site locations (yellow crosses). 89
Figure 4-16 12 Thenkabail et al. (2000) narrow bands (labelled in nm) versus the selected Probe-1 Bands that best matched the recommended band centers (band widths Table 4-7) superimposed on an average sunlit canola spectral measurement. The portion of the spectrum where leaf pigment and cell structure drives spectral response are shown at top. 93
Figure 4-17 Establishing the soil line from the Probe-1 hyperspectral imagery. Only the study area (307 acre farm) was included in the analysis. The red band (660.1 nm) is shown on the x-axis, and the NIR band (721.6nm) is shown on the y-axis. 94
Figure 4-18 Linear regression analysis of pixel values selected from Probe-1 imagery to represent bare soil line required for TSAVI. 95
Figure 4-19 Original endmembers (solid line) and calibrated endmembers (dashed line) for sunlit crop, sunlit residue, and sunlit soil endmembers. 101
Figure 4-20 Manually selected Image Endmembers using two spectral bands (Probe-1 red band 660 nm and NIR band 721 nm) in the ENVI n-dimensional visualizer. 104
Figure 4-21 ENVI Automatic Image Endmember selection for 12 Probe-1 spectral bands. 104
Figure 5-1 Magnitude of coefficient of determination (r^2) for vegetation indices as a predictor of biomass and LAI for all three crop types. Note: "*" not significant at the 95% confidence level. 114
Figure 5-2 Ground based nadir picture of the wheat crop in June 2000. 116
Figure 5-3 Ground based nadir pictures of peas, canola, and wheat (clockwise) showing predominantly crop residue rather than bare soil contribution to the background. 118
Figure 5-4 Magnitude of coefficient of determination (r^2) for SMA using fractions from reference endmembers for predicting biomass and LAI for all three crop types. Note: "*" indicates not statistically significant at the 95% confidence level. 122
Figure 5-5 Magnitude of coefficient of determination (r^2) from SMA image endmember fractions for predicting biomass and LAI for all three crop types. Note"*" indicates not statistically significant at the 95% confidence level. 126
Figure 5-6 Comparison of reference and image endmembers in 2 dimensional spectral space. 127
Figure 5-7 Flow diagram illustrating the different integrated endmember sets tested for the reference (Ref) and image (Img) cases for sunlit crop (C), shadowed crop (S),

and sunlit background (B) endmembers. Bold text highlights the endmember that was substituted from the previous entry. 131
Figure 5-8 Magnitude of coefficient of determination (r^2) from SMA integrated tests for predicting biomass and LAI of pea crop. Image (Img) and reference (Ref) endmembers shown for sunlit crop(C), shadowed crop (S), sunlit background (B) fractions. Boxes highlight the endmember that was substituted from the previous entry. Note:* indicates not statistically significant at the 95% confidence level.... 137
Figure 5-9 Magnitude of coefficient of determination (r^2) from SMA integrated tests for predicting biomass and LAI of canola crop. Image (Img) and reference (Ref) endmembers shown for sunlit crop(C), shadowed crop (S), sunlit background (B) fractions. Boxes highlight the endmember that was substituted from the previous entry. Note: "*" indicates not statistically significant at the 95% confidence level. 138
Figure 5-10 Magnitude of coefficient of determination (r^2) from SMA integrated tests for predicting biomass and LAI of wheat crop. Image (Img) and reference (Ref) endmembers shown for sunlit crop(C), shadowed crop (S), sunlit background (B) fractions. Boxes highlight the endmember that was substituted from the previous entry. Note: "*" indicates not statistically significant at the 95% confidence level. 139
Figure 5-11 Summary of results for the prediction of pea biomass using remote sensing. 143
Figure 5-12 Summary of results for the prediction of canola biomass using remote sensing. Note"*" not statistically significant at the 95% confidence level..... 144
Figure 5-13 Summary of results for the prediction of pea LAI using remote sensing. Note"*" not statistically significant at the 95% confidence level..... 145
Figure 5-14 Summary of results for the prediction of canola LAI using remote sensing. Note"*" not statistically significant at the 95% confidence level..... 146
Figure 5-15 Summary of results for the prediction of wheat LAI using remote sensing. Note"*" not statistically significant at the 95% confidence level..... 147
Figure 5-16 Summary of best results obtained in terms of magnitude of the coefficient of determination (r^2) for each remote sensing method tested to predict biomass for each crop type. Note: "*" not statistically significant at the 95% confidence level. 148
Figure 5-17 Summary of best results obtained in terms of magnitude of the coefficient of determination (r^2) for each remote sensing method tested to predict LAI for each crop type..... 149

List of Equations

Equation 2-1 Leaf Area to Leaf Mass Relationship for deriving LAI 23
Equation 2-2 Simple Ratio (SR) Vegetation Index 29
Equation 2-3 Normalized Difference Vegetation Index (NDVI) 29
Equation 2-4 Green Difference Vegetation Index (GDVI) 30
Equation 2-5 Perpendicular Vegetation Index (PVI) 30
Equation 2-6 Soil Adjusted Vegetation Index (SAVI) 30
Equation 2-7 Transformed Soil Adjusted Vegetation Index (TSAVI) 31
Equation 2-8 Optimized Soil Adjusted Vegetation Index (OSAVI) 32
Equation 3-1 Spectral Mixture Analysis (SMA) Algorithm 39
Equation 3-2 Unconstrained Spectral Mixture Analysis (SMA) 39
Equation 3-3 Minimizing the Least Squares Error 40
Equation 3-4 Root Mean Square Error (RMSE) 41
Equation 3-5 SMA Constrained to Unity 41
Equation 3-6 Estimating Ground Cover using SMA 56
Equation 4-1 Spectral Mixture Analysis (SMA) in Agriculture 96
Equation 4-2 Spectral Reflectance Equation for Endmember Spectra 99

List of Tables

Table 4-1 Comparison of Historical (AAFC, 1976) and 2000 Precipitation Data 69
Table 4-2 Comparison of Historical Temperature (AAFC, 1976) and 2000 Temperature Data 70
Table 4-3 Study area field identification number, crop type and variety, seeding date and rate, plant count date, and harvest date in 2000. 71
Table 4-4 2000 fertilizer, chemical, and seeding application strategies. 71
Table 4-5 IKONOS Spectral band Characteristics (Space Imaging, 2003) 80
Table 4-6 Recommended bands for characterizing crop biophysical variables by Thenkabail et al., 2000. 91
Table 4-7 Characteristics of Spectral Bands Recommended by Thenkabail et al. (2000) and equivalent Probe-1 bands 92
Table 4-8 Input Probe-1 Hyperspectral Bands for SMA 106
Table 5-1 Crop heights measured at the time of airborne image acquisition. 110
Table 5-2 Crop biomass measurements based on fresh weight 110
Table 5-3 Leaf Area Index (LAI) 110
Table 5-4 Linear regression analysis results for vegetation index prediction of LAI and biomass based on magnitude of coefficient of determination (r^2), standard error (SE), and F-statistic (F). Note: "*" indicates not statistically significant at the 95% percent confidence level and highest r^2 value per crop type in bold. 112
Table 5-5 Linear regression results using reference endmembers for SMA prediction of LAI and biomass based on magnitude of coefficient of determination (r^2), standard error (SE), and F-statistic (F). Note: "*" indicates not statistically significant at the 95% percent confidence level and highest r^2 value per crop shown in bold 120
Table 5-6 Linear regression analysis results using image endmembers for SMA prediction of LAI and biomass based magnitude of coefficient of determination (r^2), standard error (SE), and the F-statistic (F). Note: "*" indicates not statistically significant at the 95% percent confidence level and highest r^2 value per crop shown in bold. 124
Table 5-7 Paired-samples T-test of integrated endmember SMA test #1 & #2 for all crop types. Note: Reference (Ref) and image (Img) automatically derived (a) or manually derived (m) endmembers shown for sunlit crop image endmember (C), shadowed crop (S), sunlit background (B). Bold text highlights the endmember that was substituted. 129
Table 5-8 Paired-samples T-test of integrated endmember SMA test #3 & #4 for all crop types. Note: Reference (Ref) and image (Img) automatically derived (a) or manually derived (m) endmembers shown for sunlit crop image endmember (C), shadowed crop (S), sunlit background (B). Bold text highlights the endmember that was substituted. 129
Table 5-9 Linear regression analysis results for integrated SMA prediction of LAI and biomass of pea crop based on the magnitude of coefficient of determination (r^2), the standard error (SE), and F-statistic (F). Note: "*" indicates not statistically

significant at the 95% percent confidence level. Bold text highlights the endmember that was substituted from the previous entry and the highest r^2 value per test. 132
Table 5-10 Linear regression analysis results for integrated SMA prediction of LAI and biomass of canola crop based on the magnitude of coefficient of determination (r^2), standard error (SE), and F-statistic (F). Note: "*" indicates not statistically significant at the 95% percent confidence level. Bold text highlights the endmember that was substituted from the previous entry and the highest r^2 value per test. 133
Table 5-11 Linear regression analysis results for integrated SMA prediction of LAI and biomass of wheat crop based on the magnitude of coefficient of determination (r^2), the standard error (SE), and F-statistic (F). Note: "*" indicates not statistically significant at the 95% percent confidence level. Bold text highlights the endmember that was substituted from the previous entry and the highest r^2 value per test. 134

CHAPTER I

1.0 INTRODUCTION

1.1 Introduction

In today's world, there is increasing concern with respect to the agriculture sector and the estimated longevity of a sufficient food production system. Environmental issues can hinder food production systems (e.g. soil erosion, water quality, climatic change), while socioeconomic issues can be equally as damaging. Concern from both the consumer and the farm community stems from issues surrounding the volatility of the international agricultural marketplace, and the requirement of farmers to meet the food demands of an increasing population while maintaining quality. These factors coupled with increasing production costs have resulted in a substantial decrease in the number of North American "family" farms and public concern surrounds the subsequent increase in industrial and corporate farms (Brklacich et al., 1991).

The adoption of sustainable agriculture practices by farmers involves daily management strategies that strive to protect the land resources required to grow food. A sustainable food production system has been defined as an agri-food sector that over the long term can simultaneously maintain environmental quality, provide economic and social rewards for all individuals involved in the system, and produce an adequate and accessible food supply (Brklacich et al., 1991). Essentially, if the food production system cannot meet these criteria then the system is deemed unsustainable.

Site-specific agriculture is one approach to farm management that can promote sustainable agriculture. Site-specific agriculture, also known as precision agriculture, can be defined as the application of technologies and principles to manage spatial and

temporal variability associated with all aspects of agricultural production to improve crop performance and environmental quality (Pierce and Nowak, 1999). This style of agriculture practice refers to a "knowledge-based system" that allows farmers to manage variability at scales that are within a defined farm unit (e.g. section, quarter section) and to specific spatial regions of the farm unit where required (Lu et al., 1991). Spatially variable crop yield can exist due to many factors such as soil nutrient and moisture content, topography, as well as insect and weed infestations that change over time. Site-specific agriculture requires both spatial and temporal management, which in the case of farming can require highly time-sensitive information over large agricultural fields. In the past this type of real-time information has not been easily accessible and farmers have treated fields as homogenous units applying average rates of crop inputs over the entire field. As a result of this practice, farmers tend to over or under-apply crop inputs (e.g. fertilizer) which can result in both economic loss and environmental contamination (Lu et al., 1997).

More recently, the increased availability of remote sensing imagery accompanied by comprehensive site-specific crop management plans has offered farmers a more definitive means of implementing sustainable agricultural practices in large agricultural areas. Remote sensing can play a unique role in agriculture because it is a non-invasive, time-specific method of acquiring information about seasonally variable crop and soil conditions. Remote sensing is a geospatial tool often incorporated into a management strategy for the whole farm operation that together with the benefits of Global Positioning Systems (GPS) and Geographic Information Systems (GIS) can be used to develop Variable Rate Application (VRA) maps for crop inputs (Lu et al., 1997; Pierce and

Nowak, 1999; Batte, 2000). Recently launched commercial Earth Observation (EO) satellites can provide the spatial resolution, timeliness, and high quality imagery that site-specific agriculture requires (Moran et al., 1997). This thesis research has examined the potential of narrow band hyperspectral imagery in site-specific agriculture rather than more traditional multispectral sensors. Narrow band hyperspectral imagery provides increased spectral definition, and this is addressed in this thesis research by assessing new sub-pixel remote sensing image processing methods. Remote sensing as part of a site-specific agriculture management strategy can provide the farm enterprise with the ability to satisfy increasing environmental, economic, and market demands (Stafford, 2000)

The remote sensing and ground-based data collected for this research were part of a much larger multi-organizational and multi-disciplinary project undertaken at the Indian Head Agricultural Research Foundation (IHARF) in Indian Head, Saskatchewan to demonstrate the full potential of remote sensing in site-specific agriculture. The IHARF project was led by the Canada Centre for Remote Sensing (CCRS) with contributions from partners including Agriculture and Agri-Food Canada (AAFC) as well as a number of Canadian universities.

The IHARF project had 5 main scientific objectives (CCRS, 2000):

- validate remote sensing algorithms for estimating biophysical parameters such as leaf area index (LAI) and biomass, as well as plant water content and percent cover from hyperspectral data sets for agricultural crops
- explore the potential of hyperspectral sensors to estimate biochemical parameters such as chlorophyll and nitrogen in crops

- investigate whether hyperspectral, multispectral and radar imagery can detect the presence of water, nutrient and weed stresses in crops
- determine at what growth stage and how early crop stressors can be detected using both satellite based and ground based remote sensing data
- demonstrate that remote sensing data can be delivered in near-real time for use in assessing crop condition

The research objectives for this thesis work concentrate on the estimation of biophysical parameters using hyperspectral remote sensing, as described next.

1.2 Research Objectives

Vegetation indices (VIs) have been used with some success for characterizing crop biophysical parameters (Weigand and Richardson, 1990; Weigand et al., 1991; Thenkabail and Ward, 1994; Rondeaux, 1995). However, vegetation indices have been criticized since they use only two spectral bands yet many more are available from multispectral and hyperspectral data, and they do not account for mixtures of scene components at sub-pixel scales (Peddle et al., 2001b). Identifying scene components at sub-pixel scales is important since background soil, residue and shadow have significant influence on pixel-scale reflectance. Furthermore, vegetation indices tend to saturate in mature crop stages with higher leaf area index (LAI), thus providing very little information about crop biophysical parameters when LAI exceeds two (Major et al., 1990; Rondeaux, 1995).

The SMA method can use more than two spectral bands and explicitly examines the various sub-pixel components that contribute to the overall pixel signal. SMA is dependent on the accurate spectral characterization of endmembers by determining the

purest (without the presence of other surface material) spectral response pattern of each scene component (Davidson, 2002). In an agricultural context, three components were identified: sunlit vegetation, sunlit background (soil and residue), and shadow. The product from SMA is a set of fraction values for each scene component that can then be used as a physical and spatial descriptor of crop biophysical parameters and can contribute to the management of variability site-specifically.

In this research, the purpose of comparing the conventional vegetation indices to SMA was to evaluate the advantages of using the new method to provide an improved spectral and spatial management tool for site-specific agriculture. SMA has been used effectively for the estimation of biophysical parameters in forestry (Hall et al., 1995; Radelhoff et al., 1999; Peddle et al., 1999a; Peddle and Johnson, 2000), but only limited research has been completed with respect to SMA in agricultural applications for defining crop biophysical parameters (Staenz et al., 1997b; Deguise et al., 1998; Lelong et al., 1998; Peddle et al., 1999b; Maas, 2000; Peddle and Smith, 2003). In agricultural applications of SMA, very little research has included narrow band remote sensing imagery, and more importantly, research has not fully addressed the variety of crops that are found predominantly in western Canada. This research concentrated on remote sensing of three prominent crop types found in the prairie region of western Canada: peas (*Pisum sativum L.*), wheat (*Triticum aestivum L.*) and canola (*Brassica napus L.*) all of which play a substantial economic role in the national and international agriculture market.

Accordingly, the main science objectives for this thesis research were to:

1. *Investigate spectral mixture analysis (SMA) as a relatively new remote sensing image processing method that provides sub-pixel scale fractions (sunlit vegetation, sunlit background, and shadow) to estimate crop biophysical parameters (LAI and biomass) in site-specific agriculture.*
2. *Compare SMA with conventional vegetation indices (VIs) for the prediction of crop biophysical parameters*

1.3 Organization of Thesis

This thesis is organized into six chapters. In this chapter, the thesis has been introduced and the research objectives have been stated.

In Chapter Two, the literature is reviewed, starting with the broader context of this research in agriculture and site-specific management. The role of remote sensing in site-specific agriculture is defined in terms of how spatial management tools contribute to the practice of sustainable agriculture. Environmental factors that influence leaf and canopy spectral reflectance are outlined, and crop biophysical parameters are described. The final section of this chapter provides a review of conventional remote sensing image analysis methods.

Chapter Three provides an extensive review of spectral mixture analysis (SMA). The theory of SMA is described, an overview of various algorithms is provided, and parameters of the algorithm are reviewed. Several advanced approaches to SMA are discussed briefly, and specific SMA applications in agriculture are reviewed.

In Chapter Four, the research methodologies are presented. The study area, field data collection and image data set are described. All image pre-processing tasks including radiometric correction and surface reflectance retrieval are outlined. Various types of spectral measurements are summarized, including endmember sets (reference, image, and integrated) which were used as input into the SMA. The vegetation indices and the SMA algorithms used in this research are defined, and finally statistical methods are presented which were used to assess each remote sensing method for predicting crop biophysical parameters.

In Chapter Five the results are presented and discussed. Statistical results are presented for the vegetation indices and SMA fractions as predictors of crop biophysical parameters. The discussion of the results is presented for each individual crop type, and followed by a synthesis and comparison of all results from the SMA and VIs.

In Chapter Six, major conclusions from the research are drawn. Contributions to the research community are presented, and suggestions for future research are highlighted.

CHAPTER II

2.0 LITERATURE REVIEW

2.1 Introduction

In this chapter, a review of the literature is given with respect to remote sensing in site-specific agricultural applications. The first section refers to the broader research context of sustainable agriculture, the role of site-specific agriculture within this context, and the use of remote sensing as a site-specific management tool. Next, crop biophysical parameters are identified and defined. Following this, the spectral properties of crops are discussed at the leaf and canopy level, and the effects of environmental stress on the spectral characteristics of the crop are presented. Finally, a review of conventional remote sensing image processing methods is presented. The emphasis for this portion of the review is placed on traditional vegetation indices (VIs) and soil adjusted vegetation indices (SAVIs) as these are more pertinent to this research and are used in a direct comparison with spectral mixture analysis.

2.2 Sustainability and Site-Specific Agriculture

2.2.1 Sustainable Agriculture

The broader context of this thesis research falls within the domain of sustainable agriculture. The implementation of sustainable farm practices is closely related to the way the agricultural sector has historically evolved. In the 1950s through to the 1980s, the emphasis in farming was placed on the modernization and industrialization of agriculture to increase farm output (Ilbery and Bowler, 1998). This time period is also referred to as the "green revolution" that was conceptually adopted on the farm due to the introduction of higher yielding grain varieties, an increased number of irrigation

facilities, increased access to inorganic fertilizers, and changes to redundant government policies (Khush, 1999). A key factor in this era of agricultural intensification was global consideration for the food-balance equation that focused on meeting higher demands for food due to population growth in underdeveloped countries (Khush, 2001). Higher demand for production led to intensified agricultural land use which resulted in environmental degradation (e.g. over use of chemicals, soil erosion). These environmental consequences were realized through an international movement that focused on sustainable development and conscious use of the world's limited natural resources (World Commission on Environment and Development, 1987). It was through this paradigm shift that both the public and the farm community became aware of the environmental damage which occurred due to intensive agriculture practices.

By the 1990's, the focus changed from increasing food output to concern over food quality and sustainable food production (Ilbery and Bowler, 1998). The 1990's were not only characterized by reduced output of food, but also progressive withdrawal of subsidies, resulting in an increasingly competitive market, and growing environmental regulation of agriculture (Ilbery and Bowler, 1998). During this time period there were vast advances in biotechnology which also affected how farmers implemented sustainable agriculture practices (Mannion, 1998). Overall, farmers became more aware of alternative sustainable practices (e.g. organic farming, improved crop rotation, no-till practices, site-specific agriculture) and the implementation of these practices became more common (Sivakumar et al, 2000; Rigby et al., 2001).

As farmers began to recognize the importance of sustainable agriculture, the adoption of alternative practices on the farm involved a transition from substituting

capital for labor, to substituting management for capital (Petrzelka et al., 1997). Measuring management as capital can be quite difficult to quantify, and the literature describes the issues surrounding the development of an adequate definition for sustainable agriculture (Brklacich et al., 1991). Ilbery and Bowler (1998) summarized the work of Brklacich et al. (1991) by defining a sustainable agriculture system in terms of simultaneously satisfying three types of sustainability:

- *Environmental sustainability* - the capacity of an agricultural system to be projected into the future without unacceptable pollution, depletion or physical destruction of its natural resources such as soil, water, air, and natural or semi-natural habitats.
- *Socio-economic sustainability* - the capacity of an agricultural system to provide an acceptable economic return to those employed in the productive system.
- *Productive sustainability* - the capacity of an agricultural system to supply sufficient food and support the non-farm population.

In order to simultaneously promote these three types of sustainability adequately, farmers recognize there is a need to balance and define what is to be 'sustained' in terms of level and scale (i.e. international, national and regional scales) (Ilbery and Bowler, 1998), as well as defining what is "acceptable" and "unacceptable" within each type.

The 1990's was also a period where climate change was identified as a key factor in the future success of the agricultural sector (Sivakumar et al., 2000). Climate change will impact agriculture in Canada greatly as the nation begins to experience warmer conditions, longer frost-free seasons and increased evapotranspiration (Brklacich et al., 1998). Although one would expect longer growing seasons and increased carbon dioxide

(CO_2) concentrations to benefit the agriculture sector in Canada, other factors such as reduced soil moisture, extreme climate events, soil degradation and increased disease and pests may counteract any potential benefits (Natural Resources Canada, 2002). Since 1992, Canada has supported the United Nations Framework Convention on Climate Change (Government of Canada, 2003) and in 1990 it was estimated that 5% of Canada's greenhouse house gas emissions were directly related to methane and nitrous oxide emissions from agricultural activities (Environment Canada, 1995). In 1995, the federal government released The National Action Program on Climate Change which called for an increase in the carbon content of agricultural soils, a decrease in equipment usage through reduced tillage practices, and the control of methane and nitrous oxide emissions related to livestock production and fertilizer applications (Environment Canada, 1995). The storage of carbon in agricultural soils is known as a carbon sink. Carbon sinks are based on the premise that agricultural crops absorb atmospheric CO_2 during the growing season then convert CO_2 into the soil as organic carbon which is not released back to the atmosphere. Increasing agricultural carbon sinks can happen if farmers increase their yields, and reduce soil disturbance due to tillage methods (Government of Canada, 2002).

More recent ratification of environmental policy, such as the Kyoto Protocol, will put pressure on Canadian farmers to rapidly adopt the aforementioned practices. Under the Kyoto Protocol Canada has committed to reducing greenhouse gas emissions to 6% below 1990 levels, on average, through the first commitment period (2008-2012). This is equivalent to a 240 MT (megatonne) reduction in the nation's projected "business-as-usual" emission levels for 2010 (Government of Canada, 2003). Since 1991, the agriculture sector has adopted a considerable portion of the recommended conservation

practices, and at current rates it is estimated that the agriculture sector will generate a carbon sink of 10 MT in the first commitment period (Government of Canada, 2003). The agricultural policy framework within the Climate Change Plan for Canada indicates that there is a strong "national incentive to promote sustainable land use and expand the area covered by perennial forage and trees" (Government of Canada, 2003). Sustainable agricultural land use initiatives will involve adaptation options in farm technology developments, government programs and insurance, farm production practices, and farm financial management (Natural Resources Canada, 2002). New technological developments in site-specific agriculture practices, including crop monitoring using remote sensing, will not only enable farm level implementation of sustainable land use practices, but will also aid in monitoring results of the adaptation process nationally and over time.

2.2.2 Site-Specific Agriculture

Site-specific agriculture is a knowledge-based system that enables farmers to apply precise amounts of fertilizers, pesticides, water, seeds or other inputs to specific areas where and when they are needed for optimal crop growth (Lu et al., 1997). Successful site-specific agricultural management systems are well documented in the literature (Stafford, 2000; Macy et al., 1994; Mulla, 1991, Stafford et al., 1991; Wollenhaupt and Buchholz, 1992). Schilfgaarde (1999) emphasized that this type of management is very information intensive, and is not based solely on spatial technology but also on rapidly evolving information technologies that contribute to the site-specific modification of land management as conditions change spatially and temporally. One of the most important factors in farm practices is managing more static natural field

variability (i.e. soil type, topography) and variability that is in flux due to environmental stressors (i.e. weather induced, pests). Managing crop variability successfully considers two domains: (1) the spatial variability of the land under production (e.g. soil sampling to establish the amount of phosphorus in the soil), and (2) how that variability changes over time with improved management practices (e.g. applying more phosphorus to those regions of the field that require more for optimal crop production). Successful site-specific farming is dependent on how well practices can be used to assess, manage, and evaluate the 'space-time continuum' in crop production (Pierce and Nowak, 1999).

A quality food production system requires optimal yield performance from the land, and farmers employ site-specific management practices to reduce production costs and increase crop yields (Mulla, 1991). Other reasons for employing site-specific farming practices are not just economic in nature, but include environmental benefits (Hammond, 1992). However, the environmental benefits are not widely documented in the literature (Pierce and Nowak, 1999) and are not easily quantified (Perez-Munoz and Colvin, 1996).

Site-specific farming has been primarily 'technology-driven' (Stafford, 2000) and involves the use of four primary enabling technologies: (a) Geographic Information Systems (GIS), (b) Global Positioning Systems (GPS), (c) Sensors and (d) Variable Rate Technology (VRT). A GIS is an organized collection of computer hardware, software, geographic data, and personnel designed to efficiently capture, store, update, manipulate, analyze, and display all forms of geographically referenced information (ESRI, 1995). A GIS is a key tool in extracting and quantifying crop variability within agricultural fields (Pierce and Nowak, 1999). Å GIS not only establishes where the variability is, but can

address the variability through the application of crop inputs using maps (e.g. variable rate fertilizer maps). Over time, the GIS is a record keeping tool that can provide a cost-benefit analysis for the farmer (e.g. assess if adding more fertilizer to a specific region of the field resulted in more crop yield and more economic return).

The second enabling technology, GPS, became widely accessible in the early 1990s and was originally a constellation of military satellites known as the NAVSTAR (NAVigation System with Time And Ranging) system. In 1994, NAVSTAR became available for general civilian use, including agriculture (Pierce and Nowak, 1999). In 1995, a Russian constellation of satellites was also launched for civilian use and is known as the GLObal Navigation Satellite System or GLONASS (Stafford, 2000). GPS provides location control in site–specific agriculture and is essential to delineate within field spatial variability and to deliver site-specific applications using variable rate technology (VRT) (Tyler et al, 1997).

The third enabling technology involves the use of sensors that can be defined as devices that transmit or receive an impulse in response to physical stimulus such as heat, light, magnetism, motion, pressure and sound (Pierce and Nowak, 1999). The sensors include yield monitors, remote sensing, and soil sensors that measure surface and sub-surface features. Remote sensing and visual image interpretation of individual fields has been used in agricultural research and development for the last 25 years (Bullock et al., 2000). Remote sensing has been used in agriculture in the laboratory, in the field, and from the sky. The advantages of remote sensing in agriculture stems from its non-destructive, non-intrusive measurement capabilities and its flexibility of scale.

The fourth enabling technology, VRT, involves the controlled application of crop

inputs. Variable Rate Technology (VRT) is a remediation tool that ingests the 'map' results derived from the GIS, remote sensing and GPS technologies and is available with farm equipment. Examples of a VRT tool are fertilizer or pesticide applicators, and yield monitors, both of which have evolved rapidly and have resulted in the growth of site-specific agriculture significantly (Brisco et al., 1998). The degree to which a farmer will invest in "high technology" or expensive VRT equipment is not only dependent on the size of operation but also on the type of crop and the current market value of that crop (Batte, 2000). It is important to recognize that all of the technology components listed above work together to form a viable site-specific farm management system. GPS is used to spatially record the location of field activities, sensors are used to spatially characterize the physiological properties of the crop, a GIS ingests the GPS and sensor derived information to create management maps, and VRT is used to implement the management strategies back in the field. As described next, remote sensing in agriculture is an important component of this comprehensive approach to site-specific management.

2.3 Remote Sensing of Crop Information

Remote sensing is the practice of deriving information about the earth's land and water surfaces using images acquired from an overhead perspective, using electromagnetic radiation in one or more regions of the electromagnetic spectrum, reflected or emitted from the earth's surface (Campell, 1996). Optical remote sensing provides an indirect method of observing the physical processes in plant canopies. Radar and other remote sensing methods can provide structural information about the crop but are not as successful in identifying the physiological processes of the crop canopy. Recognition of the value of remote sensing by the agriculture community provides

additional motivation for further research within the context of site-specific agriculture (Moran et al., 1997; Brisco et al., 1998; McNairn and Brown, 1999; McNairn et al., 2001a). It wasn't until the mid 1970's to early 1980's when the first Earth Observing (EO) satellites were launched that a significant research effort was initiated to investigate the use of multispectral images for crop inventory and crop production (Moran et al., 1997).

In site-specific agriculture, three types of information can be obtained: (1) information on seasonally stable conditions, (2) information on seasonally variable conditions, and (3) information required to diagnose the cause of the crop yield variability and develop a management strategy (Moran et al., 1997). This research primarily focuses on the use of remote sensing to derive the third type of information. Remote sensing can be used as a diagnostic management strategy to estimate crop yield variability, aid in the creation of field management zones based on crop vigour and soil variability, and in turn guide in-field soil sampling to derive zone-based variable application maps (Bullock et al., 2000). Remote sensing is also an efficient method of spatially characterizing both site-specific crop biophysical parameters as well as broader ecological information and for modelling (Wiegand and Richardson, 1990; Mack et al., 1990; Wiegand et al., 1991; Thenkabail et al., 1994; Cihlar et al., 1991). The advantage of remote sensing is that it allows the farmer access to information about the health of the crop at more mature growth stages and much later in the growing season. Other ground-based technologies (e.g. plant tissue sampling) may be too impractical and labour intensive in mature crop stages. Using remote sensing throughout the growing season to define crop variability potentially provides farmers with a pro-active method of

remedying crop stress prior to actual yield loss.

2.3.1 Factors Affecting the Spectral Properties of Crops

The focus of this research is to better analyse crop conditions that are important in farm management, such as biophysical parameters (e.g. LAI) that can aid in the identification of poorer yielding regions of the farm. All plants, both native and cultivated, respond to environmental stresses in the same way: through a decline in growth rate and in the rate of acquisition of all resources (Chapin, 1991). Many studies have been conducted on the ability of remote sensing to detect stresses in crops such as nutrient deficiencies (Milton et al., 1991; Yoder and Pettigrew-Crosby, 1995; Masoni et al, 1996; Marrioti et al., 1996). To fully understand canopy level reflectance in airborne agricultural applications of remote sensing, one must first understand leaf spectral properties and how the leaf is linked to morphological and physiological conditions (Mariotti et al., 1996).

2.3.1.1 Leaf Spectral Properties

The leaf of a plant is the primary photosynthesizing organ. Photosynthesis occurs in the chloroplasts where the chlorophyll pigment is located (Gates et al., 1965). When examining the spectral properties of a single leaf, only part of the incident energy is reflected with the balance either absorbed or transmitted. Figure 2-1 demonstrates how these components are closely related and it is necessary to consider the interplay among all three to evaluate the physical and physiological basis for leaf reflectance (Knipling, 1970). A plant leaf typically has low reflectance in the visible (except in the green

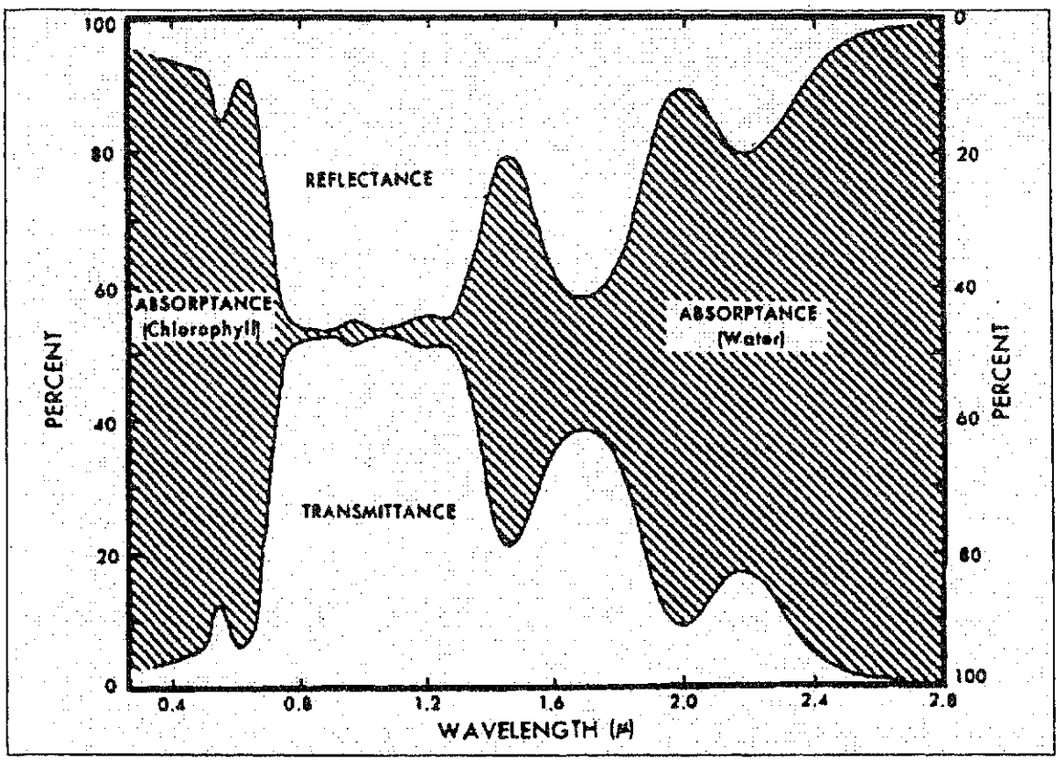

Figure 2-1 Reflectance, absorptance, and transmittance spectra of a plant leaf (from Knipling, 1970).

region) because of strong chlorophyll absorption, relatively high reflectance in the near infrared because of internal leaf scattering and no absorption, and relatively low reflectance in the infrared beyond 1.3μm because of strong absorption by water (Knipling, 1970). This strong absorption beyond 1.3 μm due to water is shown in Figure 2-2 as a function of dehydration of a bean leaf. Water content in the leaf is a dynamic feature because cell structure scatters light as it passes through air and water interfaces of the leaf (Yoder and Pettigrew-Crosby, 1995).

Leaf photosynthetic rate is linked to the amount of absorbed radiation, which depends on incident radiation and leaf absorptance. Leaf absorptance is affected by

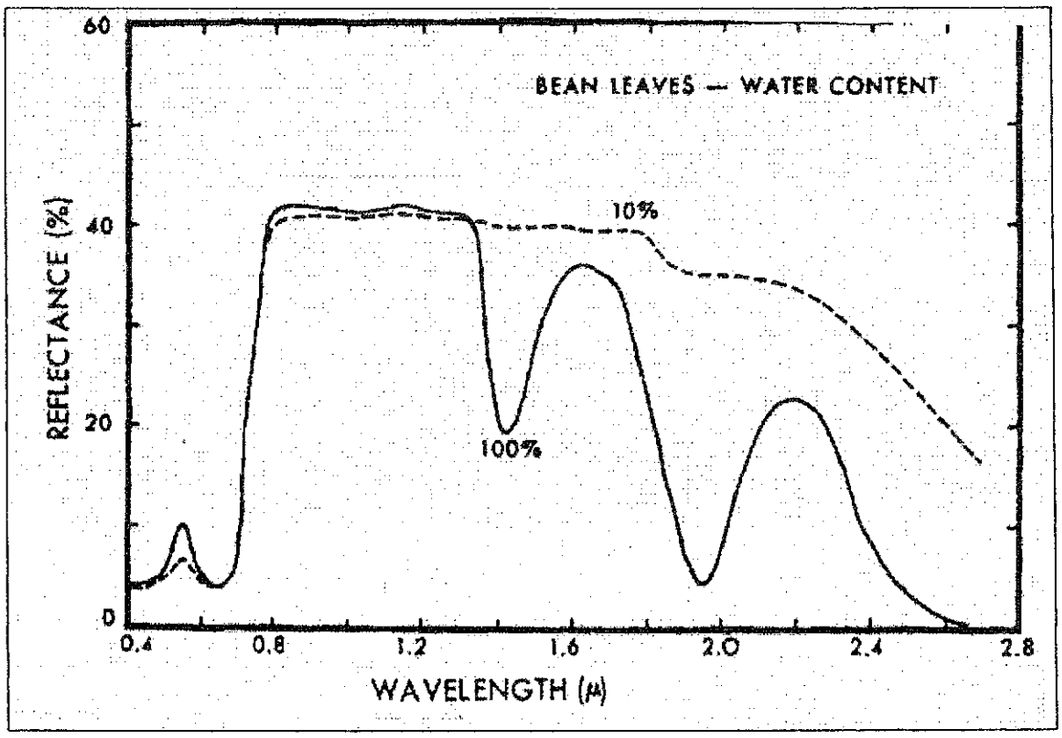

Figure 2-2 The effect of leaf dehydration on the spectral reflectance of bean leaves. The numbers on the curves (10% and 100%) refer to the water content of the leaves at the time of sampling as a percentage of their water content when fully hydrated (from Knipling, 1970).

external and internal reflectance and by leaf pigment content that is essentially represented by chlorophyll content (Masoni et al, 1996). The distribution of chemical constituents within the leaf is not uniform because proteins and chlorophylls are packed into chloroplasts that migrate and clump as the light environment changes, and due to the distribution of lignin in the cell walls (Yoder and Pettigrew-Crosby, 1995). There have been many studies that have examined the relationship between regions of the electromagnetic spectrum, crop leaf structure, and chemical constituents (Wolley, 1971; Thomas and Gausman, 1977; Wiegand and Richardson, 1984; Maas and Dunlap, 1989; Walter-Shea et al., 1991; Horler et al., 1983; Buschmann and Nagel, 1993). Leaf reflectance responses to environmental conditions that inhibit growth (i.e. plant stress)

usually involve increased reflectance in the visible region of the electromagnetic spectrum and in the infrared regions if the stress is severe enough to cause dehydration (Carter, 1992). Remote sensing, and the ability to analyze specific regions of the electromagnetic spectrum, provides a method to examine crop stress at the leaf level, and at the canopy level as described next.

2.3.1.2 Canopy Spectral Properties

The dynamic spectral nature of individual crop leaves contributes to the non-uniformity of the canopy, and furthermore the spectral characteristics of a crop canopy change due to variation in landscape (e.g. topography, soil fertility and texture). Under varying conditions, the reflectance of a plant canopy is modified by the non-uniformity of incident solar radiation, plant structure, leaf area, shadow, and background reflectivities (Knipling, 1970). One significant difference between the amount of infrared energy reflected from a leaf versus a canopy is that a portion of the incident infrared energy is transmitted through the uppermost leaves, reflected from lower leaves, and retransmitted up through the upper leaves to enhance their reflectance (Knipling, 1970). In agricultural applications of remote sensing, it is important to understand how the canopy structure and crop geometry (i.e. size, shape and orientation of the plants and their leaves) plays a role in what is being sensed from the target. The size, shape and orientation of plants are also heavily influenced by human management practices and seasonal growing conditions. All of these factors contribute to the optical properties of crop leaves, and in turn the canopy with respect to the remotely sensed reflection patterns (Knipling, 1970).

2.4 Biophysical Parameters

In the case of agricultural remote sensing applications, biophysical parameters are measured either directly or indirectly from the field of interest during the growing season to evaluate how the crop is performing. The information collected by an optical sensor (e.g. reflected and transmitted solar energy) must be related to the ground based biophysical parameters of the crop. If biophysical parameters are strongly correlated with remote sensed data, then these data can be used to predict those biophysical characteristics for variable scene and sensor characteristics over large areas (Treitz and Howarth, 1999). Empirical relationships established in the literature has led to the development of indirect methods for quantifying crop biophysical parameters using remote sensing imagery.

2.4.1 Ground Based Biophysical Parameters

In remote sensing studies, ground based biophysical sample site locations are typically mapped using GPS to enable a direct comparison of the biophysical parameter with the imagery. Sampling methods may be designed based on the size of the study area, and more importantly the spatial resolution of the imagery or pixel size. Ground based biophysical parameters commonly reviewed in the literature for agricultural studies are; percent crop cover, leaf area index (LAI), biomass, and yield (post-harvest).

2.4.1.1 Percent Crop Cover

Vegetation cover can be defined as the vertical projection of the shoot area of vegetation to the ground surface and is expressed as fraction or percent of the reference area (Purevdorj et al., 1998). In remote sensing applications, this definition can be elaborated to include all "green vegetated areas that are directly detected by the sensor

from any view direction" (Purevdorj et al., 1998). Percent crop cover during the growing season can be measured using in-field photographs taken directly above the crop. The photographs are imported into an image analysis software and classified to obtain the percent ground cover for each cover type (McNairn et al., 2001b). Percent crop cover is measured to deduce the percentage of each ground cover component in the image (i.e. percent crop, percent shadow, percent crop residue or dead matter, percent bare soil). This tool is a method of spatial validation for both traditional and new remote sensing image processing methods.

2.4.1.2 Leaf Area Index (LAI)

In assessing the health of the crop, it is very important to understand not only health but also how much plant is present. LAI is defined as the leaf area per unit area of soil surface (Daughtry, 1990). Norman and Campbell (1989) defined both direct and indirect methods of collecting LAI of a vegetation canopy. Compared to direct methods, the indirect methods are less labour intensive. Predicting LAI from remotely sensed imagery or physically measuring LAI is important in characterizing how the field is producing site-specifically. LAI prediction can aid in defining within field variability and if done early enough in the growing season could allow the farmer to remedy problems before actual yield loss results. In remote sensing studies, LAI field measurements are typically acquired at a limited number of representative sites and used for remote sensing input and/or validation over large areas.

2.4.1.2.1 Direct Measurements of LAI

One of the earliest direct methods of collecting LAI was leaf tracing. A sample of

leaves would be harvested and their contours traced onto graph paper and the area measured by counting the squares within the leaf outline (Daughtry, 1990). The leaf tracing may be weighed and area calculated based on the area to weight ratio for the paper tracing. This method was very accurate, but not time efficient. Other similar methods involved matching leaf shapes and sizes to standard sets of leaves by species, and calculations were based on linear measurements (Daughtry, 1990).

In the interest of time efficiency, direct LAI measurements have been developed in recent years to include the use of laboratory instruments that measure leaf area such as the LI-3100 (Figure 2-3) from LICOR (2003a). With the LAI-3100, a sub-sample of the crop is harvested and the leaves are placed through the optical planimetric instrument. This instrument measures the leaf area of the sub-sample in cm^2. This direct method requires additional calculations to determine the leaf area index of the entire canopy from the sub-sample measurements. Daughtry (1990) defines LAI as a function of the leaf area to leaf mass relationship, according to the following equation:

Equation 2-1 Leaf Area to Leaf Mass Relationship for deriving LAI

$$A_L = (A_S / M_S)M_L$$

Where:
A_L = Leaf Area Index
As = Leaf Area of sub-sample of leaves
Ms = Leaf Mass of sub-sample of leaves
M_L = Total leaf mass for a larger sample of leaves

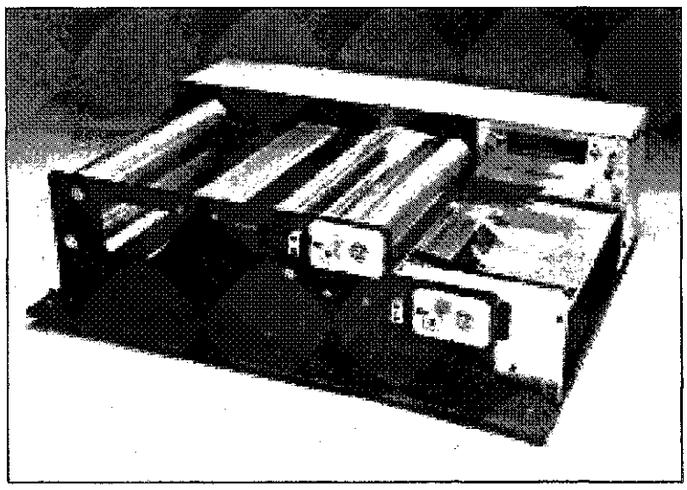

Figure 2-3 LI-3100 instrument. Leaves are measured by a camera with cumulative area reported in cm^2 on the LED display (LI-COR, 2003a).

2.4.1.2.2 Indirect Measurements of LAI

There are many methods and instruments used in measuring LAI indirectly such as hemispherical photography, crown meters, and line quantum sensors all of which are described in Welles (1990). In this review only the indirect methods that are pertinent to agricultural studies will be discussed. A common indirect field instrument used in agricultural applications is the LAI-2000 (Figure 2-4) developed by LI-COR (2003b). The LAI-2000 measures the gap fraction in foliage and is an optical instrument that does not involve destructive sampling. The LAI-2000 instrument measures all light blocking objects simultaneously in five equal zenith angles from 0 to 75 degrees and therefore is

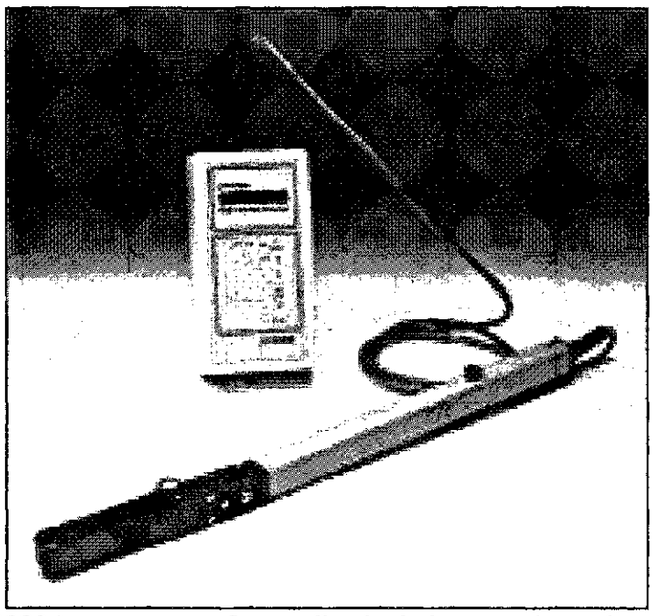

Figure 2-4 LAI-2000 instrument performs all calculations on-site and results are available for immediate inspection (LI-COR, 2003b).

considered to provide a "foliage area index" (LI-COR, 1992). The units of this instrument are dimensionless, but can in theory be thought of as (m^2 foliage area/m^2 ground area). This instrument makes the assumption that the canopy has random foliage distribution, and the clumping properties of the canopy are not considered (Leblanc and Chen, 1998). Not accommodating for a clumping index results in a measure of effective LAI (*e*LAI) and not absolute LAI. In the field, the LAI-2000 measurements are generally collected in overcast conditions to minimize the effect of scattering within the canopy. Other factors to consider in the measurement of LAI in an agricultural setting is the orientation of the foliage, foliage size, and gaps in the foliage (Welles and Norman, 1991).

The Tracing Radiation and Architecture of Canopies (TRAC) instrument (Chen and Chilar,1995) is an optical instrument that measures the gap fraction, however it considers clumping properties (e.g. boreal forests have a non-random and 'clumped' leaf

architecture). Unlike the LAI-2000, the TRAC foliage clumping index allows for the calculation of absolute LAI values. Pacheco et al. (2001b) compared the LAI-2000 and TRAC instruments for three crop types in southern Ontario and found that the LAI-2000 and *e*LAI values correlated more strongly with the percent crop cover derived from photographs than the TRAC instrument.

2.4.1.3 Biomass

Biomass is the total dry-matter production of a crop, the net result from photosynthesis, respiration, and mineral uptake (Stoskopf, 1981). Quantifying crop biomass can help a farmer to locate inadequately producing regions, and aid in developing crop input management strategies (e.g. fertilizer and pesticide application). In remote sensing agricultural applications above ground biomass measurements should be taken within a day of acquiring the remote sensing image to ensure that the derived empirical relationships are valid. The collection of biomass data involves harvesting plants from the field within a specified sampling area that adequately represents the corresponding pixel size in the imagery. Plants are weighed wet (fresh weight), dried and then reweighed (dry weight). The plant water content is calculated from the wet minus the dry weight (Staenz et al, 1997b; 1998a; Deguise et al., 1998). Timely pre-harvest biomass prediction from remote sensing imagery could help to quantify marketable yield and give the farmer an international competitive advantage that could lead to economic benefits for the farm operation.

2.4.1.4 Yield

In remote sensing agricultural applications, the most spatially accurate yield data

available today is obtained using a yield monitor coupled with a Differential Global Positioning System (DGPS). A DGPS yield monitor is placed on the combine at the time of harvest and captures position as well as crop volume and moisture readings on a per second basis. The DGPS receiver allows the yield data to be "stamped" with a geographic coordinate and enables the yield across the field to be mapped. Most DGPS receivers used in agriculture today are 12 channel and use phase smoothed pseudo-range positioning to permit sub-metre accuracy (Stafford, 2000). A typical example is the Trimble AgGPS 106 differential GPS antenna and receiver (Linco Equipment Inc., 2003). The yield monitor units used to represent yield data can vary by both the yield monitor and the manufacturers software used for data post-processing. In the North Amercian marketplace yield is represented as bushels per acre (bu/ac), kilograms per hectare (kg/ha), or tonnes per hectare (t/ha).

Generally, yield monitors provide an accurate and reliable source of information for farmers over time (Perez-Munoz and Colvin, 1996; DeHaan et al., 1999). Yield maps can be visualized in a raw format represented by a set of yield points (Figure 2-5), or points can be interpolated into a continuous map surface. The goal of yield map interpretation is enhanced profitability through better control of natural and management induced sources of yield variation (Doerge, 1999). Successful yield mapping is heavily dependent on the auxiliary information from the farmer such as field history (e.g. soil type, perennial weed regions, crop rotation), the analysts' geostatistical knowledge (e.g. appropriate data interpolation methods) and the available GIS tools (Doerge, 1999).

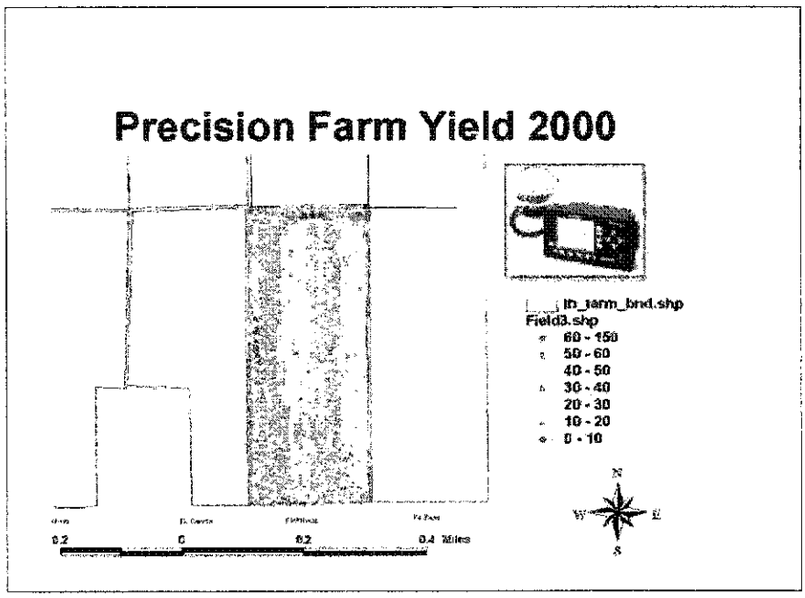

Figure 2-5 Yield map for the IHARF farm in 2000. Data were collected using an AgLeader PF300 yield mapping system and Trimble GPS (top right).

Sources of yield variation are not always easily identifiable and can be a result of weather, soil-water relationships, soil physical and chemical properties, slope and aspect of a region, pest infestation, crop inputs, field history, and cultural practices and errors (Doerge, 1999). The yield map can be used as a seasonal "report card" whereby farmers can evaluate how well the crop performed due to the implementation of new site-specific management strategies (Eghball and Varvel, 1997).

2.4.2 Conventional Remote Sensing Methods for Biophysical Information Extraction

2.4.2.1 Band Ratios and Vegetation Indices

Remote sensing has extended the usefulness of the Geographic Information System (GIS) in site-specific agriculture by incorporating non-intrusive image analysis tools for assessing crop health during the growing season. Vegetation indices, based on

the differential reflectance in the red and near-infrared wavelengths, are widely used to assess vegetation amount and/or health. Compared to non-vegetated surfaces, vegetated surfaces show a sharp contrast in the red and near infrared wavelengths (Bannari et al., 1995; Chen, 1996). Chen (1996) described the earliest form of the vegetation index which was the Simple Ratio (SR) developed by Jordan (1969) (Equation 2-2).

Equation 2-2 Simple Ratio (SR) Vegetation Index

$$SR = (\varrho_n)/(\varrho_r)$$

where ϱ_n is NIR reflectance, and ϱ_r is red reflectance.

An issue with the SR occurs when ϱ_r values are close to zero the index values increase with no bounds (Chen, 1996). Recognizing this led to the development of the Normalized Difference Vegetation Index (NDVI). The NDVI (Equation 2-3) resolves the issue by normalizing the difference between ϱ_n and ϱ_r using the sum and the difference of both values.

Equation 2-3 Normalized Difference Vegetation Index (NDVI)

$$NDVI = (\varrho_n - \varrho_r)/(\varrho_n + \varrho_r)$$

The NDVI is not an inherent physical quantity of vegetation but is correlated to the physical properties of the vegetation canopy, the LAI, percent crop cover, vegetation condition, and biomass. However, the sensitivity of the NDVI to crop biophysical parameters such as LAI becomes weak in conditions beyond a threshold value of LAI, typically 2 or 3 (Carlson and Ripley, 1997). A common variation of the NDVI used in agricultural studies is the Green Difference Vegetation Index (GDVI) in which reflectance in the green band is substituted for reflectance in the red band (Smith et al., 1999; Peddle et al., 1999b; Bannari et al., 1995) (Equation 2-4).

Equation 2-4 Green Difference Vegetation Index (GDVI)

$$GDVI = (\varrho_g - \varrho_r) / (\varrho_g + \varrho_r)$$

where ϱ_g is green reflectance, and ϱ_r is red reflectance.

A common disadvantage of the SR, NDVI and GDVI is the influence of soil background. Huete (1988) reported that for a given amount of vegetation, darker soil substrates resulted in higher vegetation index values for the SR and the NDVI. To accommodate for soil background influences in incomplete vegetation land cover Richardson and Wiegand (1977) created the Perpendicular Vegetation Index (PVI) (Equation 2-5).

Equation 2-5 Perpendicular Vegetation Index (PVI)

$$PVI = (\varrho_{soil} - \varrho_{veg})^2{}_R / (\varrho_{soil} - \varrho_{veg})^2{}_{NIR}$$

where $(\varrho_{soil} - \varrho_{veg})$ is the difference between the "bare soil-vegetation" reflectance in the corresponding spectral band (R = red and NIR = near infrared).

Similar to darker soil substrates, Huete (1988) found that brighter drier soils with sparser vegetation also resulted in higher PVI values. Several improvements have been made to the PVI, and better methods of accommodating for background soil have been implemented (Equation 2-6) in the Soil Adjusted Vegetation Index (SAVI) (Huete, 1988).

Equation 2-6 Soil Adjusted Vegetation Index (SAVI)

$$SAVI = \frac{(NIR - R)}{(NIR + R + L)}(1 + L)$$

where L is a soil adjustment factor.

Based on a simplified radiative transfer model, Huete (1988) showed that a value L= 0.5 permits the best adjustment to minimize the secondary backscattering effect of canopy-transmitted soil background reflected radiation (Bannari et al., 1995). Three versions of the SAVI were developed by Major et al. (1990) to accommodate for wet and dry soils, and varying solar inclination angles. As a result of these improvements, and other modifications by Baret and Guyot (1991), the Transformed Soil Adjusted Vegetation Index (TSAVI) (Equation 2-7) is now believed to be a better indicator than the NDVI for low vegetative covers, and is more sensitive to senescent vegetation than the NDVI (Bannari et al., 1995).

Equation 2-7 Transformed Soil Adjusted Vegetation Index (TSAVI)

$$TSAVI = \frac{[a(NIR - aR - b)]}{[(R + aNIR - ab + X(1 + a^2)]}$$

where a & b are calculated by the "soil line" or "soil brightness vector" which is NIR = aR+b, where a is the slope of the bare soil line, b is the ordinate at the origin of the bare soil line, and X=0.08 a soil effect minimization constant.

The equation of the soil line can be determined from a remote sensing image if there are enough bare soil pixels with sufficient dynamic range. If the current image being used cannot adequately provide a distinct soil line then it can be determined from a previous image of the same region with sufficient dynamic range (Bannari et al., 1995). One of the main drawbacks in the "SAVI family" of indices is that a soil line must be established for each remote sensing acquisition (Rondeaux et al., 1996). In an effort to create an index that was more universal, Rondeaux (1995) created the Optimized Soil Adjusted Vegetation Index (OSAVI) (Equation 2-8). In the SAVI indices, minimization of soil background noise is done by the adjustment of parameters X, whereas with

OSAVI, X has been re-examined to optimize the index over a variety of soils, and for high and low vegetation cover. OSAVI also incorporates bi-directional reflectance in the NIR and red bands.

Equation 2-8 Optimized Soil Adjusted Vegetation Index (OSAVI)

$$OSAVI = \frac{(\varrho_{nir} - \varrho_r)}{(\varrho_{nir} + \varrho_r + 0.16)}$$

In equation 2-8, 0.16 is a static soil adjustment coefficient that is used to minimize background noise due to soil type variation. It is quite similar with respect to performance as the TSAVI and other indices of the SAVI class. The advantage to this index is that it is a simplified formula that does not require *a priori* knowledge of the soil type. The residual variation in OSAVI due to soil is evenly spread across the range (0-1) of crop ground cover, and is therefore promoted as being an optimal vegetation index for agricultural applications (Steven, 1998).

This research evaluates both traditional and soil-adjusted vegetation indices using hyperspectral remote sensing imagery. Vegetation indices have been related to several biophysical parameters such as LAI (Turner et al., 1999; Wiegand and Richardson, 1990); photosynthetic activity (Mack et al., 1990; Wiegand et al., 1991); canopy chlorophyll content (Broge and Leblanc, 2000), biomass and yield (Thenkabail et al., 1994). However, in most vegetation studies there are limitations surrounding the relationship between vegetation indices, LAI, photosynthetic activity, and yield in high LAI conditions (Wiegand and Richardson, 1990). The ratio of red to NIR approaches limiting values asymptotically as LAI increases (Wiegand and Richardson, 1984). The relationship between VIs and LAI can vary with crop stage and leaf water content (Carlson and Ripley, 1997). Hatfield et al. (1985) performed a ground based remote

sensing experiment on different planting dates of wheat and found that VIs saturated at a LAI above 4.0 and did not return to the pre-emergence bare soil value at senescense. Therefore, the VI to LAI relationship is not absolutely reliable later in the growing season in mature crop stages.

In remote sensing agricultural applications, VIs calculated too early in the growing season do not relate well to actual crop yield because measurements do not represent the canopies' photosynthetic capacity (Wiegand and Richardson, 1990). There are also issues with VIs because the algorithms are performed on the entire pixel and do not discriminate for mixtures at sub-pixel scales (e.g. volunteer crops, weeds). Components of a pixel in agricultural remote sensing scene may include the crop vegetation, but also shadow, background soil and residue, and other types of vegetation (e.g. weeds), all of which contribute to the overall remote sensing signal (Peddle et al., 2001a). Spectral Mixture Analysis (SMA) attempts to discern the sub-pixel components in agricultural remote sensing scene, as described in the next Chapter.

2.5 Chapter Summary

In this chapter, a review of the pertinent literature was presented within the context of sustainable agriculture. Site-specific agriculture can be considered a management practice that encompasses the principles of sustainable agriculture. In this research, remote sensing is the primary enabling technology examined, but it is only one of the many technologies that are combined to deliver site-specific agricultural management strategies. Remote sensing can be used to delineate crop biophysical parameters, and several ground based biophysical parameters were described in this chapter that can be related to remotely sensed imagery using empirical methods. The last section of this

chapter reviewed conventional VIs that have also been used with some success in predicting crop biophysical parameters. In the next chapter, spectral mixture analysis is presented and reviewed as a potential improvement to VIs.

CHAPTER III

3.0 SPECTRAL MIXTURE ANALYSIS

3.1 Introduction

In the previous chapter, several issues were raised regarding the use of vegetation indices (VIs) to predict vegetation biophysical parameters. In this chapter, Spectral Mixture Analysis (SMA) is reviewed as an approach that is suitable to address several of these issues, and which forms an analytical framework for this thesis research. One of the key motivating factors in the remote sensing community for developing new and more advanced sub-pixel analysis techniques, was an understanding of the mixed pixel (Elmore et al., 2000). Remote sensing scientists became aware of issues surrounding the fact that the instantaneous field of view (IFOV) of a remote sensor contains a number of individual surface components that contribute to the overall pixel level radiance (Horwitz et al., 1971; Adams et al., 1993). In many cases, the mixed pixel can reduce the amount of useful information obtained from remote sensing imagery, and this was widely recognised in a variety of remote sensing applications such as geology, forestry, oceans and arctic (Ungar and Bryant, 1981; Peddle et al., 1995; Cloutis, 1996; Piwowar et al., 1998). The SMA approach to this problem is twofold: (1) identify the spectral properties of the dominant components within the image, and (2) deconvolve the spectral information of each pixel into component surface abundances (Tompkins et al., 1997).

The first to identify the significance of the mixed pixel problem was Horwitz et al. (1971) who developed early SMA algorithms in agricultural applications. As more research occurred in the development of SMA, the method also became known as spectral unmixing (Endsley, 1995; Chang, 1998) and linear spectral unmixing (Hu et

al.,1999; Petrou and Foschi, 1999). Awareness of the mixed pixel was not the only motivating factor in the development of SMA because increased availability and accessibility to sensors also initiated further research. Hyperspectral remote sensing imagery became available to the scientific community in 1982 with the introduction of an airborne imaging spectrometer (AIS) (Adams et al., 1993). As predicted by Goetz et al. (1985), the introduction of these new airborne sensors encouraged further development of analysis tools that could better handle the "high dimensionality" of the hyperspectral data.

Within the context outlined above, this chapter is intended to: (1) introduce the SMA equation and related parameters, and (2) discuss how SMA has been used in agricultural applications. The first section introduces the concept of the endmember which is a key SMA input parameter, and then two approaches to SMA are presented: the constrained and unconstrained methods. The next section of the chapter outlines various methods for endmember acquisition, and the final section presents a review of how SMA has been applied in agricultural applications.

3.2 Endmembers

SMA is a physically based model in which a mixed spectrum or pixel is modeled as a combination of pure spectra, called endmembers (Adams et al., 1993). Therefore endmembers can be defined as a set of unique spectra that represent each scene component found in the imagery (Bateson et al., 2000). However, the identification of endmembers is highly dependent on the region being characterized, and can be scale dependent (Rahman et al., 2003). For example, endmembers identified for a national or global land cover project that use low resolution sensors (e.g. MODIS or AVHRR

imagery) may be quite different from those endmembers identified for site-specific agriculture using a higher resolution sensor (e.g. IKONOS or airborne hyperspectral imagery). The scale of the mixed components in the imagery is a function of the instantaneous field of view (IFOV) of the sensor, and the endmembers selected to represent each component should include consideration for what scene components are smaller or larger than the IFOV of the sensor being used. For example, scene components found within an AVHRR 4km pixel are much more general and may only involve the selection of endmembers for land cover classes (i.e. water, roads, forest). However, an IKONOS 4m pixel may include more detailed spectral information that can further define each land cover class as being comprised of a vegetation component, a background component (e.g. underlying soil) and a canopy shadow component.

Adams et al. (1993) described two methods of collecting endmembers for the purpose of performing SMA on remote sensing imagery: (1) 'image endmembers' which are extracted directly from the imagery and (2) 'reference endmembers' which are typically collected on the ground but can be measured in the field or in a laboratory environment. Endmembers selected from the imagery can be more practical in operational applications, but do not guarantee spectra that have 100% abundance of one scene component (Nielson, 2001). Reference endmembers are spectrally pure, but can be very labour intensive to collect (provided they are not already defined in a spectral library), and furthermore the endmember spectra and image data must be in the same units, which typically results in the need for radiometric image correction to spectral reflectance. SMA input variables will be discussed more thoroughly in section 3-4, but first the theory of SMA is discussed next.

3.3 Spectral Mixture Analysis Theory

SMA is used to identify the spectral contribution of components within the instantaneous field of view (IFOV) of the remote sensing instrument (Piwowar et al., 1998). Once the endmember components are identified, and their spectral properties are obtained, the SMA algorithm evaluates each pixel and estimates the spatial abundance of each component contributing to the overall pixel brightness value (Johnson, 2000). The algorithm computes the amount of each component as a fraction of the total pixel area. The fraction values fall between 0 and 1, where 0 is no contribution of the component, and 1 is complete contribution of the component.

In SMA, there are two basic spectral mixture assumptions when performing SMA. The linear spectral assumption requires that the components of the scene be arranged in spatially separate areas of the pixel (Elmore et al., 2000). However, when incident electromagnetic energy reacts with more than one component before being reflected from the surface, non-linear mixing occurs (Mustard and Pieters, 1987). There have been some successful attempts at non-linear SMA in vegetation studies (Borel and Gerstl, 1986; Ray and Murray, 1996). However, non-linear unmixing can be complicated mathematically and a computationally demanding task that is often impractical to solve. In most vegetation applications, the linear method can provide a satisfactory approach to SMA provided there is limited multiple scattering in the NIR portion of the electromagnetic spectrum (Quarmby et al., 1992, Quarmby, 1992; Adams et al., 1993; Lelong et al., 1998; Peddle et al., 1999a; Elmore et al., 2000). Imagery that is input into the SMA equation are assumed to contain spectrally mixed data, and are "unmixed" to find the fractional contribution of each endmember (Piwowar et al, 1998).

3.3.1 Unconstrained SMA

In an unconstrained SMA model, fraction values do not always range from 0 to 1. In other words, fraction maps may have values that fall outside the range of 0% to 100% contribution of a component to a pixel. Out of range fractions, or "fraction underflow or overflow", occur if the endmembers and the mixture model do not adequately characterize the image (Adams et al., 1993). The simplified form of the SMA equation can be expressed as:

Equation 3-1 Spectral Mixture Analysis (SMA) Algorithm

$$DN_b = (EM_1 \bullet F_1) + (EM_2 \bullet F_2) + ... + (EM_n \bullet F_n) + \in,$$

where:

DN_b	pixel's digital number at wavelength b
EM_1	spectrum of the i th endmember (where there are n endmembers in the model)
F_1	fractional contribution of the i th endmember
$\in$	any residual contribution not accounted for by the endmember set

In Equation 3-1, the pixel's digital number at a specific wavelength (DN_b) is from the image, and we specify *EM*. Therefore, a system of equations is used to solve for the fractions *(F)* (Adams et al., 1993; Piwowar et al., 1998). In this equation, SMA produces one fraction image for each endmember, with a root mean square value computed as an estimate of the residual spectral components not accounted for by the input endmember set. This equation can also be expressed in more general terms, as shown in Equation 3-2.

Equation 3-2 Unconstrained Spectral Mixture Analysis (SMA)

$$DN_b = \sum_{i=1}^{n} F_i DN_{i,b} + \in_b$$

where DN_b is the intensity of a given pixel in band pass or wavelength b, F_i is the fraction abundance of endmember i, $DN_{i,b}$ is the intensity of image endmember i at wavelength b, n is the number of endmembers, and $\in$ is the error of the fit for band b (Elmore et al., 2000). In either approach, the ideal number of endmembers for any given SMA model should be lower than the input dimensionality (Adams and Smith, 1986). Therefore, the number of spectral bands (m) should be greater than the number of endmembers (n), hence the maximum number of endmembers in SMA should be m-1 (Boardman, 1989).

There are a number of ways that the linear SMA equation can be solved. One method presented quite early in the literature was singular value decomposition (Boardman, 1989). A more common method presented in the literature is the least squares approach described by Shimabukaro and Smith (1991) where the proportion of each component inside the pixel is solved for by minimizing the sum of squares of the errors (Equation 3-3).

Equation 3-3 Minimizing the Least Squares Error

$$f = \sum_{i=1}^{m} \in_i^2$$

Where f is the function to be minimized, and m is the number of spectral bands. This component of the equation ensures that the total error is minimized for each spectral band included in the SMA equation.

As mentioned previously, SMA model accuracy can be assessed using a measurement of Root Mean Square Error (RMSE). Equation 3-4 is the total root-mean square error (RMSE) output from the unconstrained approach where b is the number of spectral bands.

Equation 3-4 Root Mean Square Error (RMSE)

$$RMSE = \sqrt{\sum_{i=1}^{b} \frac{(\in_1)^2}{b}}$$

The RMSE is an excellent measurement of validity for the endmembers selected as input for the SMA model. Elmore et al. (2000) tested this method for Landsat TM imagery over a semi-arid region, and model accuracy was based on the precision of the input image data (i.e. RMSE = ± 1 to 2 DN's).

3.3.2 Constrained SMA

The SMA model can be constrained using one or both of the following: (i) constraining the equation to unity so that fraction values must sum to 1, and (ii) constraining the equation to ensure that fractions values fall between 0 and 1. A properly constructed unconstrained mixture model should return values that fall between 0 and 1, however constraining to unity tends to stabilize the solutions (Elmore et al., 2000). In the first case (Equation 3-5) all resulting fraction values sum to 1.

Equation 3-5 SMA Constrained to Unity

$$\sum_{i=1}^{n} F_i = 1$$

In reference to Equation 3-2, n is the number of endmembers, and F_i is the fraction abundance of endmember i. In the second case, when an SMA equation is fully constrained, the fraction values will not only sum to 1 but all fractions values will fall between 0 and 1. In the example of solving the equation for three endmember components, the constraint becomes $x_1 + x_2 + x_3 = 1$ (or $x_3 = 1 - x_1 - x_2$). The use of a fully constrained equation implies that the pixel is well defined and there are no unknown contributors to the spectral components of the image (Adams et al., 1993). There has

been some disagreement with this approach because the resulting fraction maps have the appearance of always being reasonable. For example, each pixel is always between 0 and 1 regardless of how well the input endmembers characterize the components of the image, and this can lead to erroneous results (Elmore et al., 2000; RSI, Personal Communication, 2001).

3.4 SMA Inputs

As mentioned in section 3.2, the selection of endmembers is critical to the success of the SMA model. Endmembers are the central input for any SMA equation, and can be collected from the imagery or on the ground using ground-based sensors such as a spectroradiometer. Image endmembers and reference endmembers can also be combined and used in integrated endmember approach to SMA. The integrated endmember approach to SMA is quite useful when the collection of reference endmembers may not always be practical, and when extensive reference spectral libraries are not readily available for a specific remote sensing application. The next three sections of this chapter discuss how reference, image, and integrated endmembers can be collected and used in SMA.

3.4.1 Reference Endmembers

Reference endmembers can be measured in the field, in the laboratory or selected from an existing spectral library (e.g. USGS Public Spectral Library for Minerals and Vegetation, USGS, 2003). The use of reference endmembers in SMA depends on having a well-calibrated image (Tompkins et al., 1997). Reference endmembers can be measured in two ways, one involves removing a sample of the component from the field (destructive method), and the other involves is an *in situ* measurement where the

component is left intact. For SMA studies involving the use of reference endmembers, both the endmember spectra and the airborne or satellite imagery must be converted to the same physical units, and this is usually reflectance (Piwowar et al., 1998). Both types of measurements involve a considerable amount of care in the field, and in the calibration of the ground spectra and the remote sensing imagery (Peddle et al., 2001a).

3.4.1.1 Non-Destructive *In Situ* Endmember Acquisition

Non-destructive *in situ* endmember acquisition is done in the field above the target of interest using a ground-based sensor such as a spectroradiometer. The main advantage of collecting reference endmembers using *in situ* measurements in vegetation studies is that the geometry of the image components can be maintained. Geometry of the plant canopy and background material such as soil, can play an important role in spectrally defining the complex interaction of energy before the signal is received back at the sensor. The size of the area sampled using *in situ* methods is heavily dependent upon the scale of the application, and the spatial resolution of the imagery. If the objective is to acquire near pure representations of one component with no influence from complex geometry such as shadow, then it can be difficult to find a plot location in a natural setting with minimal background and shadow noise within the IFOV of the sensor (Peddle et al., 1999b).

The difficulties associated with *in situ* sampling was demonstrated in the literature by Franklin et al. (1991) who used a pole-mounted radiometer to acquire *in situ* reflectance characteristics over different tree species in Africa. This study showed how there were distinct differences in the red and NIR reflectance characteristics of the various vegetation components in the canopy. It also illustrated how difficult it is to

locate a spectrally pure region with only one spectral component within the IFOV of the sensor. Similarly, Peddle (1998) illustrated some of the disadvantages of *in situ* sampling in forestry applications as part of the Boreal Ecosystem Atmosphere Study (BOREAS). In this case, spectral measurements were collected to represent maximum and minimum solar illumination of the background component that was a complex mixture of materials found in the forest understorey. Collecting endmembers on the forest floor proved to be challenging due to significant fluctuations in solar illumination because of differences in terrain, wind blowing the trees that caused sunflecks in the sample, and multiple scattering within the canopy. These illumination issues were less than adequate for reference endmembers, and instead samples were removed from the forest and measured at a stationary site outside of the region of interest.

In an agricultural study by Peddle et al. (1999a), endmembers were collected for the background component that in this case was primarily bare soil. The collection of endmembers for agricultural soils can involve a consideration for soil type, and tillage practices (i.e. soil roughness and orientation). In that study, *in situ* endmembers were collected for cultivated, disturbed loose soil, and an area of flat compacted soil. Similar to the forestry studies above, there was some difficulty finding bare soil patches in the field with no shadowed areas from the crop, therefore regions were selected outside of the crop and along the borders of the field. The most representative endmember for soil came from the *in situ* cultivated soil region because it more closely represented the geometry and tillage practices of the study area.

The non-destructive *in situ* method of endmember acquisition can involve sensing more than one component (e.g. canopy and canopy shadow), but can retain the natural

geometry of the sample (e.g. soil orientation and roughness). It should be noted that the spectral issue of sensing more than one component at a time using *in situ* methods are similar to those issues found in the mixed pixel problem. The success of the *in situ* endmember sampling strategy is highly dependent on the scale of the application, and if the dynamic nature of the components' geometry is important for the SMA.

3.4.1.2 Destructive Endmember Acquisition

Destructive endmember acquisition involves removing samples from their natural environment for spectral measurements. In vegetation applications, there are a variety of removal methods based on the amount of plant available, and what is acceptable in terms of the level of disturbance to the plants and the surrounding environment. Minimal destructive removal methods include cases where single leaves are extracted from the study area and transmittance and reflectance properties of the leaf are measured using an integrating sphere coupled with a spectroradiometer (e.g. Model LI-1800 from LiCor Inc.). Inversions of radiative transfer models such as the PROSPECT can simulate leaf reflectance and transmission (Jacequemoud et al., 2000), and canopy level reflectance and transmission can be simulated using the Scattering by Arbitrarily Inclined Leaves (SAIL) model (Daughtry et al., 2000). Both the SAIL and PROSPECT models can then be used to relate leaf biochemistry to the spectral properties of the plant, and to the biophysical parameters of the plant canopy (Zarco-Tejada et al., 2000; Jacquemoud et al., 2000). SMA can be performed on simulated canopy reflectance in addition to conventional remotely sensed imagery, and results can be compared and calibrated to SAIL-generated biophysical parameters such as LAI, fractions of absorbed photosynthetically active radiation (fAPAR), and soil brightness (Van Leeuwen et al.,

1997).

Other destructive endmember sampling strategies consider how the plants are arranged in a sample for optimal nadir reflectance measurements and involve the use of a ground sensor such as a spectroradiometer (Peddle, 1998). Ideally the sensor is placed at a stationary location outside of the study area and samples are transported to this site for controlled spectral measurements (Peddle, 1998). The Optically Thick Stack (OTS) method involves harvesting plants and stacking them in several layers on a black background under the IFOV of the ground-based spectroradiometer (Peddle et al., 1999b). The objective with an OTS is to maintain some of the in-field plant geometry, while minimizing the background noise.

Another method is the flat array sampling strategy. This destructive method involves removing all the leaves from the plant stem and placing them in a flat contiguous arrangement on a black background. The flat array virtually eliminates shadow and background noise within the sample, but alters the geometry of the plants relative to how they are found in their natural environment (Peddle et al., 1999b). These methods can also be used for collecting shadow endmembers. Shadow spectra can be obtained in the field by using the same sunlit samples, only the direct beam of illumination is obstructed. In this case, the shadow is induced and the sampled spectra are converted to reflectance using a shadowed target and a fully illuminated reference panel. This is a measurement of "apparent reflectance" (Miller et al., 1997) instead of absolute reflectance, which is an inherent property of any object and is independent of illumination (Peddle et al., 1999b).

Similar to the non-destructive *in situ* sampling method, the value of retaining

some geometry in the destructive sampling is highly dependent on the scale required for the remote sensing application. The flat array sampling method ensures that there are no external influences in the spectral measurement from background noise and shadow, whereas the OTS compromises these factors to maintain geometry. Overall, both the OTS and flat array sampling strategy provide the most spectrally pure methods and are optimal methods for establishing national spectral libraries.

3.4.2 Image Endmembers

Image endmembers provide a more practical approach to the use of SMA in real-time applications of remote sensing. However, there is no guarantee that image endmembers are derived from only one scene element (Nielson, 2001). It is unlikely that the reflectance of any one pixel in a remotely sensed image is attributable to only one component, therefore some level of mixing must be tolerated within these endmember spectra. The degrees of impurity to be tolerated, as well as the methods used to reduce it, are important considerations when using image endmembers as input for SMA.

There are several analytical and visualization methods used to extract or derive endmembers from imagery. Boardman (1993) used convex hull geometry to derive image endmembers from n-dimensional space. The linear mixed pixel problem in remote sensing shares all the defining attributes of a convex set of points in n-dimensional space, where all points are positive, sum to unity, and form what is known as a convex hull. This relationship is best shown theoretically in Figure 3-1 where the shaded area represents a mixture of three endmember materials: A, B, C. The triangle formed by the

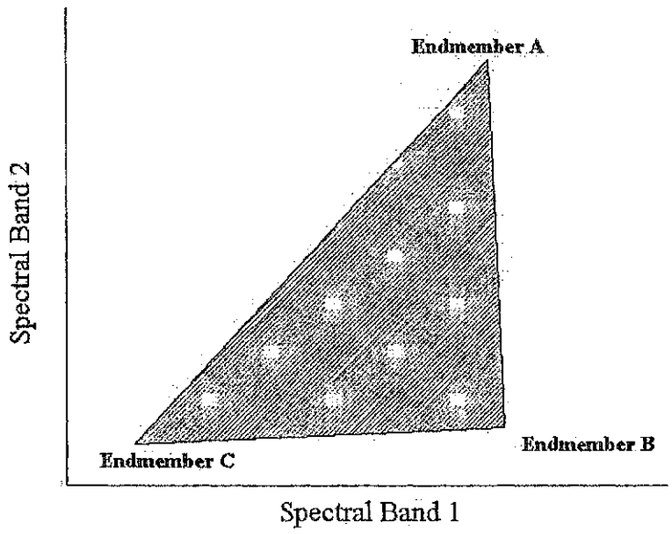

Figure 3-1Convex hull approach to image endmember selection. Above shows 2D spectral space for three components with feasible mixtures located inside the 2D simplex (triangle) (Boardman, 1995).

vertices is known as a simplex, and if there was a fourth feasible endmember then the triangle would become a tetrahedron. Depending on the dimensionality of the image data the simplex can range from 0 to *n* dimensions (Boardman, 1993). The convex hull approach is basically a measure of pixel purity, where pixels near the vertices of the data cloud have a high score in terms of spectral purity, and pixels that lie along the flat edges score low (Boardman, 1995). Figure 3-2 shows an agricultural dataset in 2D spectral space, where all pixels that fall within the simplex are mixtures of three components. In an agricultural setting the three components would be sunlit vegetation, shadow, and sunlit background (likely soil and residue). The purest pixels that would represent these three components would fall closest to the vertices of the simplex, and it is these spectra that would be selected as the image derived endmembers. Manually selecting

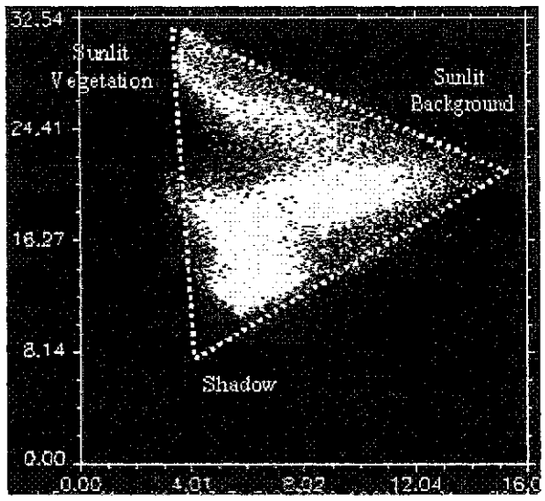

Figure 3-2 Image endmember selection in 2D spectral space where the x-axis is the red band, and y-axis is the NIR band (units in % reflectance).

endmembers using this analytical n-dimensional spectral approach is only appropriate for datasets with low dimensionality and few spectral bands, whereas data sets with much higher dimensionality would require more automatic statistical methods. The success of this technique is highly dependent on the quality of the imagery. For example, sensor or atmospheric noise can appear in spectral space as spectrally distinct pixels near the vertices of the convex hull when in fact they are artefacts of noise and can lead to erroneous endmember spectra (Boardman, 1994).

Tompkins et al. (1997) used the approach of Boardman (1993) and described it as a "fit" approach where an *n*-dimensional polyhedron was applied to the data cloud. Tompkins employed a data transformation to determine the dimensionality of the polyhedron and extracted the total number of endmembers from the imagery. The edges of the polyhedron guided the fitting process, and the endmembers were selected at the vertices of the polyhedron. The advantage of this method is that it does not require *a*

priori knowledge of the scene. Conversely, the difficulty with this endmember selection method is that the straight lines of the convex hull polyhedron prevent a unique fit to the data cloud and could result in endmembers that are not realistic in a physical sense (Tompkins et al., 1997).

Other mathematical methods of deriving image endmembers involve the use of a principal component analysis (PCA) (Deguise et al., 1999; Lelong et al., 1998; Tromp and Epema, 1999). PCA indicates the spectral variability in the data and its spatial organization in the imagery (Lelong et al., 1998). The objective of PCA is to reduce interband correlation that can be a problem in the analysis of multispectral and hyperspectral imagery (Lillesand and Kiefer, 2000). Most of the spectral variability in the image will be captured in the first principal component, and when the principal components are viewed in spectral space they can give a clearer view of where the most spectrally distinct pixels are in the imagery. PCA is also a very efficient tool for isolating noise in the imagery, and this is optimal for the endmember selection process. Thus, PCA is very effective in that it can identify endmembers that best encompass the whole spectral variability of the image (Lelong et al, 1998).

Recently, more automated endmember extraction methods have been presented in the literature. Szeredi et al. (1999) presented four methods for automatic endmember extraction from imaging spectrometer data; (a) the Iterative Target Transform Factor Analysis (ITTFA), (b) the Alternating Regression (AR), (c) the Iterative Error Analysis (IEA) and, (d) the Purest Pixel Clustering (PPC). To determine image endmembers, all four methods include an orthogonal transform of the data (e.g. PCA, Minimum Noise Fraction), and an examination of the eigenvalues from the transform versus the

eignevalue number to determine the change in slope. The total number of endmembers is determined by where this change in slope occurs. The ITTFA and AR are derived from chemistry literature and are iterative approaches that use an unconstrained least squares unmixing equation. The geometric interpretation of these iteration procedures is that the algorithm analyzes the input data and zig-zags through n-dimensional space until it encounters the extremities of the data cloud. Alternatively, the IEA uses a constrained unmixing equation, and with successive iterations endmembers are chosen by representative pixels that minimize the remaining error in the unmixing results. This algorithm will terminate when a specific criteria is reached such as a maximum error value, or a predetermined number of endmembers is met. The PPC includes a pixel purity index (PPI) that determines the purest pixels in the image and then performs a cluster analysis on these pixels. The highest weights are assigned to the purest pixels, and these are based on the number of times the pixels were selected after the iterations are complete (Szeredi et al., 1999). The ITTFA and AR methods were designed to be used in scenes where every pixel was mixed, while the IEA and the PPC methods were most useful in the extraction of endmembers from a number of scenes that had relatively pure pixels. When all four methods were compared the ITTFA and AR were determined to be the more desirable methods. The reason for this conclusion was because the condition that an endmember be absent from at least some pixels in a scene (required by the ITTFA and AR) is far more realistic than the condition that endmembers be pure in at least some pixels (required by the PPC and IEA) (Szeredi et al., 1999).

The image endmember selection process has also been researched in terms of defining the full extent of component and image variability. Bateson et al. (2000)

suggested that endmembers should represent the variability found within the remotely-sensed image, and that variability could be incorporated into SMA by representing each endmember as a set or 'bundle' of spectra. The bundles are created from the data itself and by manual extraction of the endmembers from the imagery. This approach to SMA produces minimum and maximum fractions bounding the correct cover fractions and specifiying error due to endmember variability. Similar to the latter approach, Saghri et al. (2000) proposed an improved ISODATA clustering method for the selection of image endmembers. The ISODATA clustering algorithm was altered to use a "spectral angle" criterion rather than the typical Euclidean distance criterion. The advantage of this method over manual extraction or mathematical selection is that the resulting endmembers would (a) represent physically identifiable and likely pure species on the ground, (b) the residual error would be small, and (c) minimal human interaction is required. Newer methods of image endmember selection seem promising but currently are limited in terms of software accessibility.

3.4.3 Integrated Endmember Selection Method

Reference endmembers may not always be available to a study due to logistics, equipment or location limitations. Furthermore, some of the literature has suggested that reference endmembers may not always be a realistic measurement for all the endmembers being observed (Asner and Lobell, 1999). In some cases, the best solution may involve selecting reference endmembers in combination with image endmembers, and targeting specific materials that are being remotely sensed (Small, 2001). Integrated endmember selection can be defined as a method to determine the best set of endmembers for a particular image under study. Endmembers in this case, can be combination of image,

laboratory, and in-field spectral measurements. Roberts et al. (1998) proposed a quasi-integrated method of selection known as the multiple endmember SMA (MESMA). In this case, a series of two and three endmember models were created from a number of field and laboratory measurements. A set of endmembers were chosen to model a pixel if they met a series of criteria where fractions had to fall within a specific range of absolute values, and where the RMS error was low in seven or more contiguous bands. They found that the two endmember models were the best in defining vegetation maps, and three endmember models provided greater spatial coverage but provided poorer vegetation discrimination due to model overlap (e.g. where two or more model candidates modeled the same pixel).

Tompkins et al. (1997) proposed a Modified SMA (MSMA) algorithm that utilized both reference and image endmembers. This algorithm gave the endmembers (and their fractional abundances) a starting point and then forced the endmember spectra, by a set of constraints and by data dimensionality, to move or "grow" into a new set of values referred to as a "virtual" endmember. The MSMA algorithm had two distinct differences from the conventional linear SMA model: (1) both fractional abundances and the endmember spectra were treated as unknown which in turn creates a non-linear set of equations, and (2) all pixels were solved for at one time, rather than one pixel at a time as in conventional SMA models.

Overall, the most important consideration in using any integrated endmember approach is that it takes advantage of both the spectral purity of the reference endmembers, and the uncomplicated acquisition of image endmembers. Currently, very few comprehensive vegetation reference spectral libraries exist, and the use of image-

based or integrated endmembers may be important in SMA to realistically represent the conditions at the time of image acquisition.

3.5 Agriculture Applications of SMA

The use of airborne and satellite remote sensing in agriculture is relatively new in comparison to other applications such as geology and forestry, although in agriculture remote sensing has filled a technology gap by providing information related to crop health throughout the growing season and at a variety of scales (e.g. from a quarter section to several hundred sections). In a remote sensing image of an agricultural area, the digital reflectance value for each image pixel is a result of the combined spectral contributions of various components, namely the crop, crop background (soil and/or residue), and shadow. Conventional methods such as VIs do not separate these components explicitly, yet for the most part it is only the crop for which information is sought. In theory, SMA can offer site-specific agriculture a tool to 'data mine' at sub-pixel scales and in turn provide more detailed spectral and spatial information about the crop.

As mentioned previously, Horwitz et al. (1971) was the first to begin the development of SMA equations. This work was motivated by the fact that the low spatial resolution of some of the first sensors reduced the amount of useful information which could be extracted, and that developing methods to extract information about objects that were smaller than the IFOV of the sensor would be more beneficial. The objective of the Horwitz et al. (1971) research was to extract more specific information about crop vigour, maturity and yield. A model was developed that related the signature of a combination of materials within a pixel to the signatures of individual materials. This

preliminary SMA model was based on a maximum likelihood estimate of the proportions of the various materials and included measurements of uniqueness and error (Horwitz et al., 1971).

3.5.1 SMA for Crop Area Estimation

After the initial interest in developing the fundamental SMA equation, SMA was implemented in agriculture to determine crop type area estimations. Quarmby (1992) presented results from northern Greece using linear mixture modelling on multi-temporal AVHRR data for national crop area estimations. Image endmembers were derived using ground data, and a supervised classification of multi-temporal SPOT imagery. The SMA results compared favourably with ground based agricultural statistics from the Greek Department of Agriculture with overall accuracy for the crop area estimates being 90%. The resulting image products successfully provided the % contribution of each crop type (i.e. rice, maize, cotton and wheat) on a per pixel basis in the study area. It was concluded that linear mixture modelling would be useful for operational crop monitoring on a regional basis.

3.5.2 SMA for Ground Cover Estimation

Maas (2000) presented a more simplistic SMA approach in estimating cotton canopy ground cover, which assumed scene reflectance for cotton crops is more affected by canopy ground cover than by plant canopy density. Thus, cotton fields in incomplete ground cover conditions can be decomposed into contributions from the upper surface of the plant canopy versus the soil surface between plant rows. A modified linear mixture model was implemented that used only two endmembers to estimate cotton canopy ground cover from Landsat satellite multispectral imagery (Equation 3-6).

Equation 3-6 Estimating Ground Cover using SMA

$$GC = (R_{scene} - R_{soil}) / (R_{canopy} - R_{soil})$$

where GC is the ground cover, R_{scene} is scene reflectance in a given spectral band, R_{canopy} is the reflectance of the upper surface of the plant canopy, R_{soil} is the reflectance of the bare soil surface, and GC is the ground cover. A constant value for R_{canopy} was used based on field measurements over a number of years for healthy cotton (reflectance values of 0.04 in the red band 600-700 nm, and 0.56 in the NIR 800-900 nm), constant value for R_{soil} was also used from an average of field measurements (reflectance values of 0.18 in the red band, and 0.23 in the NIR). The results suggested that Equation 3-6 works well when computed for either the red or NIR band on fields with incomplete ground cover, and when no shadows are cast on the ground between the plant rows. The absolute mean value of the estimated GC from the satellite imagery (0.579) was comparable to the mean of the in-field estimates of GC (0.582) and resulted in an r^2 of 0.832. On average, the Landsat TM estimates of GC were within 7% of the field measurements. The advantage of this method is that this calculation does not rely on additional field information such as plant size, row spacing, or row orientation.

3.5.3 SMA for the Prediction of Crop Biophysical Parameters

The value of using remote sensing imagery in site-specific agriculture becomes more apparent as one examines the potential of the infrared (IR) region of the electromagnetic spectrum. The IR region is sensitive to plant cell structural information that is not available in the visible portion of the electromagnetic spectrum, and allows for the detection of crop stress before it is apparent to the human eye. One of the advantages

of SMA is that several IR bands can be used as input to analyze distinct absorption features which may better describe the spectral features of a specific crop type. Using SMA to predict crop biophysical parameters such as LAI and biomass, can provide more detailed spatial information about the crop for site-specific applications. Understanding where the crop is highly vigorous (i.e. high LAI and biomass regions) and where it is not, can help farmers prescribe crop inputs such as fertilizer to areas of the field where they are most needed.

Lelong et al. (1998) used SMA in France to estimate leaf area index (LAI) and map stress in wheat fields. The theory was that if LAI could be accurately quantified early in the growing season then potential problem areas in a crop could be remedied before yield was impacted. Four endmembers where chosen: two wheat endmembers (W1= high vigour and W2=low vigour crop), bare soil, and shade. As an alternative to VIs, linear regression was performed to establish an empirical relationship between ground based LAI measurements and SMA fraction maps (W1 r^2=0.96, and W2 r^2=0.97). Linear regression results were then used to empirically produce image-based LAI maps for the two wheat endmembers. The high vigour wheat endmember (W1) resulted in an LAI estimate of 4.0, and the low vigour wheat endmember (W2) resulted in an LAI estimate of 0.6. Both of these estimates were within a reasonable LAI range for wheat during the particular stage of growth (from 0 to 6-8 for most developed wheat crops). The RMSE between image estimated LAI and measured LAI was 0.05. The only limitation identified for this method occurred when soil fractions exceeded 15% and higher overall RMSE resulted.

More advanced LAI estimation research was presented by Staenz et al., (1998a) using Compact Airborne Spectrographic Imager (*casi*) hyperspectral imagery over a study area that consisted of canola, wheat and beans. This research presented LAI estimates using the NDVI and SMA crop fractions as input. Using crop fraction results as input into the LAI algorithm can account for between crop row spacing, and unwanted types of vegetation such as weeds, whereas VIs cannot account for these sub-pixel variables. When the NDVI estimates of LAI were compared to those derived using SMA, the values agreed over all crop types to within one standard deviation.

The work of Staenz et al. (1998a) was expanded by Pacheco et al. (2001a,b) to include more crop types (white beans and corn) in different geographic locations. In the initial research, Pacheco et al. (2001a) measured LAI using the TRAC and LAI-2000 in fields located in southern Ontario. To validate these results, percent crop cover photographs were taken over the crop, and were classified to discern crop cover from other image components such as shadow, and soil. When LAI from each ground-based instrument was compared to the percent crop cover, the effective LAI (*e*LAI) from the LAI-2000 had a significantly higher correlation (r=0.90) than the TRAC derived LAI (r=0.49). The results of this work were then applied in Pacheco et al. (2001b) where the LAI-2000 *e*LAI measurements for the three corn fields were compared with LAI estimations from the corresponding airborne hyperspectral imagery. SMA was performed on airborne hyperspectral imagery to derive crop fractions that accounted for non-vegetated areas between the crop rows in an automated LAI algorithm. Results showed a moderate correlation (r=0.69) with in-field measurements of *e*LAI, and the LAI estimated from the hyperspectral imagery. Linear regression did not result in a high

coefficient of determination (r^2) because the relationship did not appear to be linear in nature. Overall, the derived LAI tended to be overestimated when compared to LAI collected in the field. Automatically derived image endmembers were used and this may have introduced additional error.

The ability of SMA to predict above ground crop biomass has been demonstrated in a study by Deguise et al., (1998) where hyperspectral airborne data (4m spatial resolution) was acquired in 1997 over a potato crop in Carman Manitoba using the *casi* sensor. The research showed that SMA crop fractions were related to in-field measurements of above ground biomass with an overall r^2 of 0.48. The lack of a strong relationship was in part attributed to two common problems in this type of work, namely the inability to locate the exact pixels that corresponded to the GPS sites used to mark the in-field measurements, and the inability to properly sample the pixel area on the ground (i.e. in-field samples were taken from areas smaller than 4m pixel size). This study also extracted endmembers from the imagery using PCA, and this may have contributed some error. Although there was no direct comparison to VIs, the authors recognized very basic advantages in using SMA for row crops when a substantial portion of the image contains either bare soil or other types of vegetation (i.e. weeds) that could be separated from the crop component.

3.5.4 SMA for the Detection of Weeds in Crops

Identifying weed patches that use resources and compete with growing crops is an important part of site-specific crop management. The basic principles of SMA, especially when applied to very narrow band hyperspectral imagery, can be advantageous in identifying weeds and unwanted vegetation over conventional methods such as VIs or

classification methods that operate on the whole pixel. In research by Deguise et al. (1999), high spatial resolution (4m) hyperspectral imagery was acquired using the Compact Airborne Spectrographic Imager (*casi*) over a canola field near Altona, Manitoba, with the objective to spectrally separate weed patches of Canada Thistle from the crop using SMA. The Iterative Error Analysis (IEA) automatic image endmember extraction process was implemented and compared to a manual endmember extraction method (Szeredi et al., 1999). Unlike the IEA, the manual endmember extraction method did not result in the detection of the weeds because the three pixels that defined the weed patches were not at the vertex of the data cloud. The interesting part of this study was that SMA was performed first on the radiance data and then on the atmospherically corrected data. The results from the atmospherically corrected imagery did not match the weed patches identified from the uncorrected imagery. One possible explanation was that the small spectral feature differences between weeds and canola used by the SMA algorithm might have been reduced due to uncertainties of the atmospheric modeling.

This research demonstrates that significant areas of weeds can be detected using an automated image endmember extraction technique, however this work was based on high resolution imagery with substantial regions of weeds present in the crop. A similar methodology may not work as well for low spatial resolution imagery over a study area that has very small patches of weeds in more mature crop stages. Currently, operational agricultural remote sensing applications demands real-time deliverables so that information can be used effectively in site-specific farm applications. Atmospheric correction of imagery can be a time consuming and labour intensive task and if it is not

required for adequate SMA results as demonstrated here, then this would present an operational advantage.

3.5.5 SMA in Comparison to Conventional Vegetation Indices

Similar to remote sensing applications in forestry, conventional remote sensing VIs have been used as a source of site-specific information for agricultural applications. As mentioned earlier, VIs tend to saturate and provide little information later in the growing season when LAI values are high and when the crop reaches full maturity. VIs only use two spectral bands, can only operate on the whole pixel, and must be related empirically to the biophysical parameters of the crop (e.g. LAI, biomass). The disadvantage of the empirical approach is that in-field ground data collection is not always feasible (Maas, 2000). Several studies have demonstrated that SMA can be superior to the commonly used NDVI in estimating agricultural parameters. Wessman et al. (1997) implemented SMA on AVIRIS data over a tallgrass prairie region of Kansas. In this work image endmembers were derived for soil, rock, shade and three types of green vegetation. The sum of two of the vegetation fraction results had a much higher correlation (r=74) than the NDVI (r=51) to field biomass measurements. This study demonstrated that SMA was not only a better discriminator than the NDVI in the detection of grazing treatments, but that SMA better characterized the treatments by quantifying the vertical structure, percentage cover, greenness, and distribution of soil and litter.

Staenz et al. (1997b) presented SMA fraction results from the Imaging Spectrometer Data Analysis Systems (ISDAS), a customized remote sensing software package developed by the Canada Centre for Remote Sensing (CCRS). The SMA

fraction results were qualitatively compared to the conventional NDVI for a bean and canola field in Altona, Manitoba. The purpose of this preliminary research was to examine the potential of hyperspectral image products, and more specifically the ISDAS fraction map output, as a source of data for an agricultural GIS. This work demonstrated that the within field variability of crop fractions, and a corresponding soil fraction for the study area, showed more detailed within field variability than the conventional NDVI.

Peddle et al. (1999b) and Peddle and Smith (2003) compared conventional VIs to SMA for optical data collected in a controlled ground-based study of a potato crop in southern Alberta. Ground-based endmember spectra were collected, as well as spectra from above the crop, using an ASD Fieldspec-FR spectroradiometer. A major component of this work determined what endmember sampling methods (i.e. *in situ*, optically thick stacks (OTS), and flat array) performed best in the collection of reference endmember spectra for three scene components: sunlit soil, sunlit crop and shadow (crop and soil). A comprehensive fraction validation was done by comparing the SMA fractions with manually classified ground-based photographs taken on the same day as the field spectral measurements. The study showed that the best sampling strategy for each reference endmember was the excised leaves flat array strategy for sunlit and shadowed crop, and the *in situ* sampling method for cultivated soil. This study also demonstrated that the shadow fraction outperformed the SR, NGVI, and NDVI for the prediction of potato crop biophysical parameters (e.g. biomass, LAI, plant height, and width).

3.6 Chapter Summary

This chapter included an introduction to SMA that began with an explanation of the concept of the endmember, a key SMA input. The theory of SMA was presented, as well as the linear versus non-linear spectral assumption that is important to understand prior to implementing SMA. The constrained and unconstrained SMA methods were both presented in addition to the various endmember acquisition and sampling methods. The use of SMA in agricultural research and development was reviewed, and it was evident from the literature that SMA in site-specific agriculture could provide farmers with new spatial management tools and benefit the entire farm operation. Similar to other GIS precision farming tools, the SMA technique endorses the principle of improving the characterization of management zones and only applying crop inputs (e.g. fertilizers and chemicals) to those regions of the farm that require them. This is essentially what the concept of sustainable agriculture advocates, improved farm management practices that benefit the surrounding environment and secures a better socio-economic future for the agricultural community.

CHAPTER IV

4.0 METHODS

4.1 Introduction

This chapter describes the experimental design and methods used to compare the ground-based measurements of crop biophysical parameters with estimates derived from remote sensing data. The chapter begins with a description of the Indian Head study area, and the ground-based and remote sensing data collection methods used. The next section describes the remote sensing image processing tasks for radiometric correction and surface reflectance retrieval, co-registration of the sample site locations to the hyperspectral imagery, and computation of the vegetation indices (VIs) and the Spectral Mixture Analysis (SMA) fractions. Finally, the statistical methods are presented for evaluating each image processing technique as a predictor of crop biophysical parameters (i.e. biomass and LAI).

4.2 Study Area and Field Data Set

4.2.1 Indian Head Study Area

The study area was centred at 112°50'W, 49°42'N near Indian Head, Saskatchewan (Figure 4-1). This study area is located within Canada's prairie ecozone which comprises the northern extension of open grasslands in the Great Plains of North America. This ecozone has little topographic relief and has a subhumid to semiarid climate (Environment Canada, 2003). The land selected for this project was dedicated to site-specific farming as part of an ongoing project being conducted by the Indian Head Agricultural Research Foundation (IHARF). The experimental farm is 307 acres (124 ha) and is subdivided into eight sub-sections (i.e. fields) where each section is part of a

four year crop rotation: spring wheat (*Triticum aestivum L.*), canola (*Brassica napus L.*), spring wheat, field peas (*Pisum sativum L.*) (Figure 4-2). The study area ranges in elevation from approximately 573 m to 584 m above sea level, and the landscape is relatively level to very gently undulating with slopes ranging from 0.5 to 2.5 percent (Figure 4-3). A large part of the farm slopes toward a shallow draw running diagonally from the western edge of the farm (south central) toward the northeastern corner (Kozac and Padbury, 1999). The experimental farm is under zero-till practices, therefore the amount of residue or dead matter across the study area is substantial from year to year.

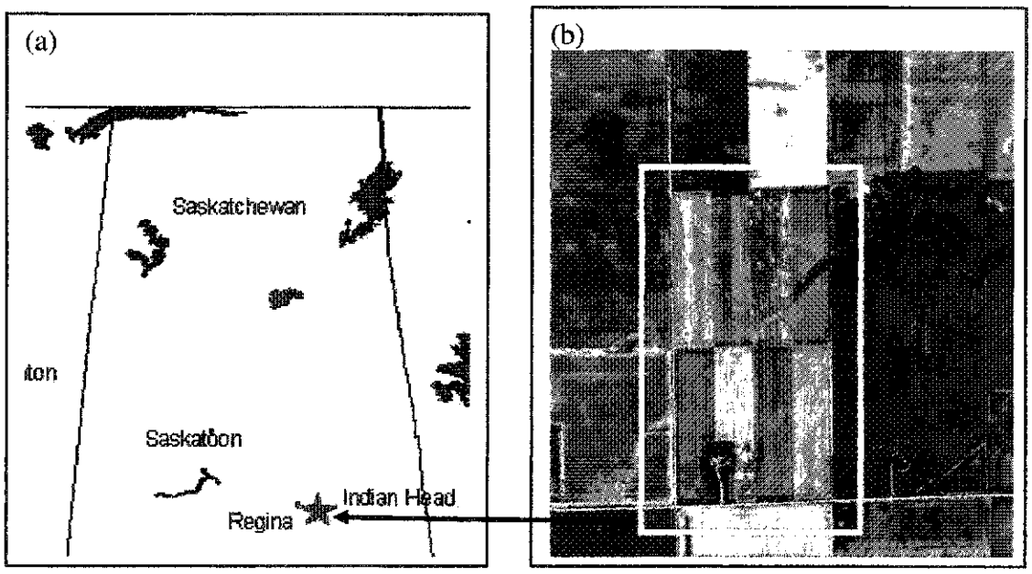

Figure 4-1 Study Area (a) provincial map showing Indian Head study site (star) east of Regina; and (b) false colour multispectral IKONOS satellite image, June 28, 2000. IHARF experimental farm shown in yellow box.

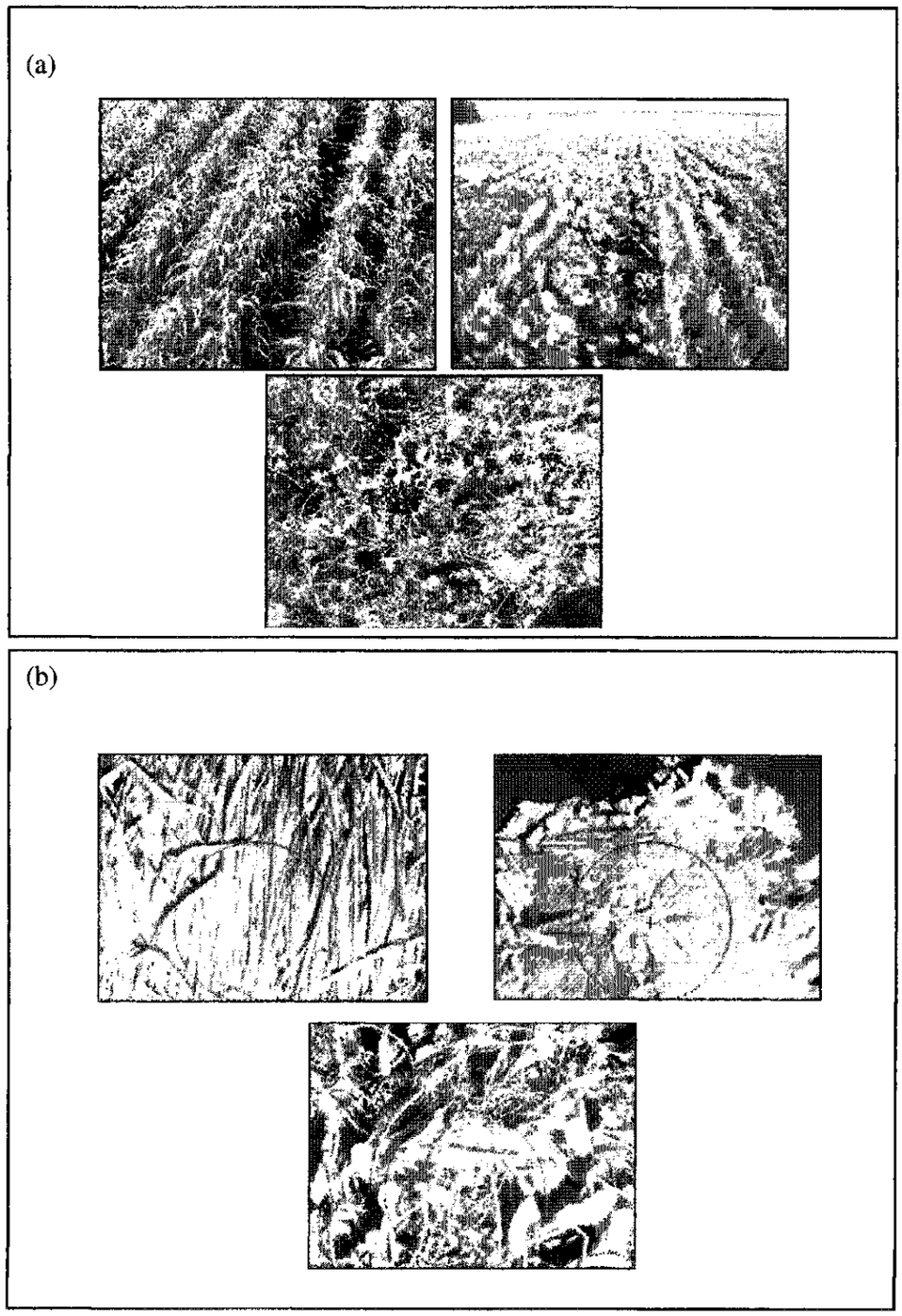

Figure 4-2 Crop types (clockwise from top left: wheat, canola, and field peas) at the IHARF study area (a) oblique photograph of each crop type, and (b) close-up view of each crop type taken from SMA endmember samples.

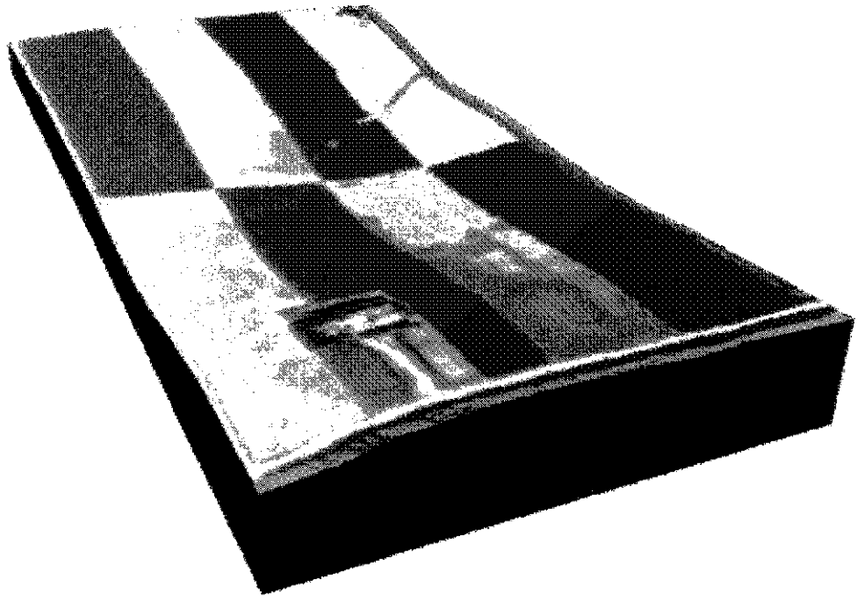

Figure 4-3 3D illustration of IHARF precision farm, created as TIN digital elevation model from 1998 elevation data. False colour 1999 aerial image was draped over the DEM and illustrates the drainage area running south central to northeast (IHARF, 2003).

4.2.1.1 Soil and Climate

A site-specific soil and topographic survey was completed for the experimental farm in 1999. The combined results of this survey are shown in Figure 4-4. The soils on the IHARF farm can be characterized as predominantly black chernozem developed on neutral to slightly alkaline uniform clayey lacustrine deposits (Kozac and Padbury, 1999). In some areas the soils are relatively shallow (< 1m thick) and can be underlain with loamy or clayey water-modified glacial till. Surface texture throughout the study area ranges from clay to heavy clay (Kozac and Padbury, 1999).

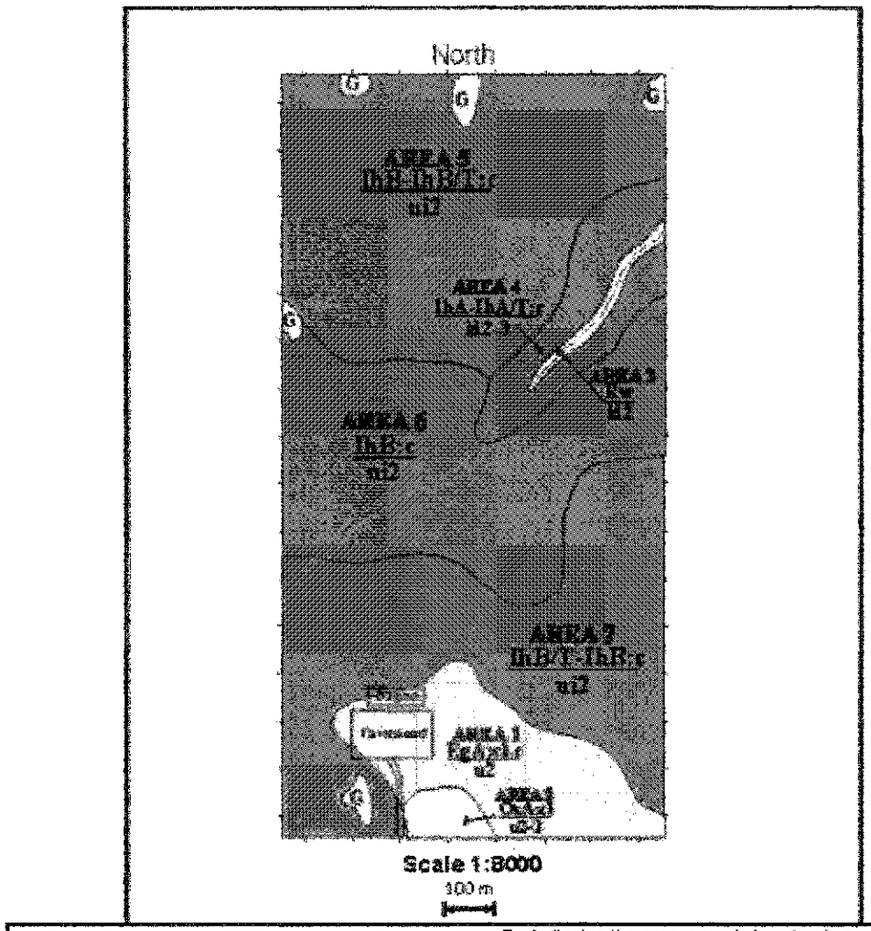

Map Legend:

EgA - Mainly a combination of rego and calcareous Edgeley soils, with some orthic Edgeley soils and thick phase Edgeley soils.
IhA - Mainly rego Indian Head soils.
IhB - Mainly rego Indian Head soils, with some orthic Indian Head soils and some thick phase Indian Head soils.
OxA - Mainly orthic Oxbow soils, with a combination of calcareous and rego Oxbow soils.
Rw - Runway soils are associated with the bottom and sides of shallow drainage channels, consequently they can be quite variable ranging from weakly developed to poorly drained. Surface textures and stone content etc. can also be extremely variable.

G - indicates the presence of gleyed or imperfectly drained soils.
/T - indicates that the soils are shallow and underlain by glacial till
cl - clay loam surface texture
c - clay surface texture
2 - slope class; nearly level, 0.5 - 2%.
3 - slope class; very gently sloping, 2 - 5%.
i - inclined surface expression; landscapes where the general slope is in one direction, only.
u - undulating surface expression, landscapes characterized by a sequence of long, gentle slopes extending from smooth rises to gentle hollows, imparting a wave-like pattern to the land surface.
d - dissected, a modifier indicating that shallow gullies occur along the slope.

Figure 4-4 Site-specific map of IHARF study area showing soil type relative to slope (Kozac and Padbury, 1999).

In the 2000 remote sensing campaign, a weather station was used to record climate data near the study area. Agriculture and Agri-Food Canada (1976) provided the historical temperature and precipitation data for the experimental farm in Indian Head (Tables 4-1 and 4-2). Historically, the average precipitation over the past 80 years (prior to 1976) for the growing growing season (April to May) was 214 mm (Table 4-1). In comparison, the spring of 2000 was exceptionally wet which contributed to delayed planting dates, slow plant emergence, and below average crop maturity at the time of the field campaign in late June and early July. Due to excess moisture, the first field on the experimental farm was not planted until May 3rd and the last field was not planted until May 20th. In an average spring season, planting dates commence in April and finish by early May. The application of herbicides for weed control was also delayed due to excess soil moisture, and consequently a substantial amount of weeds and volunteer crop from the previous year were still present during the remote sensing image acquisition on June 28th.

Table 4-1 Comparison of Historical (AAFC, 1976) and 2000 Precipitation Data

Month	Precipitation (mm) 80 year Average	2000 Precipitation (mm)	Difference
April	25	29	+4
May	48	68	+20
June	86	104	+18
July	55	46	-9
Total	*214*	*247*	

A comparison of the historical and the 2000 temperature data indicated that the spring was also cooler than average (Table 4-2). The 70 year average minimum temperature recorded for May was 2.9°C, and 8.5°C for June. However, in 2000 the minimum temperature recorded for May was -4.3°C, and 2.7 °C for June. Since the crops were planted in May, the crops would have been emerging in June and consequently in a very young, temperature sensitive growth stage. The latter minimum temperature differences indicate there were days early in the growing season with temperatures substantially below average. Temperatures that lie outside of the typical range can have severe consequences on crop development and crop yield, and in the most severe case can cease crop development all together (Porter and Gawith, 1999). Below average temperatures combined with delayed planting and weed control due to excess moisture, may have contributed to below average crop maturity at the time of the remote sensing campaign.

Table 4-2 Comparison of Historical Temperature (AAFC, 1976) and 2000 Temperature Data

	70 Year Historical Average Temperature (°C)			2000 Temperature (°C)			Mean Temp. (°C)
Month	**Mean Minimum**	**Mean Maximum**	**Mean**	**Minimum.**	**Maximum**	**Mean**	**Difference**
April	-3.3	9.1	2.8	-11.2	23.77	3.5	+0.7
May	2.9	17.4	10.2	-4.4	24.52	10.5	+0.3
June	8.5	22.1	15.2	2.7	27.88	13.1	-2.1
July	10.7	25.8	18.4	2.1	32.53	18.2	-0.2

4.2.1.2 Cropping Practices

In 2000, cropping practices were specific to each field and crop type. Table 4-3 shows the basic information for each field on the experimental farm (i.e. identification number, crop type, crop variety, planting date, and harvest date). Fertilization application

and seeding rates were implemented to test both conventional application practices (i.e. a uniform rate) and variable rate application technology. Both the wheat and canola fields had conventional and variable rate fertilizer application, whereas the peas had a uniform rate of fertilizer but the seeding rates were varied. Table 4-4 shows the fertilizer, chemical, and seeding rates, and Figure 4-5 illustrates how each treatment was applied on each field. Treating each crop differently with a number of application practices may have increased the amount of variability found within each field.

Table 4-3 Study area field identification number, crop type and variety, seeding date and rate, plant count date, and harvest date in 2000.

Field ID# and Crop Type	Variety	Planting Date	Harvest Date 2000
Field 1 – Wheat	AC Barry	May 17	Sept 14
Field 2 – Canola	Liberty Link Invigor 2573	May 17	Sept 12
Field 3 – Wheat	AC Barry	May 20	Sept 15
Field 4 – Peas	Swing	May 3	Aug 19
Field 5 - Peas	Swing	May 5	Aug 24
Field 6 - Wheat	AC Barry	May 20	Sept 14
Field 7 – Canola	Liberty Link Invigor 2573	May 9	Sept 12
Field 8 – Wheat	AC Barry	May 20	Sept 15

Table 4-4 2000 fertilizer, chemical, and seeding application strategies.

Field ID# and Crop Type	Seeding Rate (lbs per acre)	Fertilizer Application	Chemical Application
Field 1 - Wheat	120	**Phosphorus** (12-51-0): side banded 59 lb/ac **Nitrogen** (28-0-0 Liquid): Uniform Rates: ▪ High: 118 lb/ac ▪ Medium: 103.8 lb/ac ▪ Low: 47.1 lb/ac Variable Rates: 53.5 lb/ac to 132.1 lb/ac	**Puma Super:** 0.31 L/ac **Curtail M:** 0.8 L/ac **Water:** 4.5 gal/ac
Field 2 - Canola	5	**Phosphorus** (12-51-0): side banded 59 lb/ac **Sulfur** (20.5-0-0-24): side banded 62.5 lb/ac	**Liberty:** 1.35 L /ac **Select:** 0.026 L /ac **Amigo:** 0.5 L / 100 L of Solution

		Nitrogen (28-0-0): Uniform rate: 26.9 lb/ac Variable rate: • Zone 1: 33.4 gal/ac • Zone 2: 31.7 gal/ac • Zone 3: 26.9 gal/ac • Zone 4: 20.0 gal/ac	**Water:** 5.0 gal/ac
Field 3 - Wheat	120	**Phosphorus** (12-51-0): side banded 59 lb/ac **Nitrogen** (28-0-0 Liquid): Uniform Rate: • High: 73.9 lb/ac • Medium: 62.1 lb/ac • Low: 32.1 lb/ac Variable Rate: • 0 to 121.4 lb/ac	**Puma Super:** 0.31 L/ac **Curtail M:** 0.8 L/ac **Water:** 4.5 gal/ac
Field 4 - Peas	161 & 218 (10 acres per rate and 2 replicates of each rate see Figure 4-5)	**Phosphorus** (12-51-0): side banded 59 lb/ac	**Odyssey:** 0.017 kg/ac **Merge:** 0.5 L / 100 L solution **Water:** 6.5 gal /ac **Lefatech soil inoculant:** 3.8 lb/ac
Field 5 - Peas	161 & 218 (10 acres per rate and 2 replicates of each rate see Figure 4-5)	**Phosphorus** (12-51-0): side banded 59 lb/ac	**Odyssey:** 0.017 kg/ac **Merge:** 0.5 L / 100 L solution **Water:** 6.5 gal /ac **Lefatech soil inoculant:** 3.8 lb/ac
Field 6 - Wheat	120	**Phosphorus** (12-51-0): side banded 59 lb/ac **Nitrogen** (28-0-0 Liquid): Uniform Rates: • High: 92.8 lb/ac • Medium: 81 lb/ac • Low: 51 lb/ac Variable Rates: • 0 to 107.1 gal/ac	**Puma Super:** 0.31 L/ac **Curtail M:** 0.8 L/ac **Water:** 4.5 gal/ac
Field 7 - Canola	5	**Phosphorus** (12-51-0): side banded 59 lb/ac **Nitrogen (28-0-0):** Uniform rate: 26.6 gal / ac Variable Rates: • Zone 1: 116 lb/ac • Zone 2: 97 lb/ac • Zone 3: 76 lb/ac	**Liberty:** 1.35 L /ac **Select:** 0.026 L /ac **Amigo:** 0.5 L / 100 L of Solution **Water:** 5.0 gal/ac
Field 8 - Wheat	120	**Phosphorus** (12-51-0): side banded 59 lb/ac **Nitrogen** (28-0-0 Liquid): Uniform Rates: • High: 94 lb/ac • Medium: 82.8 lb/ac • Low: 52.8 lb/ac Variable Rates: 42.8 to 96.4 lb/ac	**Puma Super:** 0.31 L/ac **Curtail M:** 0.8 L/ac **Water:** 4.5 gal/ac

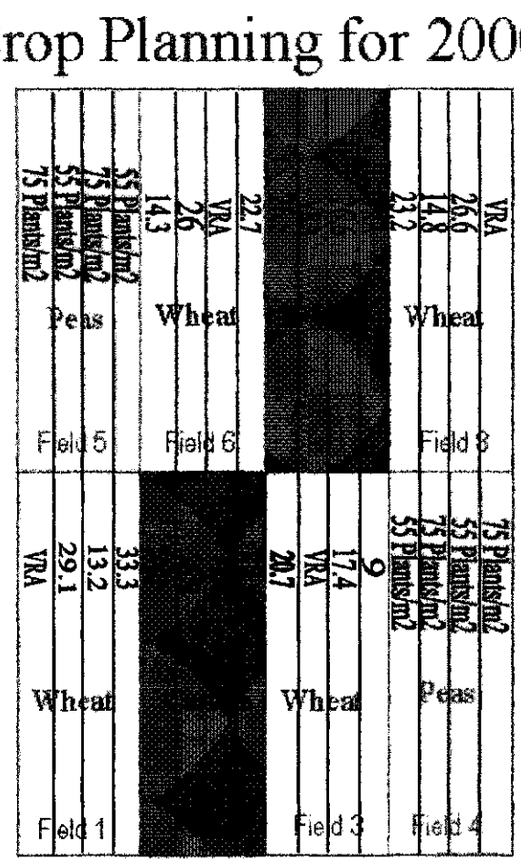

Figure 4-5 Nitrogen fertilizer application strategy for wheat and canola, seeding rates shown for peas. Units in imperial gallons per acres unless otherwise specified (from IHARF, 2003).

4.2.2 Field Data Collection

4.2.2.1 Selection of Sample Sites

In the 2000 remote sensing campaign, airborne hyperspectral and satellite multispectral imagery were acquired by the project partners in conjunction with extensive ground sampling during a two week period from June 26th to July 7th. The sampling design for each of the eight fields was based on agronomic knowledge provided by local

field managers and research scientists, soil maps, aerial photography, and GPS derived fertility and yield maps that defined the extent of within-field variability (Figure 4-6). The objective of the sampling scheme was to establish management zones (represented by one sample site location) that were homogenous over time. It was assumed by CCRS that each sampling site represents a homogenous zone with respect to crop performance, and as a result these representative zones would be used as individual units for applying site-specific management practices.

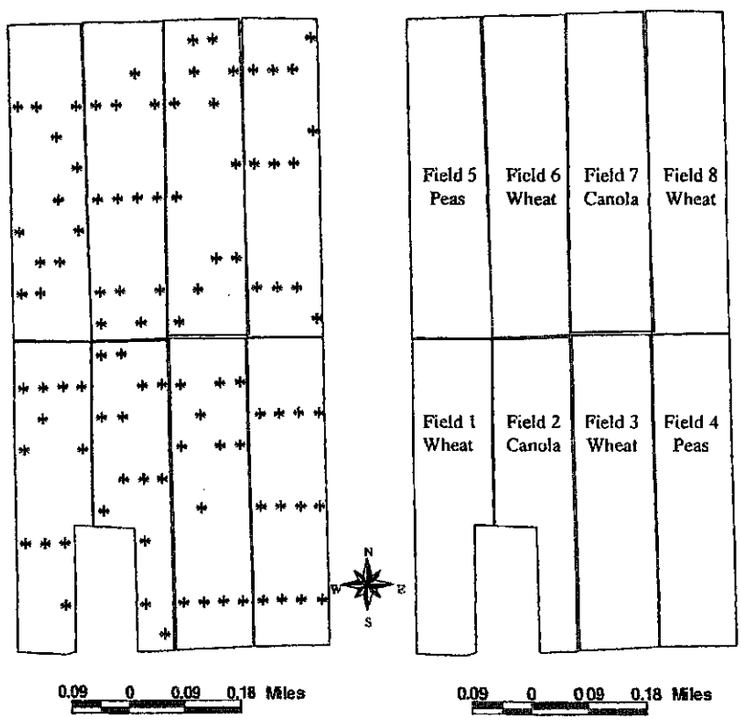

Figure 4-6 Location of 98 sample sites selected to capture the extent of within-field variability. The sample sites were mapped using GPS with an accuracy of +/-1 metre.

4.2.2.2 Crop Biophysical Measurements

Ground-based crop data were collected to characterize growth within two weeks of the image acquisition date by CCRS staff. At each sample site, plants were counted within four 0.33 m^2 areas (i.e. one north, one south, one east and one west of the sample site location) on May 30th or June 5th. The average number of emerged plants was calculated for each sample site. Plant emergence is sometimes very dependent on the weather conditions early in the spring, which can help explain within-field variability. In addition to plant counts, plant height measurements were taken between June 28th to July 2nd as indicator of crop status. Three separate measurements were made at each of the 98 sample site locations and averaged. The three measurements at each site were taken within 2m of the GPS pin location to ensure that spatial consideration was given to the corresponding resolution of the hyperspectral imagery (pixel size was 5m). The plant counts and crop height data were used only as a reference for plant emergence and crop status, these measurements were not used directly in the statistical analysis (Chapter 5)

Plant samples for biomass estimation were collected on the day of image acquisition. At each sample site, plants were harvested from three separate 0.25 m^2 areas located within 1-2 m of the sample site location. Samples were weighed within 1-2 hours of harvest to determine fresh weight, then placed in a drying oven at 105°C for 48-72 hours and reweighed to derive dry weight. To prevent water loss, samples were placed in brown paper bags and kept cool until fresh weights were determined and until transportation to the drying oven was completed. The difference between the fresh weights and dry weights was used to derive Plant Water Content (PWC) at the time of image acquisition. For this research, because it was the fresh plant matter (living crop)

that was remotely sensed by the airborne sensor, the fresh biomass weights were used in the analysis.

A Licor LAI-2000 plant canopy analyzer was used by the projects' field staff to measure ground-based LAI, and to provide further biophysical characteristics of each crop type. The LAI-2000 is an optical instrument that measures canopy gap fraction based on radiation transmission through the canopy (Chen et al., 1997). LAI is used to describe the percentage of vegetation cover and to estimate productivity of agriculture and forestry (Pacheco et al., 2001a). LAI is defined as one half the total green leaf area per unit ground surface (Chen and Black, 1992). This definition takes into account that foliage of plant canopies can be oriented in various directions, and the projected area in one direction does not contain all of the information for estimating radiation interception (Chen et al., 1997).

The LAI-2000 instrument only measures effective LAI (*e*LAI) (LI-COR, 1992) because it does not take into account the clumping characteristics within the crop canopy (Pacheco et al., 2001a). The foliage of plant canopies are generally clumped, but the LAI-2000 can calculate LAI without information about the foliage angle distribution because it measures at five zenith angles (Chen et al., 1997). In an earlier agriculture project it was shown that *e*LAI values acquired with the LAI-2000 had very strong correlation (r=0.90) to percent crop cover measurements (Pacheco et al., 2001b). In this research, the LAI-2000 was fixed with a lens cap that restricts the instrument FOV to sensing 90° of the hemisphere and output is a measurement of how much light is attenuated into the five zenith angles simultaneously (Figure 4-7). When the instrument is below the crop it views upward through the canopy and sense approximately 3.5m

away from the user and not below a zenith angle of 74 degrees (Peter White, personal communication, August 14, 2002). In agricultural applications, the size of crop leaves at a particular growth stage should be considered and zenith angles that are too small in comparison to leaf size should be omitted before outputting the final LAI-2000 values (Peter White, electronic mail, August 14, 2002). In this research, the sensing was done early enough in the growing season that leaf size was not a factor.

Ground based LAI measurements were acquired in overcast conditions using the LAI-2000 instrument oriented perpendicular to the sun. Samples were collected along 20m transects (Figure 4-8) on a diagonal between two plant rows to accommodate for row spacing (Pacheco et al., 2001a,b). Within each transect, a reference measurement was taken above the canopy, and then four measurements were acquired below the canopy which resulted in the final *e*LAI value for the whole transect. Three transects were measured at each sample site location and averaged to return the final *e*LAI value.

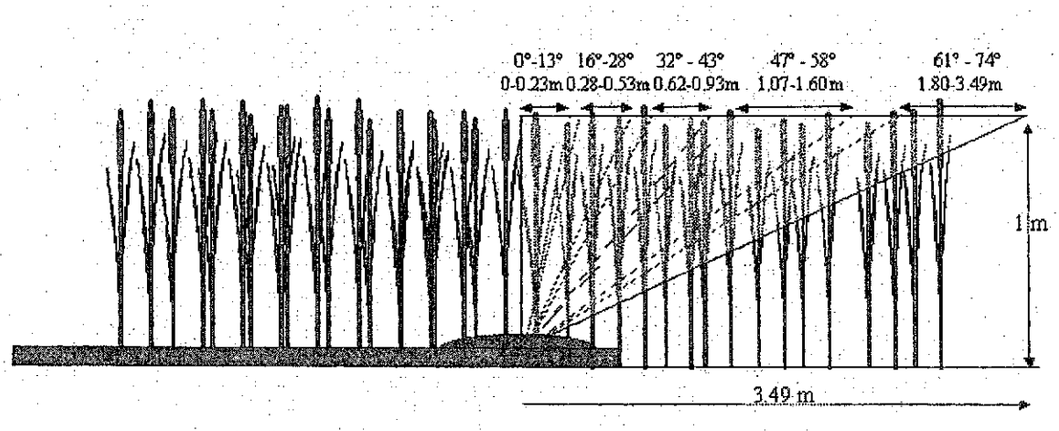

Figure 4-7 The above diagram is a profile of the LAI-2000 instrument pointed away from the field technician.

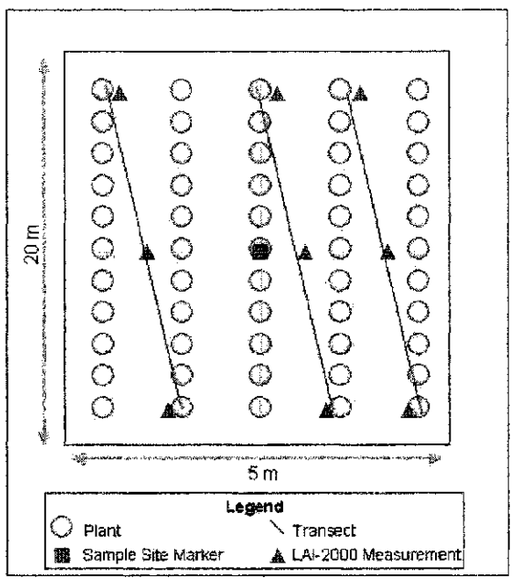

Figure 4-8 Ground based LAI-2000 sampling method.

4.3 Remote Sensing Imagery

4.3.1 Airborne Imagery

Airborne hyperspectral imagery was acquired using the Probe-1 sensor (Figure 4-10) which is a "whiskbroom style" instrument that collects data in a cross-track direction by movement of an airborne platform (Earth Search Sciences Inc., 2002). The Probe-1 is mounted on a three-axis gyrostabilizer to minimize geometric distortion from aircraft movement. The flying altitude for this research was 2500 m, producing a swath width of 3 km and spatial resolution of 5 metres. The sensor collects upwelling radiance in 128 spectral bands in the visible, NIR and SWIR between 440 to 2500 nm. The bandwidths are between 11 and 18 nm at full width half maximum (FWHM). Two flightlines were collected over the study area on June 28th. The first flightline was acquired between

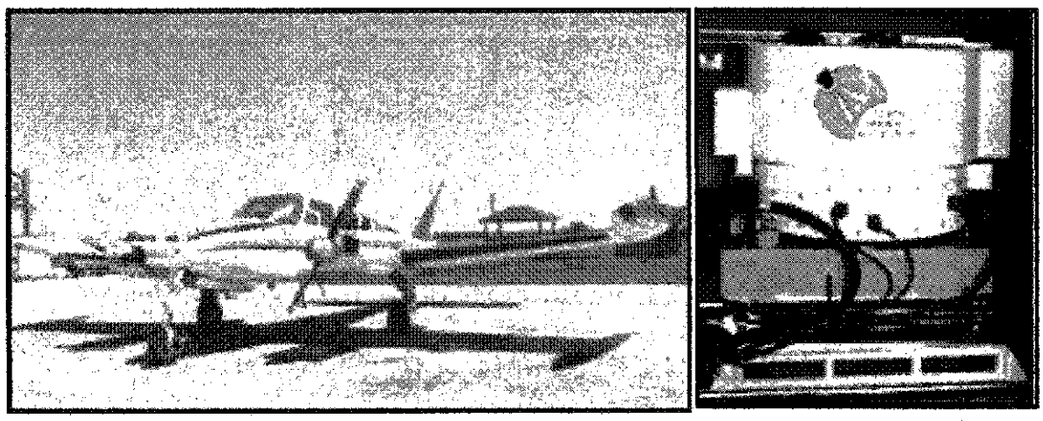

Figure 4-9 The aircraft and Probe-1 sensor that were used in the 2000 campaign. Services provided by Earth Search Systems Inc.

10:40 a.m. and 10:42 a.m., and the second between 11:09 and 11:11a.m local time. Portions of both flightlines were used in the image analysis (SMA and VIs), and the portion being used was heavily dependent upon the co-registration of the imagery and the sample site locations which is explained in more detail in section 4.3.3.4. Upon examination, CCRS deemed the last 11 bands too noisy and the dataset was reduced to 117 bands (Appendix A).

4.3.2 Satellite Imagery

Multispectral satellite imagery was also acquired on the same day as the airborne acquisition. The Space Imaging IKONOS II satellite acquired a 11.2 km x 7.7 km image at 11:37 a.m local time on June 28, 2000. This multispectral sensor has four spectral bands in the visible and NIR between 444.7 to 852.7 nm. This sensor collects information in one panchromatic and four multispectral (Table 4-5). The altitude of the satellite sensor is 681 km and the sensor has a nominal swath width of 11 km at nadir. All default IKONOS products are radiometrically corrected to in-band radiance (mW/cm^2*sr) and are available in 11 bit or 8 bit format. In this research, 11 bit imagery

was used in the image rectification and co-registration of the sample site locations to the hyperspectral imagery.

Table 4-5 IKONOS Spectral band Characteristics (Space Imaging, 2003)

Band	Lower 50% (nm)	Upper 50% (nm)	Bandwidth (nm)	Center (nm)	Spatial Resolution (m)
Pan	525.8	928.5	403.0	727.1	1
MS-1 (Blue)	444.7	516.0	71.3	480.3	4
MS-2 (Green)	506.4	595.0	88.6	550.7	4
MS-3 (Red)	631.9	697.7	65.8	664.8	4
MS-4 (VNIR)	757.3	852.7	95.4	805.0	4

4.3.3 Image Pre-Processing

4.3.3.1 Ground-based Spectral Measurements

Two types of ground-based spectral measurements were acquired in this research. Calibration spectral measurements were collected for use in deriving surface reflectance from the airborne hyperspectral imagery. An asphalt parking lot that could be readily identified on the airborne imagery was used as the radiometric calibration target. Spectral measurements were collected of individual scene components to serve as reference endmembers in the SMA. Ground-based reference endmembers were collected in this research to acquire the most spectrally pure measurement of each scene component that was expected to be present in the imagery.

Spectroradiometers were used to obtain ground based spectral measurements. A spectroradiometer measures reflected energy and the magnitude of the measurement is highly dependent on incoming solar radiation (spectral irradiance) reaching the target which varies due to the time of day (due to changing solar zenith angle and atmospheric

path length), atmospheric conditions, weather, topography of the surface, and intervening features which alter incoming radiation (e.g. canopy structure) (Peddle, 1998). Spectral reflectance is the ratio of incident-to-reflected radiant flux measured from an object or area over specified wavelengths and is an inherent property of an object, regardless of time, location, illumination intensity, atmospheric condition and weather. For the latter reasons, spectral reflectance is a key unit in remote sensing especially over time, but it is not measured directly and must be derived (Peddle et al., 2001a). To calculate spectral reflectance from the energy measurements collected with a field spectroradiometer it is imperative to acquire a measurement of irradiance coincident to the target radiance measurement (Johnson, 2000). In most cases a white reference panel is used which has known spectral and angular reflective properties. For this research, a white Spectralon™ panel was used that is composed of pressed polytetrafluoroethylene (PTFE) and has near lambertian properties over a wide spectral range (Labsphere, 2002).

Two models of spectroradiometers were used in this research: (i) an Analytical Spectral Device (ASD) FieldSpec® Pro (Analytical Spectral Devices Ltd., 2003) and (ii) a GER3700™ (Geophysical and Environmental Research Corporation, 2003). Each spectroradiometer was used for very specific tasks that were essential to the project, and the use of both instruments distributed the time-critical workload amongst field staff on the days on or near the airborne image acquisition date. In this research, the ASD FieldSpec® Pro was used to collect endmembers for each scene component, and the GER3700™ was used to collect spectral measurements of the calibration targets used in radiometric correction of the hyperspectral imagery.

The ASD FieldSpec® Pro instrument was made available in this research by Agriculture and Agri-Food Canada (AAFC) Lethbridge, and measurements were acquired by AAFC staff in Indian Head. The ASD FieldSpec® Pro is designed with a fibre-optic cable that extends a custom foreoptic to which is attached a digital video camera. The digital camera is configured to view the same FOV on the ground as the spectroradiometer and enables simultaneous capture of video frames for each ground-based spectral measurement (Figure 4-10a and b). The ASD FieldSpec® Pro spectroradiometer used in this research measures reflected energy over a wide spectral range (350-2500 nm), and band widths vary from 3 nm (between 350-700 nm) to 10 nm (between 1400-2100 nm) at FWHM which are then sampled and interpolated to output data in 1nm intervals (ASD, 2001). In the scene endmember collection, the foreoptic was attached to a tripod so that view angle and sensor height above the target could be controlled precisely. A 12° foreoptic was used for all measurements, and to ensure an acceptable signal to noise ratio each sample was the average of three spectral scans. To remove noise internal to the spectroradiometer, a dark current was measured prior to each scan set and substracted from each target measurement.

CCRS provided a GER3700™ spectroradiometer (Geophysical and Environmental Research Corporation, 2003) for the project. This instrument has 642 channels spanning the wavelength interval between 301.56 to 2523.06 nm, and bands vary from 1.5 nm to 9.5 nm in width (Figure 4-11). An asphalt parking lot was chosen as the radiometric calibration target with spectral measurements taken on the day of airborne image acquisition. The GER3700™ was configured with a 10° FOV lens giving a 0.26 m diameter ground field of view (GFOV) from a height of 1.5 m above the target. To

ensure an acceptable signal to noise ratio, each sample was the average of seven spectral scans. To remove signal to noise internal to the spectroradiometer, a wavelength dependent dark current signal was obtained and subtracted from each channel before the GER3700™ output the target measurement.

(a)

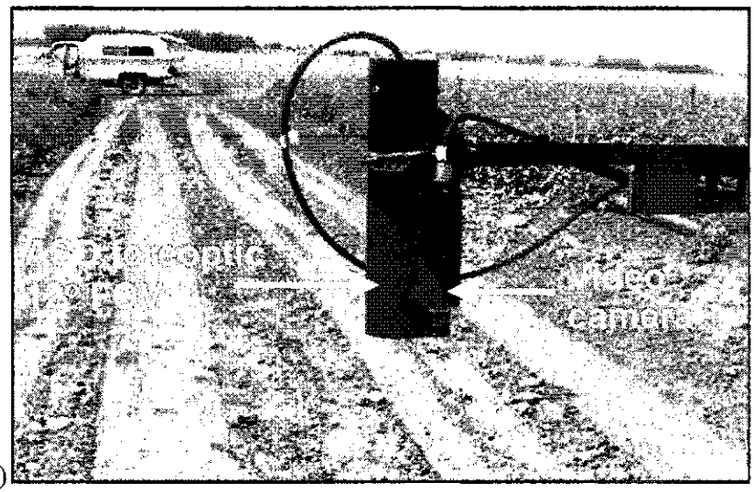

(b)

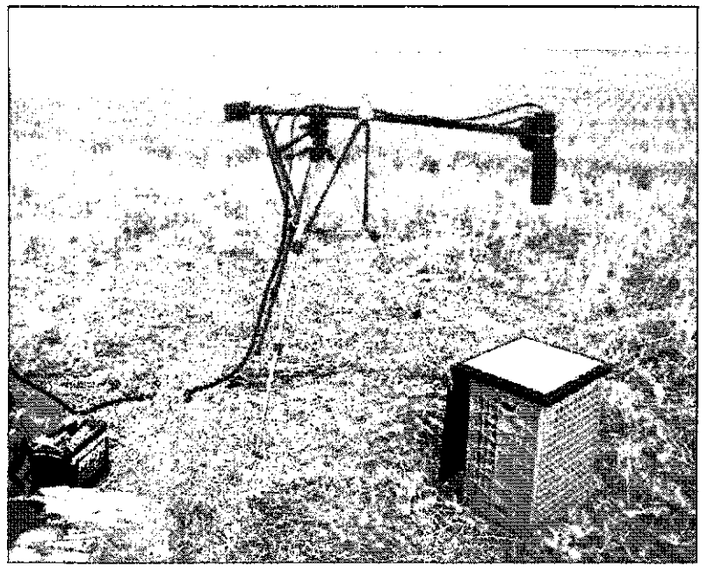

Figure 4-10 (a) ASD FieldSpec® Pro spectroradiometer FOV and video camera mount (b) ASD FieldSpec® Pro stationary field set-up, target shown is the Spectralon™ panel.

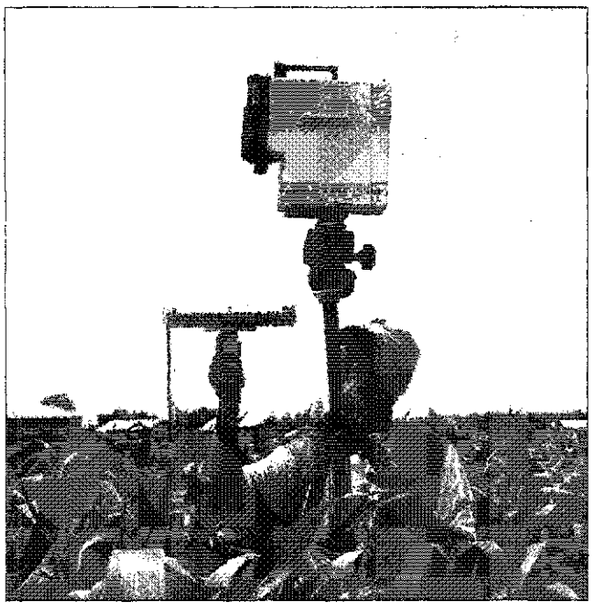

Figure 4-11 GER3700™ Spectroradiometer used by CCRS to measure the radiometric calibration target for radiometric correction.

4.3.3.2 Radiometric Correction

Radiometric correction of the airborne hyperspectral imagery was performed by CCRS based on 39 spectral measurements of a uniform dark target (i.e. asphalt parking lot without painted lines) using the GER3700™ field spectroradiometer and a white reference panel on the day of image acquisition. The reflectance was derived as the ratio of the raw GER3700™ radiance measurements of the target, and the radiance of the calibrated Spectralon™ panel reference. The resulting reflectance values were pre-processed to correct for angular (bi-directional reflectance factor – BRF) and spectral variations in the reflectance of the near lambertian surface of the Spectralon™ panel (Secker et al., 2001). The correction factors for the Spectralon™ panel were measured at the University of Arizona's Optical Sciences Center in March 1999, and values at the appropriate solar zenith angle (SZA) and wavelength were obtained via interpolation. Spectral reflectance retrieval was completed using the CCRS software package ISDAS

(Imaging Spectrometer Data Analysis System), and all reflectance spectra were averaged to yield a single mean corrected reflectance spectrum for the calibration site. The result was then convolved to the band centres of the Probe-1 hyperspectral sensor.

The airborne hyperspectral imagery was radiometrically calibrated using reflectance-based vicarious calibration (RBVC) and the calibration target reflectance (Secker et al., 1999, 2001). RBVC provides a method for the absolute calibration of remote sensors via reference to accurate spectral measurements made separately from the airborne sensor (Secker et al., 20001). RBVC was used in this research to replace laboratory coefficients for the Probe-1 sensor with a new set of radiometric coefficients. The calibrated mean of 39 spectral measurements from the asphalt uniform target were applied with this method to generate new coefficients, and consequently allowed for the conversion from raw digital numbers (DN) to at-sensor radiance (Appendix A). Atmospheric correction was performed on the calibrated Probe-1 radiance data (Figure 4-12). The MODTRAN3 radiative transfer code was implemented within ISDAS using a look-up table (LUT) approach to correct the Probe-1 radiance data to surface reflectance (Staenz and Williams, 1997; Staenz et al., 1998b).

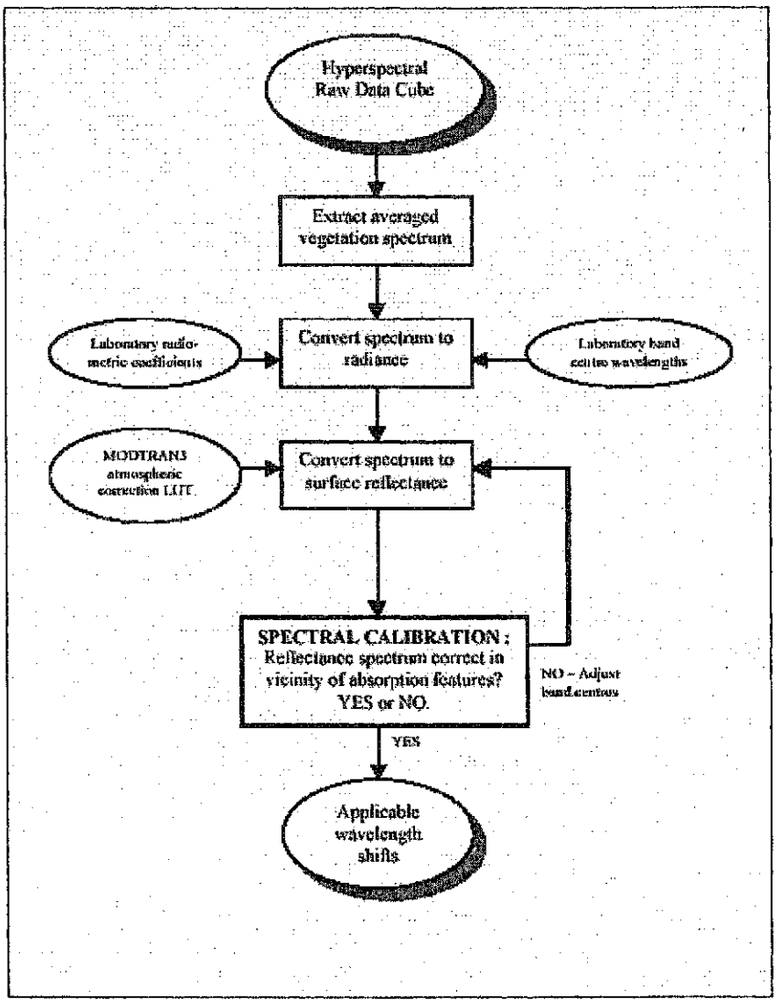

Figure 4-12 Flow diagram illustrating the pre-processing steps applied to the airborne hyperspectral data (Secker et al., 2001).

Early in the radiometric correction of the Probe-1 imagery, CCRS detected a harmonic signal in the GER3700^{TM} spectral measurements from 1465 to 1777 nm. This was initially detected in the multiple asphalt spectra of the uniform target used in the vicarious calibration procedure. The harmonic signal could not be corrected by the calibrated gain values provided by the manufacturer because only radiance data (not the digital raw data) were recorded by the GER3700^{TM}. Alternatively, the signal was

corrected by using a filtering function on the reflectance data with a second order polynomial on a moving window of 100 nm in the 1465 to 1777 nm range. Due to the uncertainty of this correction, this thesis research only considered bands up to 1350 nm for analysis and this effectively reduced the number of bands in the data set to 63.

4.3.3.3 Image Rectification

It is important to establish positional control in remote sensing imagery to correctly locate ground sites and to enable co-registration with other spatial data. In addition to the sample site locations within the study area located using GPS (Figure 4-6), ground control points (GCP's) were also collected outside of the experimental farm (Figure 4-13) to facilitate sufficient spatial coverage for geometric correction of the hyperspectral imagery with the IKONOS satellite imagery. Twelve GCP's were chosen based on static features in the image that would not change significantly over time (e.g. road intersections).

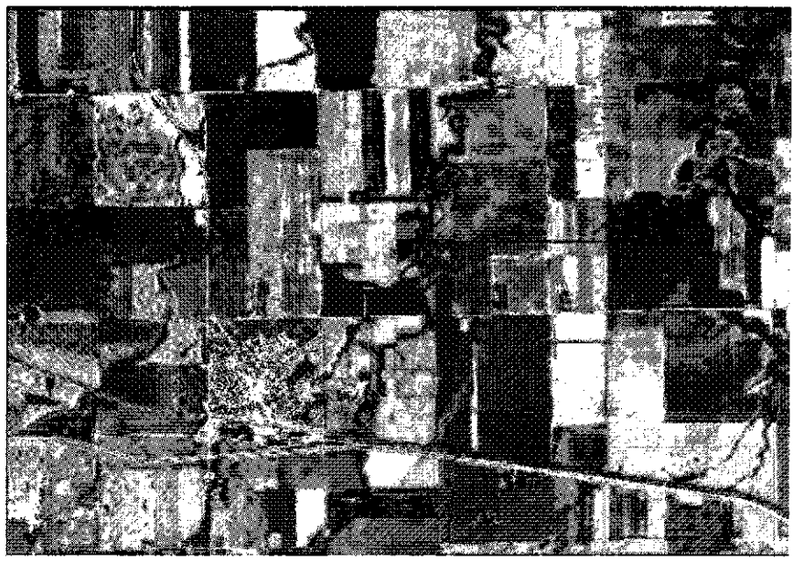

Figure 4-13 False colour multispectral IKONOS imagery showing the location of the 12 GCPs (yellow asterisk).

4.3.3.4 Co-Registration of Imagery and Sample Site Locations

Substantial geometric distortion was present in the Probe-1 imagery due to the mechanical failure of the hydraulic mount used to stabilize the sensor on board the aircraft (Figures 4-14 and 4-15). To preserve the spectral integrity of the hyperspectral imagery, the Probe-1 imagery was not geometrically corrected using conventional methods. Instead, to locate the Probe-1 pixels that corresponded to the field sample site locations, a reverse image-to-image registration was performed by CCRS. The 4m multispectral IKONOS image was ortho-corrected using 12 GCP's collected using GPS around the fields of interest (Figure 4-13), a national topographic database (NTDB) sheet (1:50 000), and the GPS derived sample site locations within each field (Figure 4-6). Each field in the study area was registered using a total of 10-12 GCP's. The sample sites were located on the IKONOS imagery and then the IKONOS image with sample site locations were transformed to the Probe-1 imagery using a second order polynomial. Sample site locations (x and y coordinates) were extracted from both Probe-1 flightlines by evaluating the accuracy of the transformation for each sample site location, and choosing the flightline with the least distortion.

Spectral data from the Probe-1 imagery for each ground based sample site location was extracted using ENVI image analysis software. An average of a 3x3 pixel window surrounding each sample site location was extracted as input for the VIs and the SMA. Due to the presence of co-registration error, a 3x3 pixel window helped to ensure that the absolute location of each ground based sample site would be included within the pixel window. Upon closer examination of the sample site locations, Field #1 wheat (Figure 4-6) was excluded from this research due to geometric distortion and lack of

confidence in the co-registration process. Sample site locations were omitted from the analysis if they were too close to the next field (border locations) and where a complete 3x3 window could not be extracted with confidence within the field boundary.

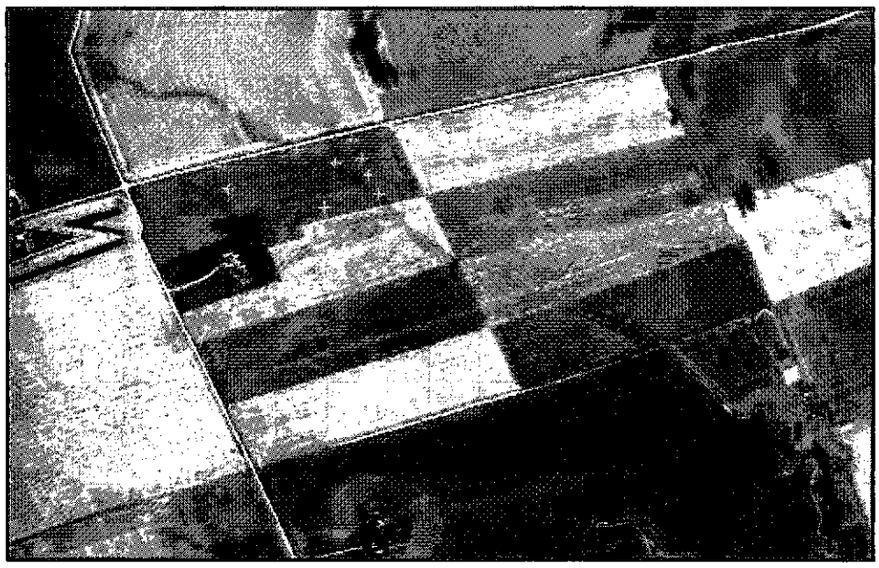

Figure 4-14 Natural colour composite of Probe-1 flightline one showing the co-registered sample site locations (yellow crosses).

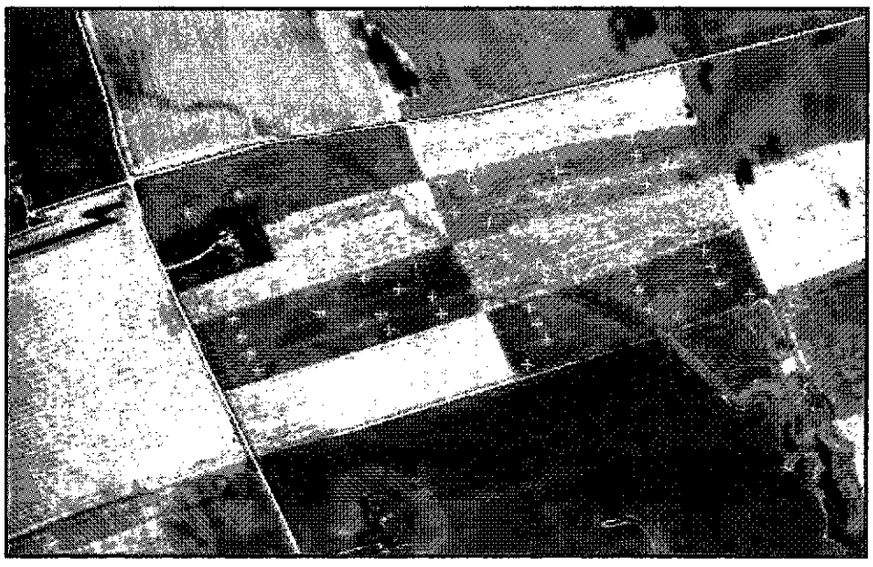

Figure 4-15 Natural colour composite of Probe-1 flightline 2 showing the co-registered sample site locations (yellow crosses).

4.3.3.5 Band Selection

From the 63 band Probe-1 dataset a reduced number of image bands was sought that would sufficiently characterize the spectral response of the crops being observed. It was determined that it is unlikely 60 or more bands would be required spectrally for optimal characterization of crop biophysical parameters using hyperspectral imagery (Thenkabail et al., 2000). It should also be noted that in practical terms, future hyperspectral satellites may not have a payload that allows for 60 or more bands while maintaining high enough spatial resolution for site-specific applications at a local scale (Chabrillat et al., 2002; Rahman et al, 2003). In this research the number of bands was reduced while maintaining good spectral coverage of discrete crop response features, and as a result allowed for a more manageable interpretation of the SMA results. Thenkabail et al. (2000) presented hyperspectral band centers and band widths specifically for agricultural crops from ground based spectral measurements collected in the field using an ASD FieldSpec® on five irrigated crops at distinct growth stages. The five crop types were potatoes, cotton, soybeans, corn, and sunflowers and only spectral data between 350-1050nm were analyzed (Table 4-6). Research by Thenkabail et al. (2000) demonstrated that the use of 12 narrow bands could be used more effectively than broad bands in quantifying the biophysical characteristics of crops.

Table 4-6 Recommended bands for characterizing crop biophysical variables by Thenkabail et al., 2000.

Band	*Region of EM Spectrum*	*Band Center λ (nm)*	*Band Width λ (nm)*	*λ Minimum (nm)*	*λ Maximum (nm)*	*Band Description*
1	Blue	495	30	480	510	Longer wavelength portion of the blue band. Crop-to-soil reflectance ratio minima for the blue and green bands.
2	Green	525	20	515	535	Positive change in reflectance per unit change in wavelength of visible spectrum is maximum around this "green" band (1st order derivative plot of crop spectra will show this)
3	Green	550	20	540	560	Green band peak in the visible (maxima reflectance). Best of 3 green bands.
4	Green	568	10	563	573	Negative change in reflectance per unit change in wavelength of visible spectrum is maximum around this "green" wavelength (1st order derivative plot of crop spectra will show this)
5	Red	668	4	666	670	Chlorophyll absorption pre-maxima (or reflectance minima 1) narrow bands more sensitive to crop variables.
6	Red	682	4	680	684	Greatest crop-soil contrast. Chlorophyll absorption maxima anywhere in 350-1050nm range (reflectance minima).
7	Red	696	4	694	698	Chlorophyll absorption post-maxima (reflectance minima 2). Sudden change in reflectance from near-maximum absorption in red to dramatic increase along red-edge.
8	Red-edge	720	10	715	725	Point on red edge around which there is a maximum change in slope of the reflectance spectra per unit change in wavelength
9	NIR	845	70	810	880	Center of "NIR shoulder". A broad band or a narrow band will provide the same results due to near-uniform reflectance throughout NIR shoulder.
10	NIR peak	920	20	910	930	Peak or maxima reflectance region of the NIR spectrum.
11	NIR moisture sensitive	982	30	967	997	Centre of moisture sensitive trough portion of NIR. The 'trough' is 940-1040nm and had minimum reflectance around 982nm (or point of maximum"dip" in the trough portion).
12	NIR late	1025	10	1020	1030	Portion of sudden rise in reflectance soon after the moisture sensitive band or reflectance minimum

In this research, the 12 Probe-1 bands closest to those recommended by Thenkabail et al. (2000) were chosen for investigation (Table 4-7). Examination of the 12 band reflectance spectra indicates that the selection of these bands accurately characterize the spectral response over the observed wavelength range (350-1050nm) of the crops studied in this research (Figure 4-16). The Probe-1 bands shown in Figure 4-16 demonstrate the peak and valley configuration of spectral response described by Thenkabail et al. (2000) and it was determined that the these bands would be appropriate for defining the biophysical parameters of the crops studied in this research. The objective of this research falls within the confines of testing new image processing methods using several input bands versus traditional methods that only utilise two bands.

Table 4-7 Characteristics of Spectral Bands Recommended by Thenkabail et al. (2000) and equivalent Probe-1 bands

Band Number	Thenkabail et al. (2000)				Equivalent Probe-1 Bands			
	Band Center (nm)	Band Width (nm)	λ Min. (nm)	λ Max. (nm)	Band Center (nm)	Band Width (nm)	λ Min. (nm)	λ Max. (nm)
1	495	30	480	510	491.0	16.0	483.00	499
2	525	20	515	535	521.6	16.3	513.45	529.75
3	550	20	540	560	552.8	15.7	544.95	560.65
4	568	10	563	573	567.5	15.5	559.75	575.25
5	668	4	666	670	660.1	16.5	651.85	668.35
6	682	4	680	684	675.7	16.4	667.50	683.90
7	696	4	694	698	690.9	15.9	682.95	698.85
8	720	10	715	725	721.6	15.3	713.95	729.25
9	845	70	810	880	843.1	17.0	834.60	851.60
10	920	20	910	930	929.0	13.8	922.10	935.90
11	982	30	967	997	972.9	19.1	963.35	982.45
12	1025	10	1020	1030	1021.4	15.4	1013.7	1029.10

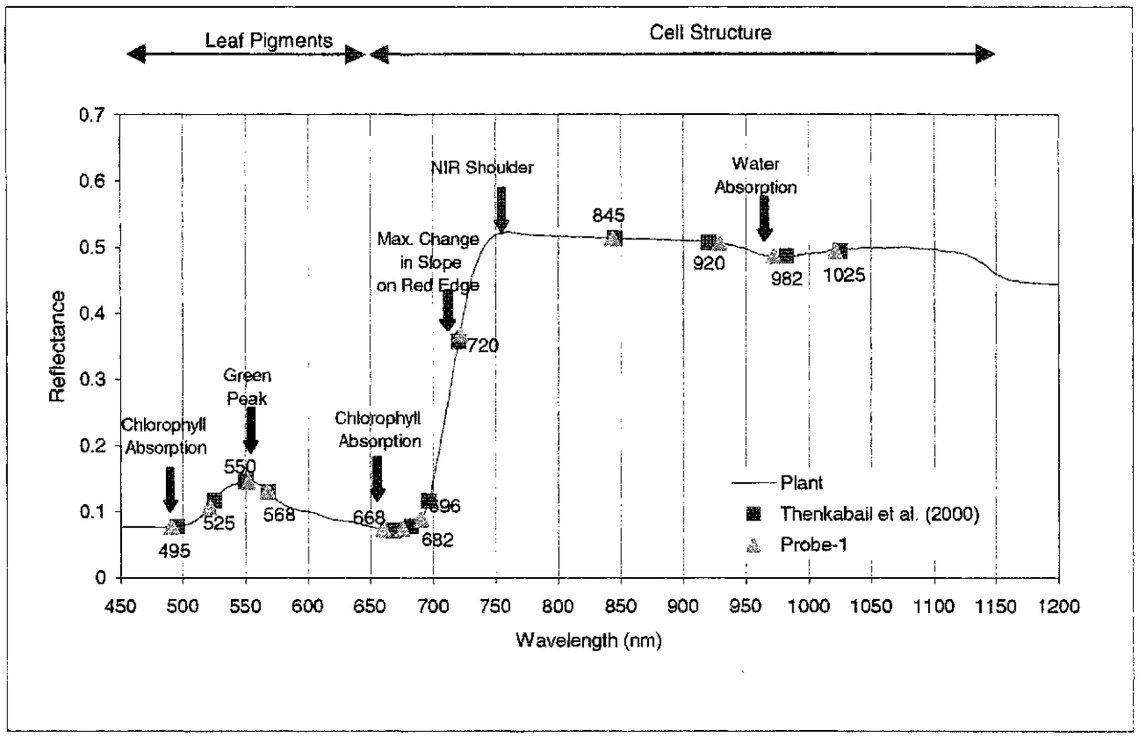

Figure 4-16 12 Thenkabail et al. (2000) narrow bands (labelled in nm) versus the selected Probe-1 Bands that best matched the recommended band centers (band widths Table 4-7) superimposed on an average sunlit canola spectral measurement. The portion of the spectrum where leaf pigment and cell structure drives spectral response are shown at top.

4.4 Experimental Design

4.4.1 Vegetation Indices

The SR, NDVI, GDVI, TSAVI, and OSAVI were computed from the hyperspectral imagery (see equations in Section 2.4.1). For indices, the Probe-1 bands centered at 660.1 nm and 721.6 nm were used as the red and NIR bands, respectively. Spectral data for each sample site location was extracted from the imagery for the two bands using an average of a 3x3 pixel window (refer to section 4.3.3.4). The soil line required for the TSAVI was extracted from the imagery by viewing the red and NIR bands in spectral space (Figure 4-17). Corresponding pixels were examined in the imagery to ensure they were in spatial locations that consisted of bare soil. One should

note that dry residue and dead matter are spectrally similar to a dry light textured soil, but given the nature of a zero-till plot this was considered to be an important component of the background noise that would negatively affect the VIs not adjusted for soil (e.g. SR, NDVI, GDVI). Selecting representative pixels from the imagery for the soil line provided the dynamic range necessary to accommodate any soil type variation in the study area. These pixel values for the red and NIR bands were input into a regression test that resulted in a coefficient of determination (r^2) of 0.99 (Figure 4-19). The linear regression equation provided in Figure 4-18 provide the slope (a) and intercept (b) soil coefficients required for the TSAVI (Equation 2-6).

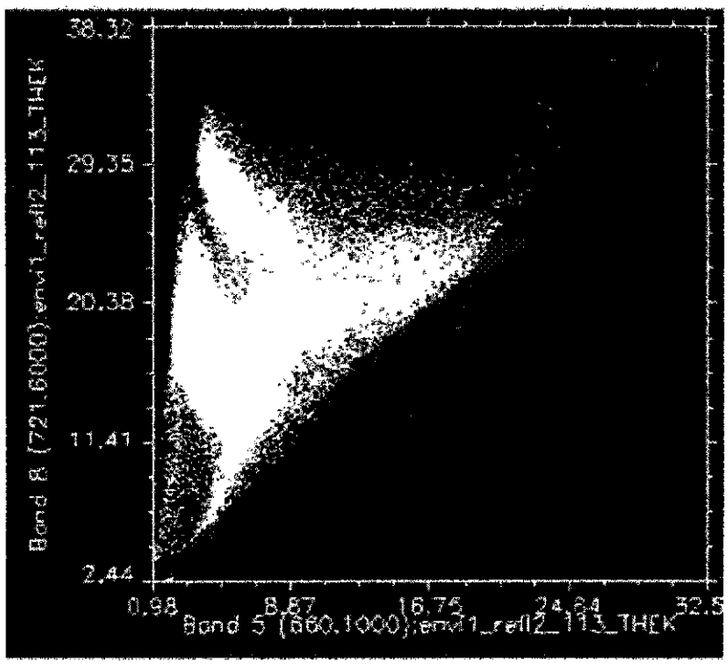

Figure 4-17 Establishing the soil line from the Probe-1 hyperspectral imagery. Only the study area (307 acre farm) was included in the analysis. The red band (660.1 nm) is shown on the x-axis, and the NIR band (721.6nm) is shown on the y-axis.

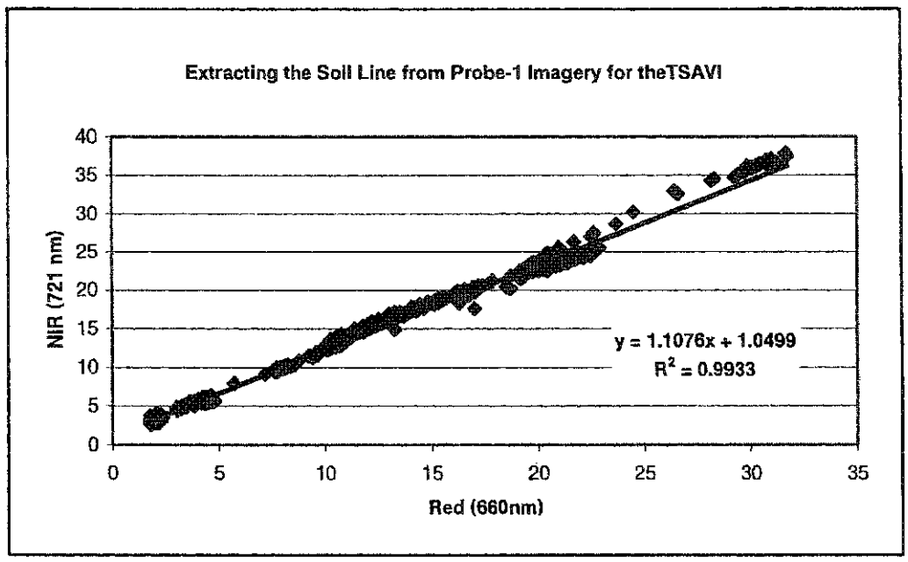

Figure 4-18 Linear regression analysis of pixel values selected from Probe-1 imagery to represent bare soil line required for TSAVI.

4.4.2 Spectral Mixture Analysis

Spectral mixtures analysis (SMA) quantifies the abundance of subpixel scene components within an image (Adams et al., 1993). SMA is dependent on the accurate spectral characterization of endmembers by determining the purest (without the presence of other surface material) spectral response pattern of each scene component (Davidson, 2002; Small, 2001). In this agricultural context, three endmembers were identified: sunlit crop (C), sunlit background (B), and shadow (S). The spectral reflectance of each endmember ($\varrho_c\ \varrho_b\ \varrho_s$) in each band was input into the SMA together with the overall pixel band reflectance values (ϱ_y) to be unmixed (Peddle et al., 2000; 1999a; Hall et al., 1995).

Equation 4-1 Spectral Mixture Analysis (SMA) in Agriculture

$$\varrho_y = C\varrho_c + B\varrho_b + S\varrho_s$$

where:

ϱ_y = overall pixel level reflectance value

C = fraction of crop

B = fraction of background

S = fraction of shadow

ϱ_c = spectral reflectance of crop

ϱ_b = spectral reflectance of background

ϱ_s = spectral reflectance of shadow

Each SMA component is represented by a spectral measurement comprised of only one scene component that is referred to as endmember. In this research, three types of endmember sets were tested for each respective field and crop type: (1) reference endmembers collected in the field within 48 hours of the image acquisition date, (2) image endmembers extracted from the hyperspectral imagery, and (3) integrated endmember sets that comprised of both reference and image endmembers.

The use of the three endmember approaches stems from the fact that even though reference endmembers are spectrally superior, the collection process can be very labour intensive and invasive, in-field collection may not always be feasible in an agricultural environment (i.e. in more mature crop stages), and the successful use of reference endmembers in SMA is heavily dependent on the accurate radiometric correction and surface reflectance retrieval in the associated imagery (Note: radiometric correction is also a labour intensive task). Image endmembers can be extracted from the imagery in a

less labour and time intensive fashion, and can circumvent issues that may surface in SMA due to discrepancies between ground collected reference endmembers and the radiometric correction of the associated imagery. Image endmembers do not guarantee that spectra will contain only one scene component, yet they offer a practical approach to real-time site-specific agriculture applications of remote sensing.

Integrated endmember sets included the use of both reference and image endmembers, and in order to take advantage of both the spectral quality of the reference endmembers as well as the efficiency of the image endmembers. In the future, practical use of SMA in site-specific agriculture may involve the use of integrated endmember sets because it is likely that national reference agricultural spectral libraries will be under development for many years (i.e. complex task to develop a library for numerous crop types, crop varieties and growth stages). The methods used to select the reference and image endemembers are described next.

4.4.2.1 Reference Endmembers

The collection of reference endmembers involved the establishment of a stationary measurement site for the ASD FieldSpec® Pro in the field (Figure 4-10b). The excised leaf sampling strategy described by Peddle et al. (1999b) was used for the crop and residue spectral measurements. The excised leaf and residue samples were stacked in a flat array to minimize shadow and placed under the field of view (FOV) of the spectroradiometer on a dark panel. However, due to the time-critical nature of the field campaign, and the inherent complexity of maintaining the geometry of representative soil samples, all reference endmembers for the soil component were performed *in situ* on bare soil patches.

The first task in using the ASD FieldSpec® Pro involved an optimization process which included a dark current measurement to ensure internal signal-to-noise was reduced. Then a two step process was implemented for each spectral measurement; first, incident irradiance of the Spectralon™ white reference panel was measured, and secondly target radiance under the same illumination conditions was measured. The shadow reference endmember was collected under diffuse light conditions using a sheet of plywood positioned in the principal plane of the sun in order to block all direct solar illumination (Peddle, 1999b; Johnson, 2000). In addition to the diffuse measurements, a fully illuminated incident irradiance measurement was acquired at the same time using the Spectralon™ panel. Consequently, to generate a shadow component an *apparent reflectance* measure was calculated by taking the ratio of diffuse target radiance to incident irradiance (Miller et al., 1997; Peddle, 1998; Peddle et al., 1999b; Peddle et al., 2001a).

The reference endmember data were converted from radiance to reflectance for use with the airborne hyperspectral imagery that was also corrected to reflectance (Section 4.3.3.2). In previous research, Peddle et al. (2000) suggested that equation 4-1a be used to convert endmembers because the reference panel should be calibrated as they do not reflect all of the incident radiation in all regions of the electromagnetic spectrum. In this research, AAFC staff converted the reference endmembers to reflectance using Equation 4-1b which estimated the spectral response of the Spectralon™ panel at 100%. When the manufacturers' spectral response file was recovered for the AAFC Spectralon™ panel the absolute response was 99% for the wavelength range used in this thesis research, and AAFC staff remained satisfied with their initial estimation.

Equation 4-2 Spectral Reflectance Equation for Endmember Spectra

(a) Reflectance (θ,Φ) = (Target Radiance / Panel Radiance) * Panel Calibration

(b) Reflectance (θ,Φ) = (Target Radiance / Panel Radiance) * 100%

Where: Reflectance (θ,Φ) = is the spectral reflectance for a given SZA (θ) and view angle (Φ).

In this research, the imagery was calibrated using the GER3700™, whereas the reference endmembers were collected using the ASD FieldSpec® Pro. Differences in the manufacturer design of the two spectroradiometer instruments could have contributed a significant source of error in the results of the SMA. The spectroradiometer instrument discrepancy in the calibration of the imagery (GER3700™) versus the spectral measurement of the endmembers (ASD FieldSpec®) was evaluated by analysing the response of the two spectroradiometers for a series of cross-calibration targets measured on the acquisition day. The cross-calibration targets included a Spectralon™ panel, an orange tarp, a uniform cement pad, and a black panel. Both the GER3700™ and the ASD FieldSpec® Pro were used to measure each target simultaneously.

The cross-calibration sensor files from the GER3700™ and the ASD FieldSpec® Pro were convolved to match those bands (Table 4-8) selected from the Probe-1 imagery for the SMA. Ideally, this would be done with reference to the spectral response of the airborne sensor, but in this case the spectral response files for the Probe-1 sensor were not available. Instead, the data were convolved using a linear average between each instrument. To examine the statistical relationship between the two instruments a series of linear regression tests were conducted for each calibration target. Overall, the values obtained with the two instruments were similar (r^2=0.99) for all bands selected for the SMA. The linear regression equations for the cross-calibration targets were then used to

adjust the endmember spectral measurements (Figure 4-19). Calibration of the sunlit crop endmembers resulted in an adjustment of 0.5 to 1.7 % reflectance in the visible, and 2.0 to 3.0 % reflectance in the NIR (Figure 4-19a). Calibration of the sunlit residue endmembers resulted in an adjustment of 0.6 to 1.5% in the visible, and 1.5 to 2.0% in the NIR (Figure 4-19b). Calibration of the sunlit soil endmember resulted in an adjustment of 0.5 to 1.3 % reflectance in the visible, and 1.3 to 1.6 % reflectance in the NIR (Figure 4-19c).

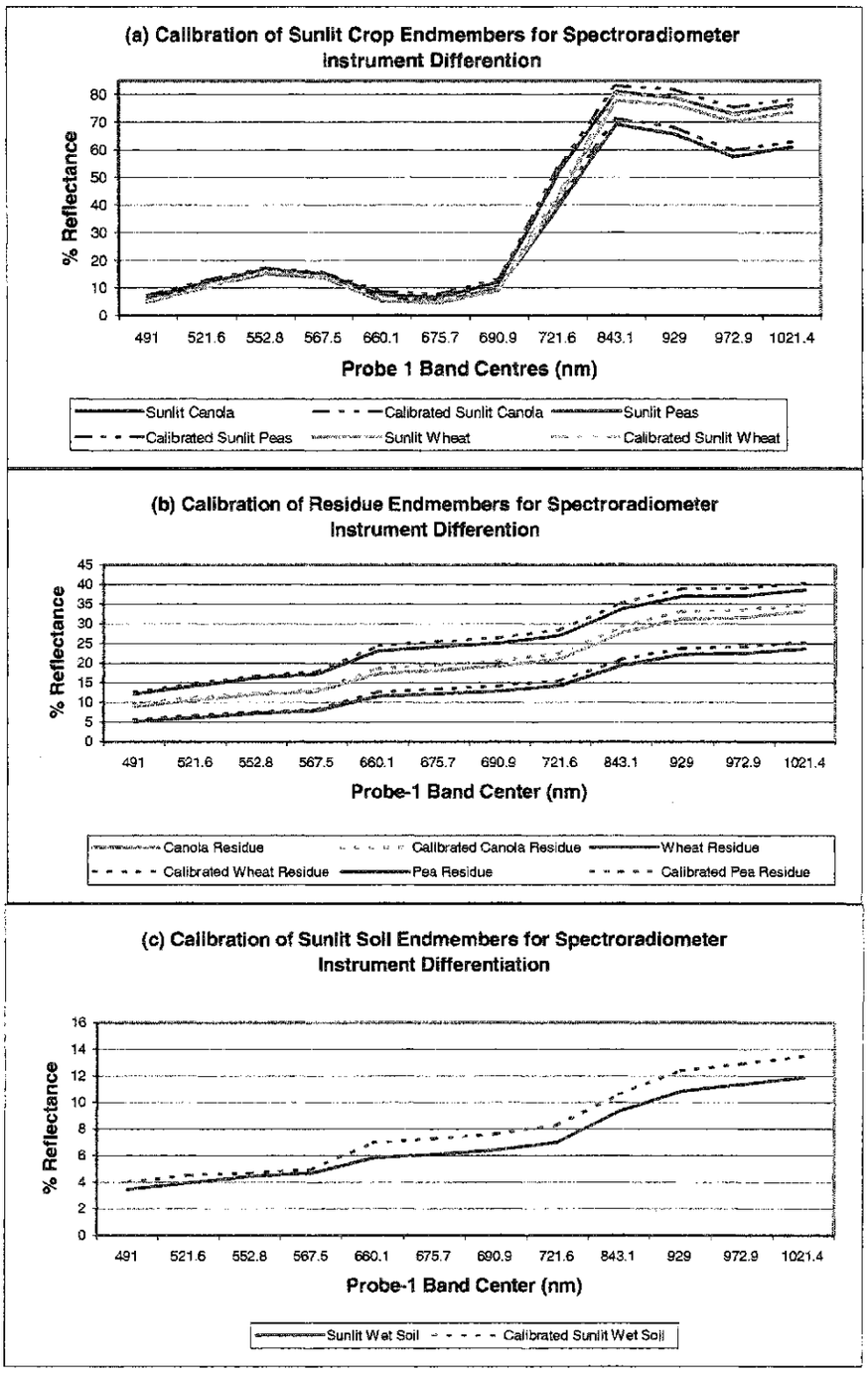

Figure 4-19 Original endmembers (solid line) and calibrated endmembers (dashed line) for sunlit crop, sunlit residue, and sunlit soil endmembers.

4.4.2.2 Image Endmembers

As discussed in section 3.4.2, and in section 4.4.2, image endmembers are not ideal for SMA primarily due to the difficulty of locating homogenous targets within the sensor FOV for all of the agricultural scene components identified for SMA. However, image endmembers are an alternative for ground based reference endmembers that may not always be feasible for a specific crop type or for a specific growth stage. At present, a complete and comprehensive spectral library of agricultural targets does not exist for Canada. Futhermore, the accuracy of image radiometric correction to surface reflectance is critical when using reference endmembers as input into SMA. In light of these realistic issues, image-based endmembers may be more practical especially for applications of SMA in large agricultural areas, when SMA is attempted later in the growing season and ground-based reference endmember collection is too cumbersome. Two methods were used in deriving the image endmembers for this research: (i) manual endmember extraction, and (ii) automatic endmember extraction.

The manual selection method included examining the reflectance of the two bands that were the basis for of all VIs calculated in this research. Reflectance values for each pixel in the 660 nm (red) and 721.6 nm (NIR) Probe-1 bands were plotted in spectral space using ENVI for the seven fields in the study area. Image endmembers for sunlit crop, shadowed crop and crop background (residue and soil) were chosen by selecting pixels from the image that fell at the extremes (vertices) of the simplex in spectral space (Figure 3-1). The n-dimensional visualizer in ENVI allowed the user to select pixels in spectral space and view their corresponding locations in the image (ENVI, 2002). The spectral curve for the pixels selected from the imagery were examined to ensure that the

values represented a realistic spectral signature for each scene component. The evaluation of the spectral signatures for each component, and the corresponding location of the pixels which represented each component, was based on an understanding of crop row structure and prior knowledge of the experimental farm. As a result, this type of selection process does involve a certain degree of estimation, and one cannot be certain that the pixels chosen do not include a shadow component or a slight mixture of components. Figure 4-20 demonstrates this mixture issue for the manually selected image shadow endmember in that the spectral response of shadow seemed to be slightly higher than the image sunlit crop endmember for two of the red Probe-1 bands (660 nm and 675 nm).

To ensure that other candidate image endmember pixels were not being excluded in a variety of other spectral band combinations, an automatic endmember selection process was also implemented. All 12 bands recommended by Thenkabail et al. (2000) were used in the ENVI automatic endmember extraction tool. The purest pixels for describing each primary scene component were located in the imagery. The n-dimensional visualizer allowed various band combinations to be viewed where the chosen pixels are located in spectral space and in the corresponding image. The values of the selected pixels can also be viewed as a spectral response curve graphed for each scene component. To select the purest crop endmember, the highest (brightest) vegetation reflectance curve was chosen to represent sunlit crop, and a curve that represented both soil and residue was chosen for the sunlit background component (Figure 4-21). The automatic method did not provide a spectral curve that definitively characterized a shadow image endmember, therefore this component was not extracted using this method.

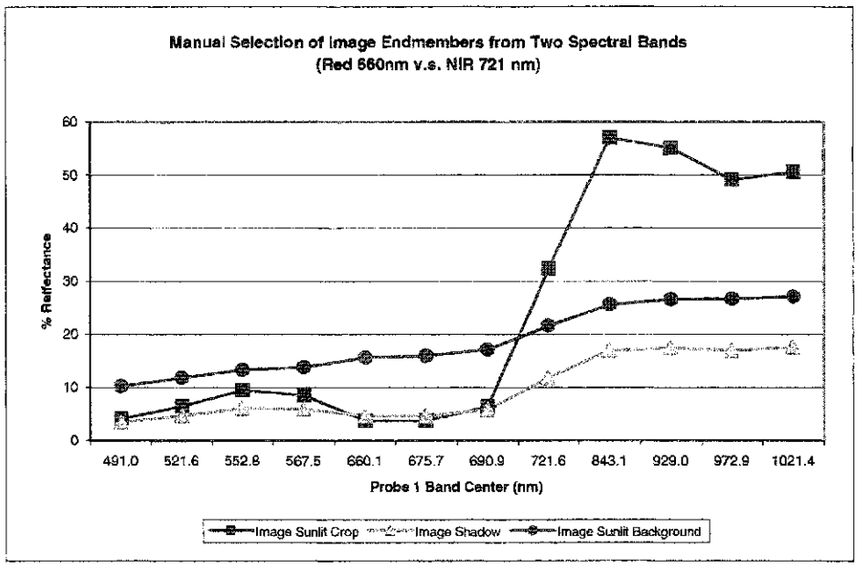

Figure 4-20 Manually selected Image Endmembers using two spectral bands (Probe-1 red band 660 nm and NIR band 721 nm) in the ENVI n-dimensional visualizer.

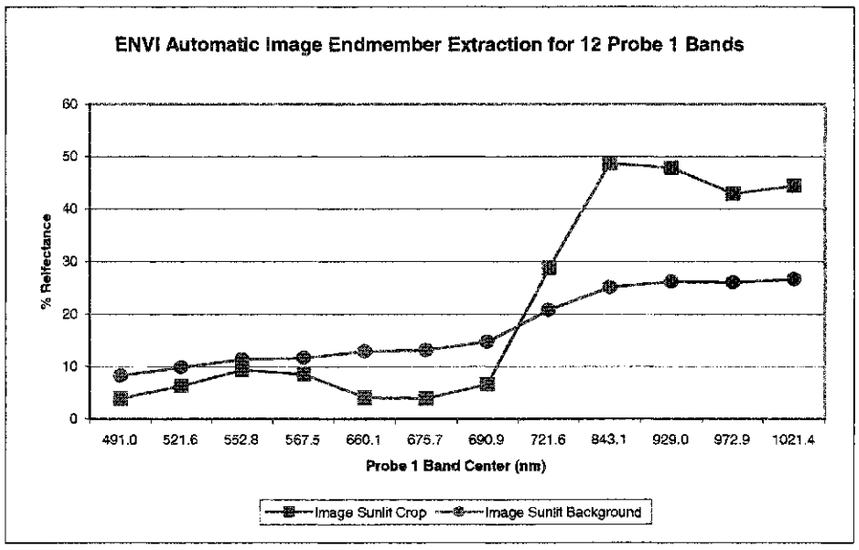

Figure 4-21 ENVI Automatic Image Endmember selection for 12 Probe-1 spectral bands.

4.4.2.3 Integrated Endmembers

An integrated endmember set was created for SMA that consisted of both reference and image endmembers. As mentioned in section 4.4.2, the integrated endmember

approach provides a method that takes advantage of the spectral purity of the reference endmembers, and the uncomplicated acquisition of image endmembers. For the image endmembers, both the automatically selected and manually selected image endmember were tested. A controlled experiment was conducted for the integrated approach, whereby the substitution process was done using each individual image endmember for one component at a time. Using this approach, the SMA model was tested to determine if the different endmembers significantly change the SMA results for predicting crop biophysical parameters.

4.4.2.4 SMA Software

Two software packages were used to assess SMA. The first is a fortran program developed by Shimabukuro and Smith (1991) and modified by Dr. D. Peddle to include both a constrained and unconstrained version of the least squares algorithm. The Shimabukuro and Smith SMA program can process a maximum of seven bands (Table 4-8). This software is a very flexible and useful program for research purposes, but it is not a commercially available software package. The unconstrained SMA algorithm chosen for this research can produce underflow or overflow fraction values (i.e. fraction values below 0, or above 1). This is a more advantageous method than the constrained algorithm because the overflow and underflow, as well as the frequency of these occurrences, can alert the user to portions of the dataset where the SMA model may not be correctly parameterized. In this case, the user can assess each sample site location in the dataset to infer why the endmembers may not adequately characterize the scene components of the imagery for certain regions of the field in the study area. The spatial abundance of each component in the imagery can also be better characterized by the

unconstrained method. If the spatial contribution of one component in the imagery is minimal, then negative fraction values for a particular scene component would indicate minimum contribution to the area being observed or error in the endmembers.

The second software package used in this research was the commercially available ENVI remote sensing software (Research Systems Inc., 2003) The Linear Spectral Unmixing (LSU) tool in ENVI (Version 3.5) is based on earlier work by Boardman (1989) however, as with all proprietary software, little has been published on the specific implementation of the LSU algorithm and therefore it was not ideal for this research environment. Similar to the Shimabukaro and Smith (1991) program, the LSU algorithm in ENVI is unconstrained (i.e. where overflow and underflow fraction values can result) but a constraint to unity can be placed on the algorithm to ensure the fraction values from each component sum to unity (Research Systems Inc., 2003). The ENVI software does provide a more convenient fraction map output than the Shimabukaro and Smith (1991) program. Results of a comparison between the two programs are shown in Appendix B, with the sole purpose being to demonstrate that similar results could be

Table 4-8 Input Probe-1 Hyperspectral Bands for SMA

Probe-1 Wavelength Center (nm)	Band Width (nm)	Wavelength Minimum (nm)	Wavelength Maximum (nm)
491.0	16.0	483.0	499.0
552.8	15.7	545.0	560.7
660.1	16.5	651.9	668.4
690.9	15.9	683.0	698.9
721.6	16.4	714.0	729.3
929.0	13.8	922.1	936.0
972.9	19.1	963.4	982.5

achieved using commercially available remote sensing software and the modified Shimabukuro and Smith (1991) fortran program.

4.4.3 Statistical Methods

The VIs and SMA fractions were analysed and compared statistically for their ability to predict crop biophysical parameters (i.e. LAI and biomass) using linear regression analysis. The predictive ability of each remote sensing method was based on the strength of coefficient of determination (r^2), the standard error (S.E.), and the F-statistic. The coefficient of determination (r^2) (also known as regression coefficient) measures the proportion of the total variability explained by fitting the regression model. As the r^2 approaches 1, a greater proportion of the variability is explained by the model, similarly as the r^2 values approach 0, less variability is explained. The S.E. for each regression model provides an estimate of the deviation of the model from the observed value. The F-statistic is a measure of significance, and if the value is large a significant proportion of variability is due to the relationship between the variables. Due to the empirical nature of this research, and the sampling scheme that was dependent on specific homogenous management zones, the statistical methods used were not inferential in nature. As a result, the predictive power of each image processing method by crop type was specific to the pre-defined management zones, and consequently the regression analysis presented in this research cannot necessarily be applied to different crop types in other geographic regions.

4.5 Chapter Summary

In this chapter, the study area was defined, and the ground-based and remote sensing data collection methods were described. The conventional image processing

method used for predicting crop biophysical parameters included the computation of a series of vegetation indices (i.e. SR, NDVI, GDVI, TSAVI, and OSAVI). The new image processing method presented in this chapter for predicting crop biophysical parameters was SMA. This chapter described the analytical and statistical methods that were used in evaluating the predictive capability of the new and conventional image processing methods for predicting crop biophysical parameters (i.e. LAI and biomass).

CHAPTER V

5.0 RESULTS AND DISCUSSION

5.1 Introduction

In this chapter, vegetation indices (VIs) and SMA fractions from airborne hyperspectral remote sensing imagery are compared for their ability to predict crop biomass and LAI for each sample site location, and each crop type. Regression analyses were used to determine the amount of variation in the dependent variable (LAI or biomass) that may be explained by the independent variable (VI value or SMA fraction value) based on the magnitude of the coefficient of determination (r^2) (also known as regression coefficient), the standard error (SE), and the F statistic (F).

This chapter is organized into four main sections. In the first section, descriptive statistics are presented for the ground based biophysical data by crop type. In the next two sections, linear regression results for predicting crop LAI and biomass are presented for VIs (section 5.3) and SMA (section 5.4). In section 5.5, the results from conventional VIs and SMA for predicting crop biomass and LAI are discussed and compared.

5.2 Biophysical Data

As presented in section 4.2.2.2, crop biophysical measurements were taken at each of the 98 sample site locations. Descriptive statistics are given for crop height, biomass and LAI in Tables 5-1 to 5-3 respectively. The pea crop was planted the earliest in the growing season (Table 4-3) and as expected, the crop had the highest mean crop height. The canola crop had a much broader leaf base than the peas, and as expected showed the highest mean biomass and LAI values. The canola crop demonstrated the most

variability across the sample sites in comparison to the other two crops. This is apparent from the wider range of LAI and biomass values. The three wheat fields used in this research were the last to be planted in 2000, and as expected, the wheat mean height, biomass and LAI were the lowest. Crop height measurements were not used directly in the regression analysis for each crop type, but instead were used as a reference for crop status since it can serve as an additional indicator of the amount of crop variability amongst the various pin locations. In a similar agricultural study, it was determined that the use of a nadir sensor did not result in a strong relationship between crop height and crop biophysical parameters, although the strength of this relationship may be improved if the imagery was captured using an off-nadir view angle (Peddle et al., 1999b).

Table 5-1 Crop heights measured at the time of airborne image acquisition.

Crop Type	Number of Samples	Minimum Height (cm)	Maximum Height (cm)	Mean Height (cm)	Standard Deviation
Peas	24	27	62	40	9
Canola	22	5	63	24	16
Wheat	34	19	44	28	7

Table 5-2 Crop biomass measurements based on fresh weight

Crop Type	Number of Samples	Minimum Biomass (g/m^2)	Maximum Biomass (g/m^2)	Mean Biomass (g/m^2)	Standard Deviation
Peas	24	629	1611	1038	274
Canola	22	274	3315	1247	1001
Wheat	34	406	1183	650	176

Table 5-3 Leaf Area Index (LAI)

Crop Type	Number of Samples	Minimum LAI	Maximum LAI	Mean LAI	Standard Deviation
Peas	24	0.66	2.74	1.58	0.54
Canola	22	0.51	4.5	1.96	1.12
Wheat	34	0.80	2.68	1.38	0.42

5.3 LAI and Biomass Prediction using Vegetation Indices

The results of the linear regression analysis to predict LAI and biomass for each crop type using the conventional VIs are presented in Table 5-4 (for linear regression figures see Appendix C). The VIs tested were; simple ratio (SR), normalized difference vegetation index (NDVI), green difference vegetation index (GDVI), transformed soil adjusted vegetation index (TSAVI), and the optimized soil adjusted vegetation index (OSAVI) which were presented in sections 2.4.1 and 4.4.1. Each VI was used as an independent variable in separate predictions of LAI and biomass for each crop type. The F statistic was consistently large (at the 95% confidence level) for all results (except wheat biomass) and indicated that a significant portion of the variability was explained by the relationship between the variables.

The highest r^2 value for predicting biomass of the pea crop was the SR with an r^2 of 0.66 and standard error (SE) of 162.95 g/m^2 with similar results (r^2 = 0.63 and 0.64) for the other vegetation indices. The highest r^2 value for predicting LAI of the peas was OSAVI with an r^2 of 0.50 (SE = 0.37), with similar results for the GDVI and TSAVI (r^2 = 0.48) and the SR (r^2 = 0.49). For the canola crop biomass, the highest r^2 value was the GDVI with an r^2 of 0.77 (SE = 489.14), although all other indices performed similarly with an r^2 of 0.75. (SE = 511.77 to 512.78 g/m^2). The highest r^2 value for predicting canola LAI was the GDVI with r^2 = 0.68 (SE = 0.64), whereas all the other indices performed similarly r^2 = 0.59 or 0.60 (SE = 0.72 to 0.74). None of the VIs were statistically significant for predicting wheat crop biomass, whereas the highest r^2 value for predicting wheat LAI was the SR with an r^2 of 0.65 (SE = 0.26). Similar to the latter

results, all other indices performed almost equally for wheat LAI prediction with r^2 of 0.62 to 0.64 (SE = 0.26).

Table 5-4 Linear regression analysis results for vegetation index prediction of LAI and biomass based on magnitude of coefficient of determination (r^2), standard error (SE), and F-statistic (F). Note: "*" indicates not statistically significant at the 95% percent confidence level and highest r^2 value per crop type in bold.

Vegetation Index	Biomass			LAI		
	r^2	SE	F	r^2	SE	F
PEAS						
SR	**0.66**	162.95	43.26	0.49	0.39	21.02
NDVI	0.63	170.55	37.57	0.48	0.40	20.31
GDVI	0.64	168.58	39.98	0.38	0.43	13.44
TSAVI	0.63	171.17	37.15	0.48	0.40	20.33
OSAVI	0.63	170.62	37.53	**0.50**	0.40	10.63
CANOLA						
SR	0.75	511.77	60.35	0.60	0.72	30.48
NDVI	0.75	512.54	60.10	0.59	0.74	28.74
GDVI	**0.77**	489.14	67.95	**0.69**	0.64	45.01
TSAVI	0.75	512.78	60.03	0.59	0.74	28.64
OSAVI	0.75	512.21	60.21	0.59	0.74	28.75
WHEAT						
SR	0.01	177.96	0.17*	**0.65**	0.26	58.24
NDVI	0.00	178.11	0.12*	0.64	0.26	56.44
GDVI	0.01	177.94	0.18*	0.62	0.27	51.96
TSAVI	0.00	178.19	0.09*	0.64	0.26	57.22
OSAVI	0.00	178.12	0.12*	0.64	0.26	56.60

There were slight differences amongst the various VI results, but overall they performed very similarly as predictors of biomass and LAI for all crop types (Figure 5-1a to 5-1c). Early in the growing season a higher portion of soil or residue (dead matter due to no-tillage practices) is present between the crop rows. Residue or senescing vegetation is also a valid consideration for soil-adjusted indices and the soil-line concept (Baret et al., 1989). In this research, one may have expected in a no-till environment that the soil-

adjusted indices would have performed better as predictors of crop biophysical parameters early in the growing season. However, the sensitivity of VIs to soil background is greatest with moderate levels of vegetation cover (>50% green cover). In low vegetation cover there is insufficient vegetation to induce a canopy-scattered, soil-reflected signal (Huete, 1988). In this research, the background was primarily residue with some bare soil, and vegetation cover was not greater than 50% (crop maturity was below average in June, see section 4.2.1.1). Therefore, the sensitivity of the soil-adjusted VIs in this research was minimized because there wasn't enough crop present in the imagery to induce a canopy-scattered background-reflected signal.

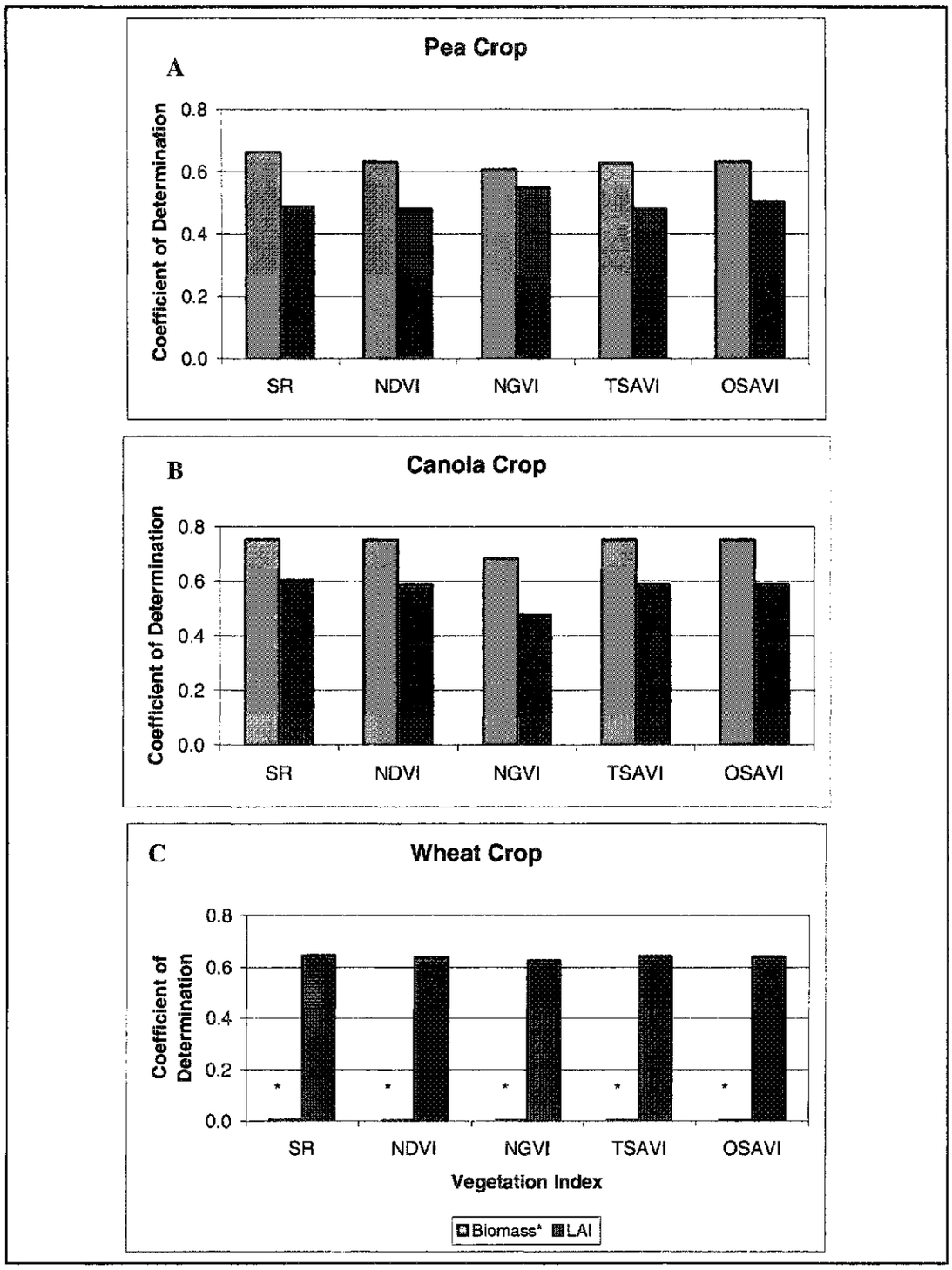

Figure 5-1 Magnitude of coefficient of determination (r^2) for vegetation indices as a predictor of biomass and LAI for all three crop types. Note: "*" not significant at the 95% confidence level.

The lack of a relationship between VIs and wheat crop biomass (Figure 5-1c) has been found in another related agricultural study performed by CCRS (Dr. Heather McNairn and Catherine Champagne, personal communication, Feb 17, 2003). Interpretation of results in this research suggests that the lack of predictive capability for wheat biomass using remote sensing imagery may be due to some or both of the following: (i) the architecture of the crop, and/or (ii) the way the biomass ground data were collected. Early in the growing season small wheat plants have a compact erectophile structure (Figure 5-2), whereas the canola and peas have a planophile structure. In wheat, the LAI derived using the LAI-2000 provides a better representation of ground cover than the biomass measurements. Although biomass is expressed in plant matter per unit area, in the case of wheat with its erectophile architecture, much of this matter is present in the vertical plane rather than the horizontal plane. In the case of peas and canola, the planophile nature of the plants results in a stronger relationship between the LAI and biomass measurements (Appendix E).

The ground based data collection methods may also have contributed to the issues surrounding wheat biomass prediction versus the wheat LAI prediction. To improve the ground-based biomass sampling technique, CCRS implemented a new sampling technique later in the growing season in the 2002 IHARF campaign that involved weighing the leaves separately from the stem of the crop. CCRS hypothesized that by weighing only the leaves, which are the portion of the plant that is primarily detected by the sensor (not the stem), the relationship between the imagery and wheat biomass may be improved. However, the results of this study have not yet been published.

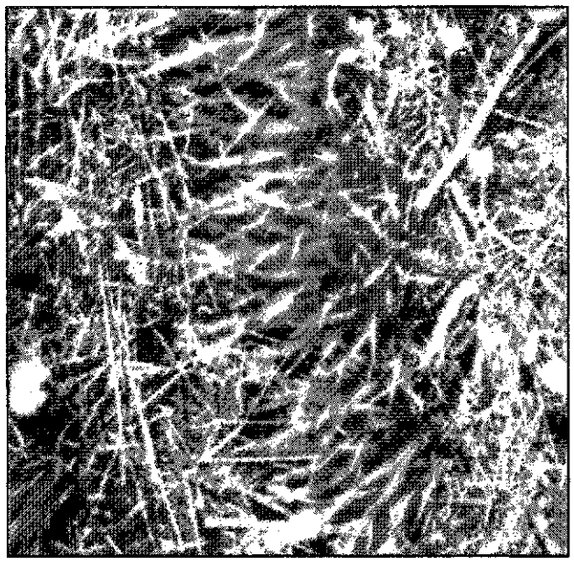

Figure 5-2 Ground based nadir picture of the wheat crop in June 2000.

In this section several VIs, including soil-adjusted VIs, were discussed and performed relatively similarly for the prediction of crop biomass and LAI. VIs are based on the magnitude of change in the spectral slope between the red and NIR regions of the electromagnetic spectrum. Therefore, VIs operate not only on the whole pixel signal, but also in a very narrow range of the spectrum and cannot accommodate the full magnitude of the spectral response curve for each crop type. Similar to results found in forestry application of VIs, it may be that complex interactions between scene components in an agricultural image (e.g. crop, soil, residue, and shadow) may not be differentiated by the linear relationship typically found in the red-NIR space of VIs (Peddle et al., 2001b). The results of this research suggest that utilizing a number of VIs early in the growing season may be empirically redundant.

5.4 LAI and Biomass Prediction Using SMA

SMA was performed using three different endmember strategies: (i) reference endmembers, (ii) image endmembers (automatic and manual), and (iii) integrated endmembers (refer to sections 3.4 and 4.4.2). Each SMA fraction value was used as the independent variable, with LAI and biomass input separately as the dependent variables in the regression analysis. The F statistic was consistently large (except in the case of wheat biomass) for all results and indicated that a significant portion of the variability was explained by the relationship between the variables (for linear regression figures see Appendix D).

5.4.1 Reference Endmembers

In this portion of the analysis reference endmembers collected on the ground using the ASD FieldSpec® Pro spectroradiometer were input into the SMA. This series of SMA tests demonstrates the use of the most spectrally pure set of endmembers for all three components defined for the experimental farm. In this case, each sunlit crop endmember was the brightest spectra collected for each respective crop type (i.e. sunlit canola, sunlit peas and sunlit wheat). The shadow reference endmember was the darkest shadowed crop spectra measured on the ground. The sunlit background was the brightest residue spectra for each individual crop type and included consideration of the sequence of the crop rotation practiced in each field (e.g. if the crop from the previous year was wheat for the current canola field, then the wheat residue endmember was used). Preliminary SMA tests showed that when the reference sunlit soil endmember was input into the SMA as the sunlit background component, the fraction results produced severe underflow values, indicating that one or more of the endmembers were inappropriate.

Visual examination of the percent crop cover photographs taken at each sample site confirmed that due to the nature of the no-till study area, in general residue was the dominant background component. Overall the soil component was spatially less abundant and therefore not appropriate for a three endmember model (Figure 5-3).

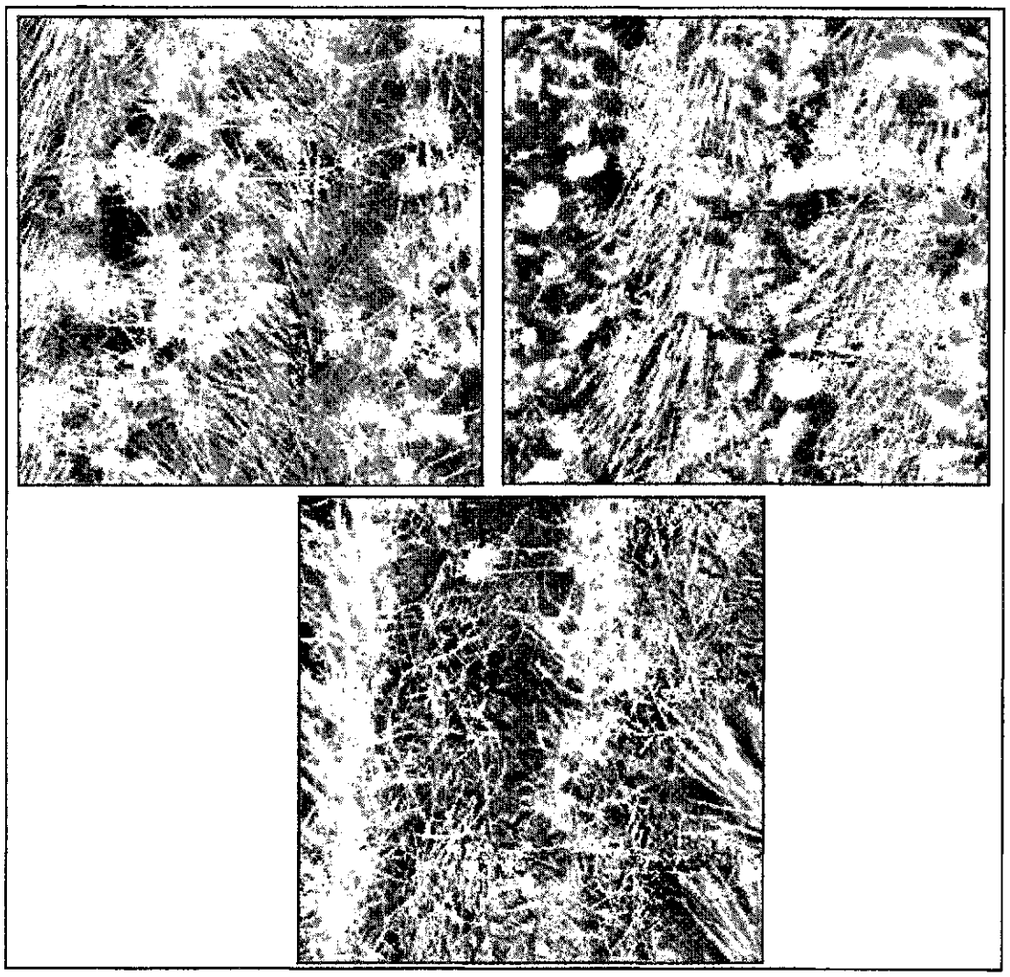

Figure 5-3 Ground based nadir pictures of peas, canola, and wheat (clockwise) showing predominantly crop residue rather than bare soil contribution to the background.

The results of the linear regression analysis to predict LAI and biomass for each crop type from the reference endmember set are presented in Table 5-5. The highest r^2 value for predicting pea biomass was sunlit background fraction with r^2 of 0.62 (SE = 173.44 g/m^2), however the sunlit crop fraction was similar (r^2 = 0.58, SE = 182.84 g/m^2). The relationship between crop background and crop biomass is inverse (Appendix D) compared to that of the sunlit crop fraction. This relationship occurs because when there is less crop on the ground, there is less biomass present in the imagery, and more background visible to the sensor. The highest r^2 value for predicting pea LAI was the sunlit crop fraction with r^2 of 0.57 (SE = 0.36), although the sunlit background fraction performed similarly with r^2 of 0.52 (SE = 0.38). The highest r^2 value for predicting canola crop biomass was the sunlit crop fraction with an r^2 of 0.80 (SE = 456.61 g/m^2). The highest r^2 value for predicting canola LAI was the sunlit crop fraction with an r^2 of 0.61 (SE = 0.72), with similar results for the sunlit background fraction (r^2 = 0.59, SE = 0.74). Similar to the results of the VIs, there was no significant relationship between the SMA fractions and the ground based biomass measurements for the wheat crop. The highest r^2 value for predicting wheat LAI was the sunlit crop fraction with an r^2 of 0.71 (SE = 0.23).

Table 5-5 Linear regression results using reference endmembers for SMA prediction of LAI and biomass based on magnitude of coefficient of determination (r^2), standard error (SE), and F-statistic (F). Note: "*" indicates not statistically significant at the 95% percent confidence level and highest r^2 value per crop shown in bold.

SMA Fraction	Biomass			LAI		
	r^2	SE	F	r^2	SE	F
PEAS						
Reference Sunlit Crop	0.58	182.84	29.84	**0.57**	0.36	29.61
Reference Shadowed Crop	0.22	247.59	6.27*	0.07	0.53	1.54*
Reference Sunlit Background	**0.62**	173.44	35.60	0.52	0.38	23.52
CANOLA						
Reference Sunlit Crop	**0.80**	456.61	80.93	**0.61**	0.72	30.82
Reference Shadowed Crop	0.04	1002.60	0.93*	0.00	1.15	0.03*
Reference Sunlit Background	0.74	520.08	57.80	0.59	0.74	28.66
WHEAT						
Reference Sunlit Crop	0.01	177.68	0.28*	**0.71**	0.23	79.09
Reference Shadowed Crop	0.04	174.56	1.44*	0.02	0.43	0.51*
Reference Sunlit Background	0.04	174.65	1.40*	0.46	0.32	27.55

The reference endmember results show that the reference sunlit crop and sunlit background fractions were the strongest predictors of biomass and LAI for all three crop types early in the growing season (except in the case of wheat biomass, which was also the case for the VIs in the last section). This result makes sense in that the most spatially abundant scene components were the crop and the crop background. Overall, Figure 5-4a to 5-4c show the shadow fraction was not generally a good predictor of crop biophysical parameters. This was expected early in the growing season because the crops were very small and it is feasible that the shadow within the canopy was minimal and thus its contribution to the image values was minimal (Figure 5-3). These results may also be due to the way the reference shadow endmembers were collected. In this research, the plant geometry and associated 'natural leaf shadowing' may have been lost in the flat-

array sampling strategy. Other methods of sampling such as the optically thick stack (Peddle et al., 1999b), or vertical bundling of crop stacks (CCRS, IHARF 2002 campaign) attempt to maintain canopy geometry and natural shadowing but these methods were not implemented in this research.

The purpose of SMA is to discriminate between scene components that contribute, or do not contribute, to the overall signal strength for each pixel. In this early growing season research, it was expected that not all fraction values would be good predictors of crop biophysical parameters (i.e. shadowed crop fraction). The advantage of implementing SMA as a sub-pixel analysis tool is that this method allows for extraction of only the relevant portions of the pixel that more closely represent real field conditions, on the acquisition date, and for a specific growth stage. The results of this research will determine for agricultural remote sensing applications early in the growing season what specific fractions more closely represented each biophysical parameter.

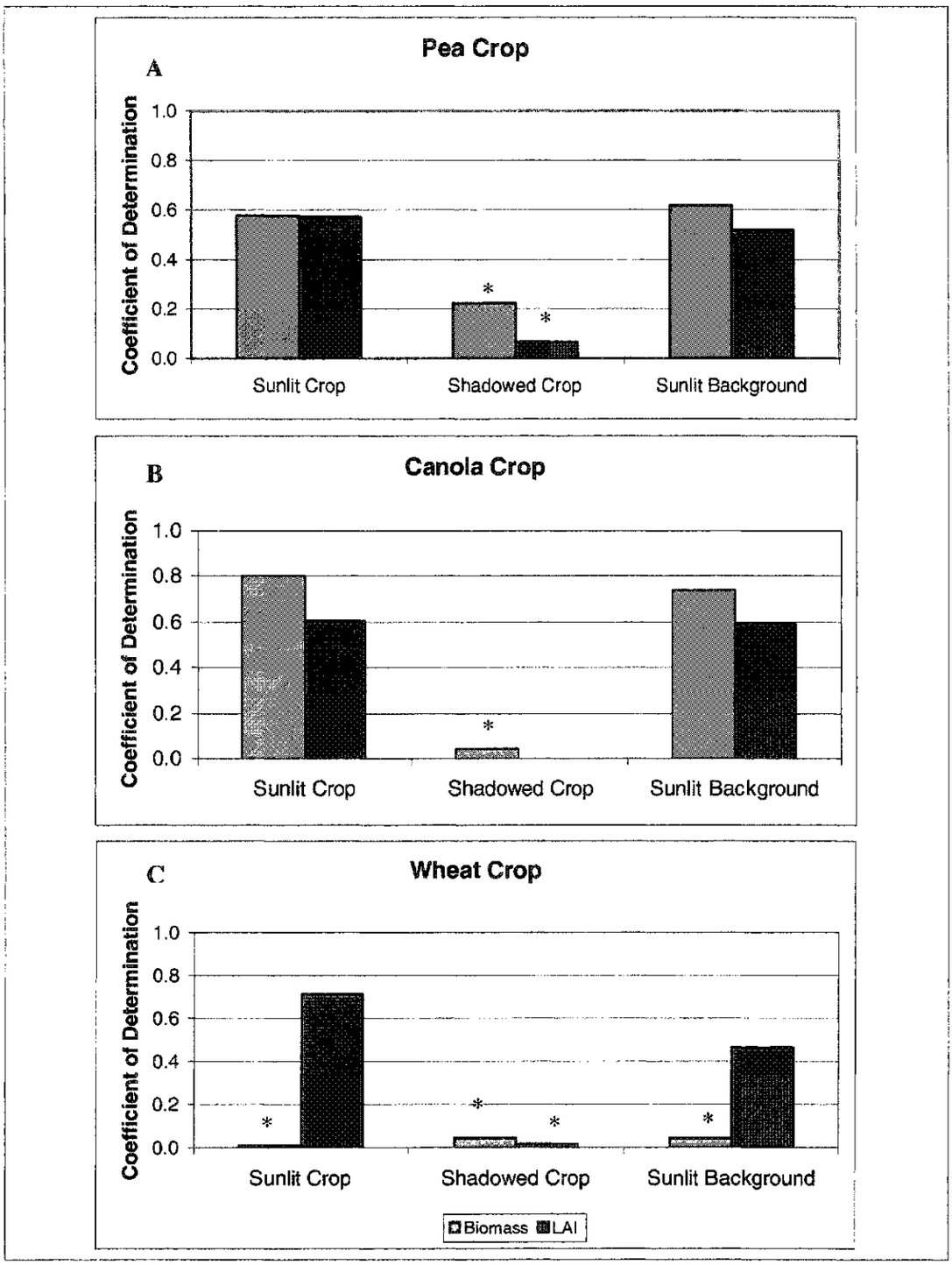

Figure 5-4 Magnitude of coefficient of determination (r^2) for SMA using fractions from reference endmembers for predicting biomass and LAI for all three crop types. Note: "*" indicates not statistically significant at the 95% confidence level.

5.4.2 Image Endmembers

As discussed in section 4.2.3, image endmembers do not guarantee that spectra will only contain one scene component, yet they can offer a potentially more practical approach to real-time agriculture applications of remote sensing. Manual and automatically derived image endmembers were extracted from the imagery (section 4.4.2.2), but the automatic method did not return an acceptable endmember for the shadowed crop component. As a result, only the manually derived endmembers were utilized for the image endmember approach to SMA.

Image endmembers were derived manually by plotting the red and NIR bands in spectral space and selecting pixels from the imagery to represent each scene component. However, the manual method did not explicitly identify each crop type, pixels were chosen from 2D spectral space that were located within the study area but only one spectra was chosen to represent all crop types (refer to Figure 3-1). This approach is not ideal, but the overriding advantage of image endmember SMA is that it does not require labour intensive (and sometimes impractical) spectral measurements of endmembers in the field, and the imagery does not have to be atmospherically corrected. It should be noted that in the future reference endmembers may be considered somewhat less labour intensive if selected from an established spectral library (i.e. no new field data collection required), although in this case atmospheric correction and surface reflectance retrieval would still be required.

The linear regression results for the image endmember SMA approach of each crop type are presented in Table 5-6. The highest r^2 value for predicting pea biomass was the image sunlit background fraction with r^2 of 0.61 (SE = 176.34 g/m^2), and the image sunlit

crop fraction had the highest r^2 value for predicting pea LAI with r^2 of 0.57 (SE = 0.36). The highest r^2 value for predicting both biomass and LAI of canola was the image sunlit crop fraction with an r^2 of 0.81 (SE = 442.84 g/m^2) and r^2 of 0.61 (SE = 0.72) respectively. Similar to the vegetation index results, there was no significant relationship between any of the image endmember derived fractions, and the ground based biomass measurements of the wheat crop. The highest r^2 value for predicting wheat LAI was image sunlit background fraction with an r^2 of 0.71 (SE = 0.23).

Table 5-6 Linear regression analysis results using image endmembers for SMA prediction of LAI and biomass based magnitude of coefficient of determination (r^2), standard error (SE), and the F-statistic (F). Note: "*" indicates not statistically significant at the 95% percent confidence level and highest r^2 value per crop shown in bold.

SMA Fraction	Biomass			LAI		
	r^2	SE	F	r^2	SE	F
PEAS						
Image Sunlit Crop	0.52	194.52	23.80	**0.57**	0.36	29.64
Image Shadowed Crop	0.35	226.25	11.85	0.17	0.50	4.38
Image Sunlit Background	**0.61**	176.34	33.73	0.48	0.39	20.41
CANOLA						
Image Sunlit Crop	**0.81**	442.84	87.31	**0.61**	0.72	30.82
Image Shadowed Crop	0.66	602.29	38.01	0.37	0.91	11.69
Image Sunlit Background	0.68	579.56	42.65	0.56	0.76	25.48
WHEAT						
Image Sunlit Crop	0.01	177.78	0.24*	**0.71**	0.23	77.70
Image Shadowed Crop	0.01	177.44	0.36*	0.18	0.39	7.16
Image Sunlit Background	0.04	174.97	1.28*	0.45	0.32	25.73

In the image endmember approach to SMA results show that, with the exception of wheat biomass, the image sunlit crop and sunlit background fractions were the strongest predictors of biomass and LAI for all crop types early in the growing season (Figure 5-5a to 5-5c). The strength of the shadow fraction as a predictor of crop biophysical parameters improved in these results in comparison to the reference endmember set. This improvement may have resulted because the shadow endmember is better characterized by image pixels. As found in previous results, the reference shadow endmember may not adequately characterize shadowing due to the loss of geometry in the flat array sampling strategy. Selecting endmembers from the imagery preserves the natural canopy geometry, and captures the transmission of energy in the IR region of the spectrum between leaves that is included in the shadowed crop signal. This research also took place early in the growing season when the crops were very small. The transmission properties of small plant leaves may have resulted in some of the soil or residue reflectance from beneath the plant being included in the returned shadowed crop signal from the imagery. An example of this is shown in Figure 5-6 which illustrates the reference endmembers and the less specific image-based endmembers. The image shadowed crop endmember falls between the purer reference shadowed crop endmember and the reference soil endmember. This mixture of components (shadow and soil) in endmembers derived from the imagery may have better characterized the shadow and background dynamic.

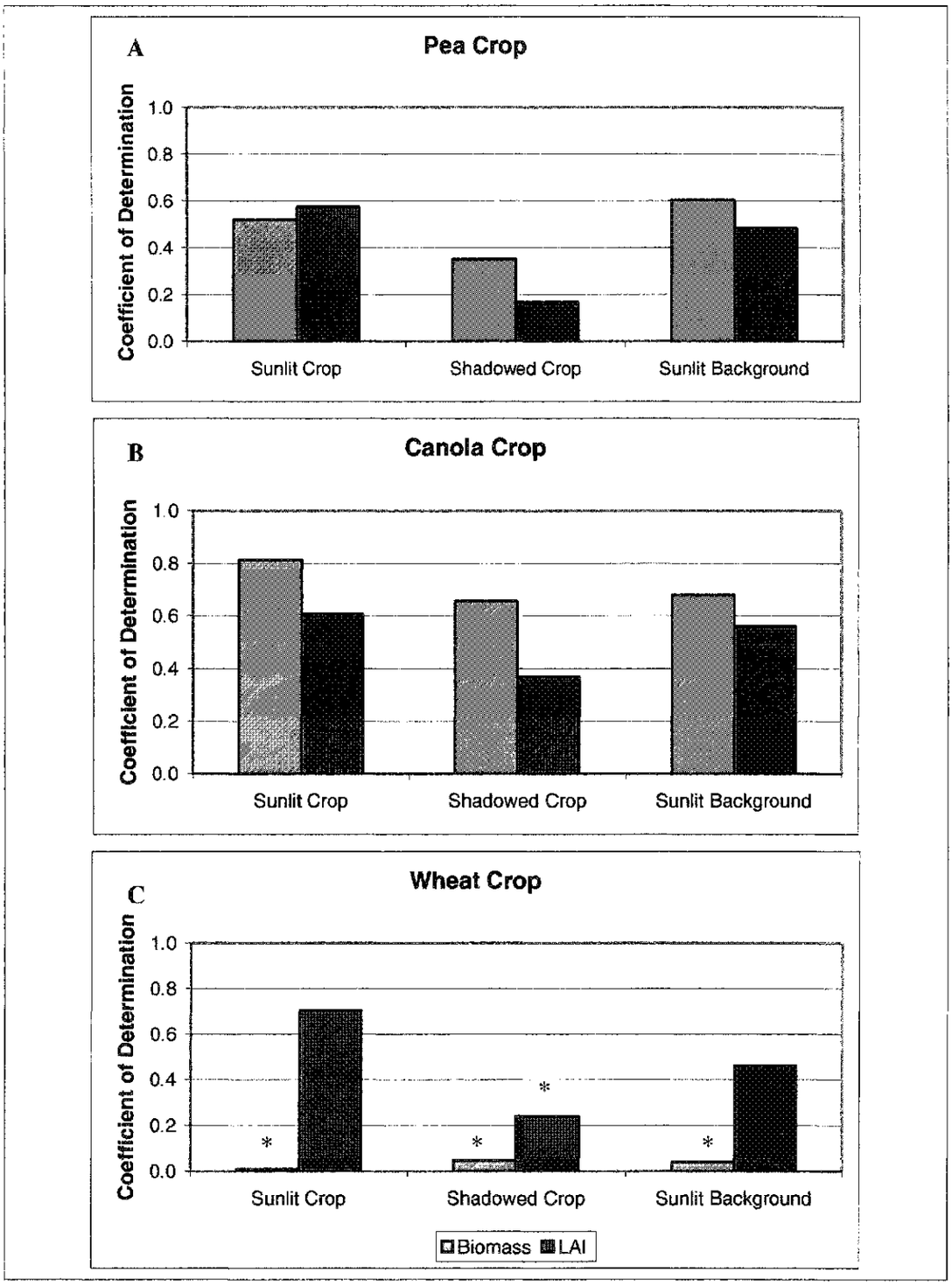

Figure 5-5 Magnitude of coefficient of determination (r^2) from SMA image endmember fractions for predicting biomass and LAI for all three crop types. Note"*" indicates not statistically significant at the 95% confidence level.

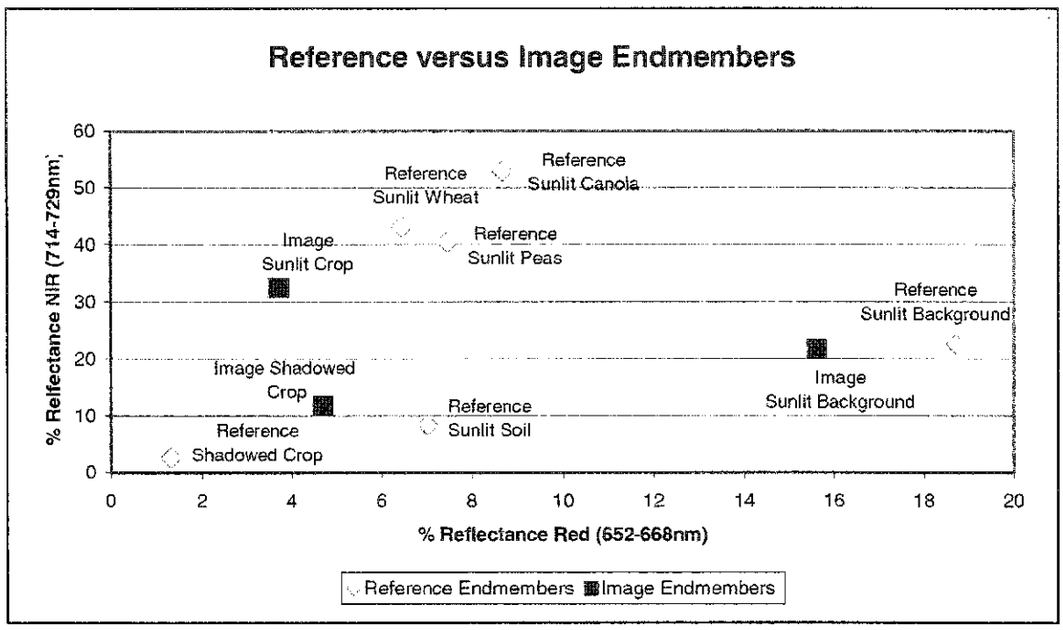

Figure 5-6 Comparison of reference and image endmembers in 2 dimensional spectral space.

5.4.3 Integrated Endmembers

As discussed in sections 4.4.2.2 and 4.4.2.3, integrated endmembers provide an approach to SMA that takes advantage of the spectral purity of the reference endmembers, and the uncomplicated acquisition of image endmembers. Image endmembers were derived using both a manual and automatic method. The difference between these two methods is a factor of the number of bands utilized to select endmembers from the imagery (i.e. ENVI automatic method utilized 7 bands whereas manual selection used only the red and NIR). Prior to performing an extensive test of integrated endmembers in SMA, the automatically and manually derived image sunlit crop and background endmembers were first compared and evaluated for similarity in two preliminary integrated tests. The automatic method did not yield an identifiable shadowed crop endmember, therefore in these preliminary tests only the manual and

automatic image sunlit crop and background endmembers were substituted for the reference sunlit crop and sunlit background endmembers.

In the statistical analysis of these SMA results, the absolute fraction values from all crop types were input to determine (for all sample sites) the amount of difference between fractions obtained from automatic and manual endmembers. First, a paired-samples T-test was used to compare the means of two variables (integrated SMA test with automatic versus manual image endmember) for a single group (fraction results for each scene component of all crop types). Then linear regression analysis was used to determine the amount of variation in the dependent variable (integrated test with automatic image endmembers) that may be explained by the independent variable (integrated test with manual image endmember). Table 5-7 and 5-8 show the results of the paired-samples T-test. Overall, the P value from the T-test indicates that the mean value for the dependent and independent variable are statistically different from one another for each fraction result (at the 95% confidence level). However, the linear regression analysis for all crop types shows that 97-100% of the variability in the dependent variable is explained by the independent variable. In the integrated SMA test that substituted the reference sunlit crop endmember with an automatically or manually derived image endmember (Table 5-7), the sunlit crop fraction had an r^2 of 1.00, the shadowed crop fraction had an r^2 of 0.97, and the sunlit background fraction had an r^2 0.99. In the integrated SMA test which substituted only the reference sunlit background endmember with an automatically or manually derived image endmember (Table 5-8), the sunlit crop fraction had an r^2 of 0.99, the shadowed crop fraction had an r^2 of 0.97, and the sunlit background fraction had an r^2 0.99. These results suggest that the

dimensionality of the image data (i.e. 2 bands for manual, and 7 for automatic) may not be crucial in the selection of image endmembers for agricultural crops, and the red to NIR relationship may be sufficient for the image endmember selection process. For the purpose of the integrated endmember approach to SMA, it was concluded that the automatically derived image endemember was considered to be a redundant input when compared to the manually derived endmember. As a result, only the manually derived image endmembers were included in the comprehensive set of integrated SMA tests.

Table 5-7 Paired-samples T-test of integrated endmember SMA test #1 & #2 for all crop types. Note: Reference (Ref) and image (Img) automatically derived (a) or manually derived (m) endmembers shown for sunlit crop image endmember (C), shadowed crop (S), sunlit background (B). Bold text highlights the endmember that was substituted.

SMA Fractions for all crop types (n=80)	Integrated Test #1 **C Img (a)** / S Ref / B Ref Mean Fraction Value	Integrated Test #2 **C Img (m)** / S Ref / B Ref Mean Fraction Value	P Value
Sunlit Crop	0.31	0.26	0.00
Shadowed Crop	0.33	0.37	0.00
Sunlit Background	0.35	0.37	0.00

Table 5-8 Paired-samples T-test of integrated endmember SMA test #3 & #4 for all crop types. Note: Reference (Ref) and image (Img) automatically derived (a) or manually derived (m) endmembers shown for sunlit crop image endmember (C), shadowed crop (S), sunlit background (B). Bold text highlights the endmember that was substituted.

SMA Fractions for all crop types (n=80)	Integrated Test #3 Ref C / S Ref / **B Img (a)** Mean Fraction Value	Integrated Test #4 Ref C / S Ref / **B Img (m)** Mean Fraction Value	P Value
Sunlit Crop	0.17	0.20	0.00
Shadowed Crop	0.35	0.43	0.00
Sunlit Background	0.47	0.37	0.00

The approach to the comprehensive set of integrated endmember SMA tests involved various combinations of both the reference and manually derived image endmembers (Figure 5-7). Results for the integrated endmember SMA tests are shown by crop type in Tables 5-9 though 5-11. In all of the integrated endmember SMA tests for the peas (Table 5-9), the highest r^2 value for predicting pea biomass was both the image and the reference sunlit background fraction with an r^2 of 0.62 (SE = 173.63 to 176.39 g/m^2). The image and reference sunlit crop fractions also performed similarly in the first two integrated tests with an r^2 of 0.58 (SE = 182.94 g/m^2). In all of the tests, the image and reference sunlit crop fraction had the highest r^2 value for predicting pea LAI (r^2 = 0.57 to 0.58, SE = 0.35 to 0.36).

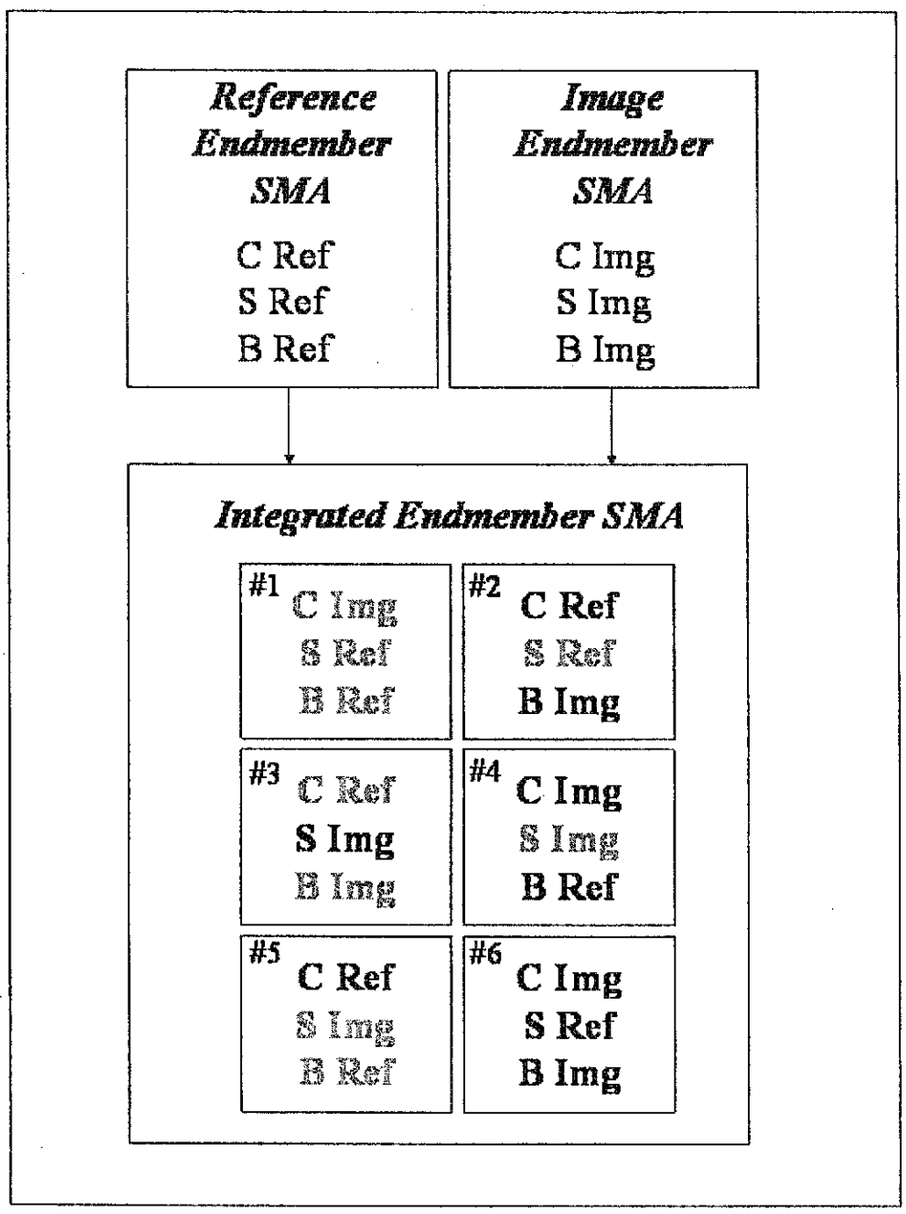

Figure 5-7 Flow diagram illustrating the different integrated endmember sets tested for the reference (Ref) and image (Img) cases for sunlit crop (C), shadowed crop (S), and sunlit background (B) endmembers. Bold text highlights the endmember that was substituted from the previous entry.

Table 5-9 Linear regression analysis results for integrated SMA prediction of LAI and biomass of pea crop based on the magnitude of coefficient of determination (r^2), the standard error (SE), and F-statistic (F). Note: "*" indicates not statistically significant at the 95% percent confidence level. Bold text highlights the endmember that was substituted from the previous entry and the highest r^2 value per test.

SMA Fractions Pea Crop	Biomass			LAI		
	r^2	SE	F	r^2	SE	F
Integrated Test #1						
Image Sunlit Crop	0.58	182.94	29.78	**0.58**	0.36	29.92
Reference Shadowed Crop	0.02	277.84	0.45*	0.12	0.51	3.05*
Reference Sunlit Background	**0.62**	174.09	35.18	0.50	0.39	22.31
Integrated Test #2						
Reference Sunlit Crop	0.58	182.96	29.77	**0.58**	0.36	30.38
Reference Shadowed Crop	0.55	188.61	26.71	0.38	0.43	13.39
Image Sunlit Background	**0.62**	173.63	35.48	0.53	0.38	24.60
Integrated Test #3						
Reference Sunlit Crop	0.52	194.49	23.81	**0.57**	0.36	29.47
Image Shadowed Crop	0.55	188.75	26.64	0.38	0.43	13.37
Image Sunlit Background	**0.62**	174.00	35.24	0.51	0.38	23.36
Integrated Test #4						
Image Sunlit Crop	0.55	188.74	26.65	**0.58**	0.36	29.85
Image Shadowed Crop	0.02	277.70	0.47*	0.12	0.51	3.13*
Reference Sunlit Background	**0.60**	176.39	33.70	0.47	0.40	19.53
Integrated Test #5						
Reference Sunlit Crop	0.55	188.80	26.61	**0.57**	0.36	29.47
Image Shadowed Crop	0.22	248.17	6.14	0.06	0.53	1.48*
Reference Sunlit Background	**0.62**	173.88	35.32	0.50	0.39	22.22
Integrated Test #6						
Image Sunlit Crop	0.57	183.10	29.69	**0.58**	0.35	30.60
Reference Shadowed Crop	0.35	226.06	11.91	0.17	0.50	4.41
Image Sunlit Background	**0.61**	174.20	35.11	0.51	0.38	23.21

Table 5-10 shows the integrated endmember SMA tests for canola. The highest r^2 value for predicting canola biomass was the image and reference shadowed crop fractions in the first and fourth integrated test with an r^2 of 0.85 (SE = 402.22 to 403.06 g/m^2). The image and reference sunlit crop fractions were similar in their prediction of canola biomass with r^2 of 0.80 (SE = 456.79 to 459.00 g/m^2). In all of the tests, the highest r^2 value for predicting canola LAI was both the reference and image sunlit crop fractions with an r^2 of 0.60 to 0.61 (SE = 0.72). However, the image and reference sunlit

background fractions performed similarly as predictors of canola LAI (r^2 of 0.56 to 0.59, SE = 0.74 to 0.76).

Table 5-10 Linear regression analysis results for integrated SMA prediction of LAI and biomass of canola crop based on the magnitude of coefficient of determination (r^2), standard error (SE), and F-statistic (F). Note: "*" indicates not statistically significant at the 95% percent confidence level. Bold text highlights the endmember that was substituted from the previous entry and the highest r^2 value per test.

SMA Fractions Canola Crop	Biomass			LAI		
	r^2	SE	F	r^2	SE	F
Integrated Test #1						
Image Sunlit Crop	0.80	457.13	80.70	**0.61**	0.72	30.81
Reference Shadowed Crop	**0.85**	402.22	110.07	0.60	0.73	29.39
Reference Sunlit Background	0.73	537.72	52.78	0.58	0.74	27.87
Integrated Test #2						
Reference Sunlit Crop	**0.80**	459.00	79.88	**0.60**	0.72	30.45
Reference Shadowed Crop	0.59	654.12	29.18	0.51	0.80	20.86
Image Sunlit Background	0.74	521.25	57.45	0.58	0.74	28.15
Integrated Test #3						
Reference Sunlit Crop	**0.81**	442.54	87.45	**0.61**	0.72	30.85
Image Shadowed Crop	0.60	651.62	29.56	0.52	0.80	21.36
Image Sunlit Background	0.73	530.75	54.70	0.58	0.74	28.00
Integrated Test #4						
Image Sunlit Crop	0.81	448.10	84.80	**0.61**	0.72	30.93
Image Shadowed Crop	**0.85**	403.06	109.53	0.59	0.73	29.25
Reference Sunlit Background	0.68	578.43	42.90	0.56	0.76	25.86
Integrated Test #5						
Reference Sunlit Crop	**0.81**	447.21	85.22	**0.61**	0.72	31.03
Image Shadowed Crop	0.05	1001.78	0.97*	0.00	1.15	0.03*
Reference Sunlit Background	0.73	530.43	54.79	0.59	0.74	28.37
Integrated Test #6						
Image Sunlit Crop	**0.80**	459.07	79.85	**0.60**	0.72	30.49
Reference Shadowed Crop	0.66	598.94	38.66	0.38	0.91	12.01
Image Sunlit Background	0.72	539.31	52.35	0.58	0.75	27.37

Similar to the results of the vegetation indices and the previous SMA results, there was no significant relationship between the integrated SMA fraction results and the ground based biomass measurements of the wheat crop (Table 5-11). The highest r^2

value for predicting wheat LAI was both the image and reference sunlit crop fractions in integrated test one, two and six the with an r^2 of 0.71 (SE = 0.23). The remaining integrated tests showed a similar result for sunlit crop fraction with an r^2 range of 0.66 to 0.67 (SE = 0.25).

Table 5-11 Linear regression analysis results for integrated SMA prediction of LAI and biomass of wheat crop based on the magnitude of coefficient of determination (r^2), the standard error (SE), and F-statistic (F). Note: "*" indicates not statistically significant at the 95% percent confidence level. Bold text highlights the endmember that was substituted from the previous entry and the highest r^2 value per test.

SMA Fractions Wheat Crop	Biomass			LAI		
	r^2	SE	F	r^2	SE	F
Integrated Test #1						
Image Sunlit Crop	0.01	177.75	0.25*	**0.71**	0.23	78.16
Reference Shadowed Crop	0.02	176.96	0.54*	0.11	0.41	4.12
Reference Sunlit Background	0.04	174.67	1.40*	0.40	0.33	21.26
Integrated Test #2						
Reference Sunlit Crop	0.01	177.61	0.30*	**0.71**	0.23	78.84
Reference Shadowed Crop	0.04	174.96	1.29*	0.01	0.43	0.47
Image Sunlit Background	0.05*	173.57	1.82	0.46	0.32	27.64
Integrated Test #3						
Reference Sunlit Crop	0.00	178.09	0.13*	**0.67**	0.25	65.07
Image Shadowed Crop	0.04	175.02	1.26*	0.02	0.43	0.49
Image Sunlit Background	0.06	173.05	2.03*	0.33	0.35	16.03
Integrated Test #4						
Image Sunlit Crop	0.00	178.24	0.07*	**0.66**	0.25	61.23
Image Shadowed Crop	0.01	177.21	0.45*	0.13	0.40	4.81
Reference Sunlit Background	0.04	174.63	1.41*	0.15	0.40	5.68
Integrated Test #5						
Reference Sunlit Crop	0.00	178.23	0.07*	**0.66**	0.25	61.09
Image Shadowed Crop	0.04	175.18	1.20*	0.01	0.43	0.25
Reference Sunlit Background	0.04	174.73	1.37*	0.34	0.35	16.31
Integrated Test #6						
Image Sunlit Crop	0.01	177.67	0.28*	**0.71**	0.23	78.21
Reference Shadowed Crop	0.01	177.58	0.31*	0.25	0.37	10.83
Image Sunlit Background	0.05	173.60	1.81*	0.41	0.33	22.66

Results from the integrated endmember tests showed that both the reference and image-based endmembers for both sunlit crop and sunlit background were consistently the strongest predictors of pea LAI and biomass, and the image sunlit crop fraction for wheat LAI (Figure 5-8 and 5-10). However, in the case of the canola crop, the shadow fraction appeared to have the highest r^2 value for predicting biomass (Figure 5-9). For wheat biomass, the remote sensing imagery available for this research did not provide adequate information content. This may be due to the nadir perspective of the imagery and the architecture of the wheat plants as discussed previously. Off nadir imagery or new biomass sampling methods as implemented by CCRS in 2002, may provide more insight on this issue in the future.

In a specific application of SMA such as agriculture, the integrated approach is advantageous in that the user can distinguish why one fraction may perform better than another simply by controlling the endmember inputs (i.e. image versus reference) throughout a series of tests. Overall, the shadow component was the most variable in terms of its predictive capability for both LAI and biomass. As discussed earlier, the reference shadow endmember may not characterize the natural shadowing of plant leaves due to a loss of geometry in the sampling technique. However, the image "shadowed crop" endmember may have been a mixture of both soil and shadow, and similarly the image sunlit crop may have been a mixture of crop and shadow. The integrated results showed improvements in the predictive capability of the shadow fraction when any image-derived endmember was introduced in to the integrated test. The image endmembers may have improved the dynamics among all scene components in a three endmember SMA model, and may have better represented the reality of the crops early in

the growing season. The reality of an agricultural scene is complex early in the growing season, and the spectrally mixed image-based endmembers may better represent the interaction between all scene components (e.g. crop, shadow, soil, and residue) in comparison to their reference endmember counterparts.

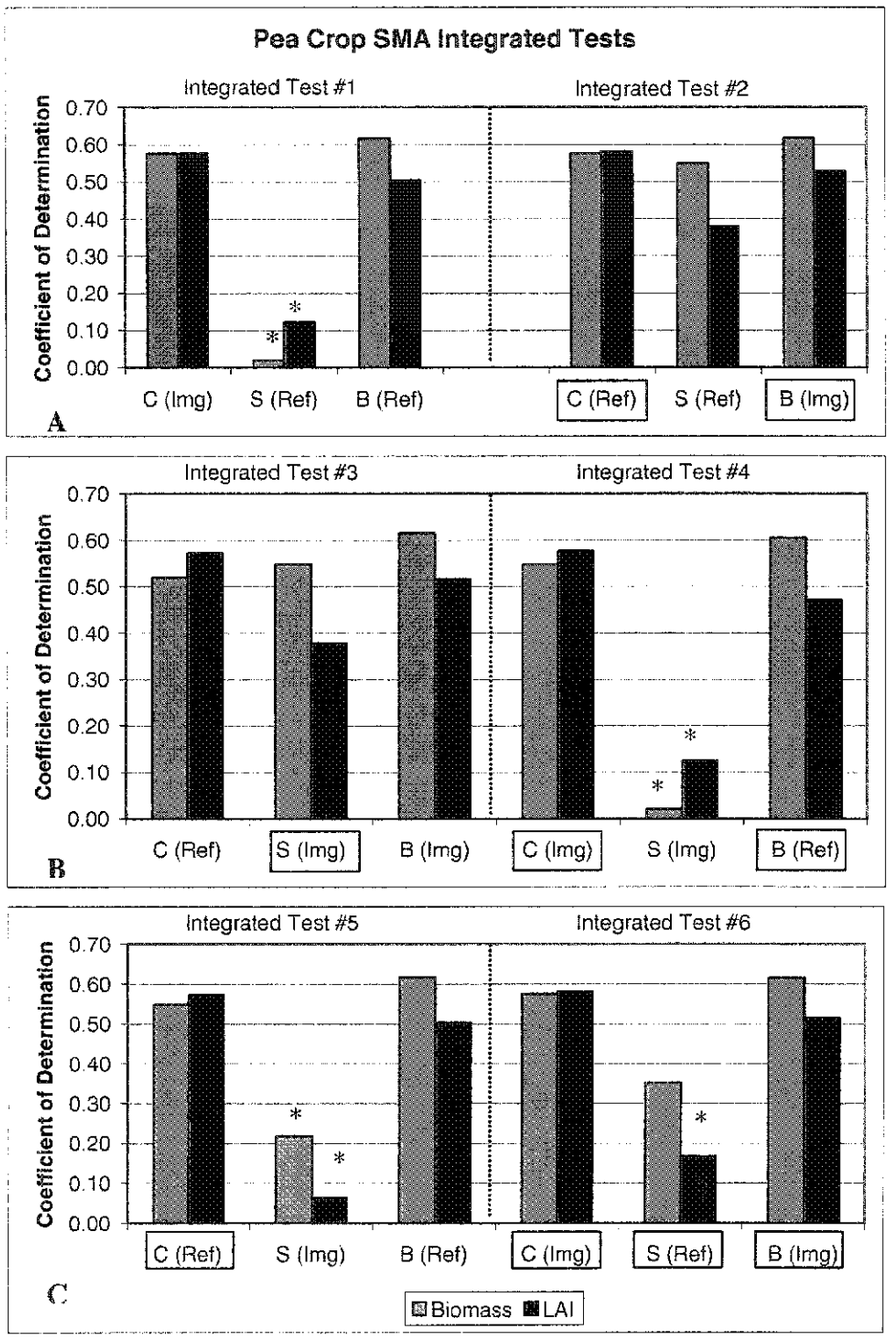

Figure 5-8 Magnitude of coefficient of determination (r^2) from SMA integrated tests for predicting biomass and LAI of pea crop. Image (Img) and reference (Ref) endmembers shown for sunlit crop(C), shadowed crop (S), sunlit background (B) fractions. Boxes highlight the endmember that was substituted from the previous entry. Note:* indicates not statistically significant at the 95% confidence level.

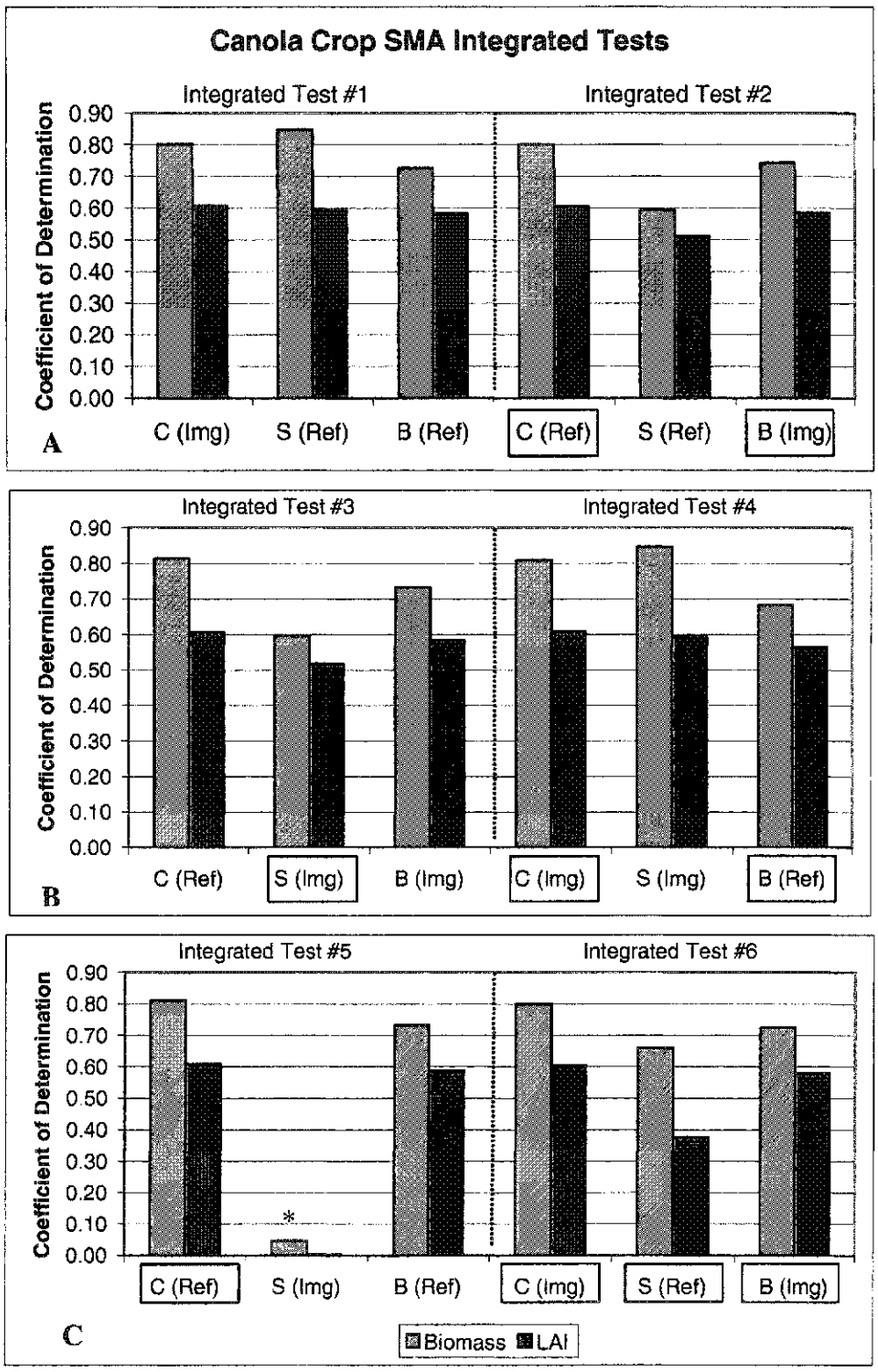

Figure 5-9 Magnitude of coefficient of determination (r^2) from SMA integrated tests for predicting biomass and LAI of canola crop. Image (Img) and reference (Ref) endmembers shown for sunlit crop(C), shadowed crop (S), sunlit background (B) fractions. Boxes highlight the endmember that was substituted from the previous entry. Note: "*" indicates not statistically significant at the 95% confidence level.

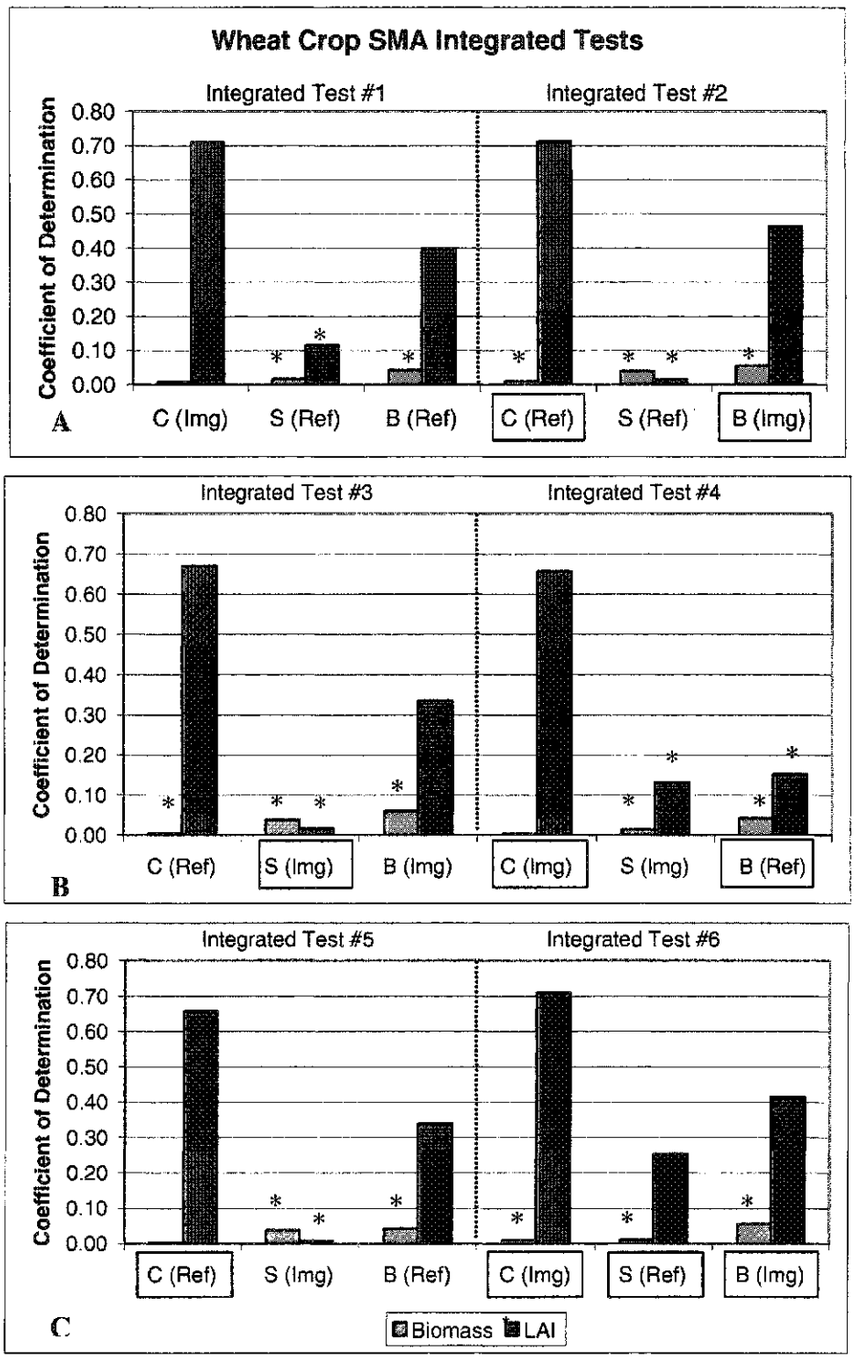

Figure 5-10 Magnitude of coefficient of determination (r^2) from SMA integrated tests for predicting biomass and LAI of wheat crop. Image (Img) and reference (Ref) endmembers shown for sunlit crop(C), shadowed crop (S), sunlit background (B) fractions. Boxes highlight the endmember that was substituted from the previous entry. Note: "*" indicates not statistically significant at the 95% confidence level.

5.5 Discussion

In this discussion it is important to recognize the practical considerations of the new SMA method versus the conventional two band VIs. The context of the discussion involves several perspectives: (i) what are the advantages to SMA for predicting biophysical parameters, (ii) what investment of resources and time is required to realize these advantages, (iii) beyond biophysical prediction what other information does SMA provide that cannot be derived from VIs, (iv) what prospects exist to further improve the SMA approach used in this research, and (v) how might SMA be applied in site-specific agriculture throughout the growing season and beyond the early growing season conditions presented in this study.

The advantages of implementing sustainable agricultural practices, and enabling technologies such as remote sensing, are driven by the ability to distinguish different contributions of various agricultural scene components. Separating remote sensing imagery into relevant and irrelevant information for the prediction of biophysical parameters using SMA could enhance the techniques farmers currently use in site-specific agriculture. One of the primary driving forces behind site-specific agriculture is the ability to define management zones based on crop performance and allow for more cost-effective and environmentally sound use of seasonal inputs (e.g. fertilizer and chemicals). In the future, if sub-pixel LAI and biomass mapping can more accurately define crop yield in the growing season at a local scale, then this could potentially help farmers and agriculture economists market crops internationally, more competitively, and prior to harvest.

The advantage of using a relatively new image processing methods such as SMA, is largely dependent on the amount of resources and time required. For example, if image derived endmembers perform adequately in agricultural applications of SMA then the processing time and resources required for SMA are reduced because there is no need for reference endmembers (i.e. labour intensive ground-based measurements). There are also other practical considerations regarding the radiometric and atmospheric correction of the imagery. If image endmembers perform adequately as predictors of biophysical parameters, then image radiometric correction is not required prior to the use of SMA (Adams et al., 1993), and thus the image pre-processing required for SMA would be the same as with VIs.

The advantages of implementing SMA go beyond the prediction of biophysical parameters. The spatial benefits of SMA should be considered in comparison to more conventional methods such as VIs that do not provide sub-pixel information. SMA fractions could be used as maps that only define the crop, not the soil, or residue, or perhaps other types of unwanted vegetation such as weeds in the future. Omitting irrelevant portions of the image may in turn increase the spatial accuracy of creating management zones that are then used in site-specific application of crop inputs (i.e. chemicals and fertilizer application strategies). For example, quantifying "crop only" pixels, or pixels which meet an end-users' threshold (e.g. a farmer decides that only pixels with less than 50% crop will be considered for application) could lead to more accurate application and spatial distribution of crop inputs.

This research presents a very preliminary approach to SMA, for three specific crop types, early in the growing season and for one geographic location. To understand the

full potential of SMA in agriculture other sensors should be tested for multiple dates and locations, and new studies should include other crop types with a variety of SMA algorithms. Throughout the course of this discussion references will be made which suggest other methods for expanding the use and flexibility of SMA in agriculture.

For each individual crop type and biophysical parameter (biomass and LAI) Figure 5-11 to 5-15 summarizes the most significant results for each approach. Each figure shows the magnitude of the coefficient of determination (r^2) for the prediction of biomass and LAI for each crop type, and provides a visual comparison of the best results obtained from different types of endmember sets (reference, image and integrated), and the different VIs.

5.5.1 Biomass Prediction by Crop Type

Figure 5-11 summarizes the performance of all of the remote sensing methods used in this research for the prediction of pea biomass. The highest r^2 value for predicting pea biomass in the VIs was the SR (r^2 of 0.66), although the GDVI performed very similarly in predicting pea biomass (r^2 of 0.64). The reference, image and integrated endmember SMA approaches showed that both the reference and image sunlit background fraction were good predictors of pea biomass (r^2 of 0.61 to 0.62). In this instance, both the conventional VI and the SMA approach performed very similarly in predicting pea biomass early in the growing season. Practical considerations may dictate that it is not advantageous to use SMA for pea biomass prediction early in the growing season, unless the objective is to obtain an improved spatial map that shows only the sunlit crop component for crop input management.

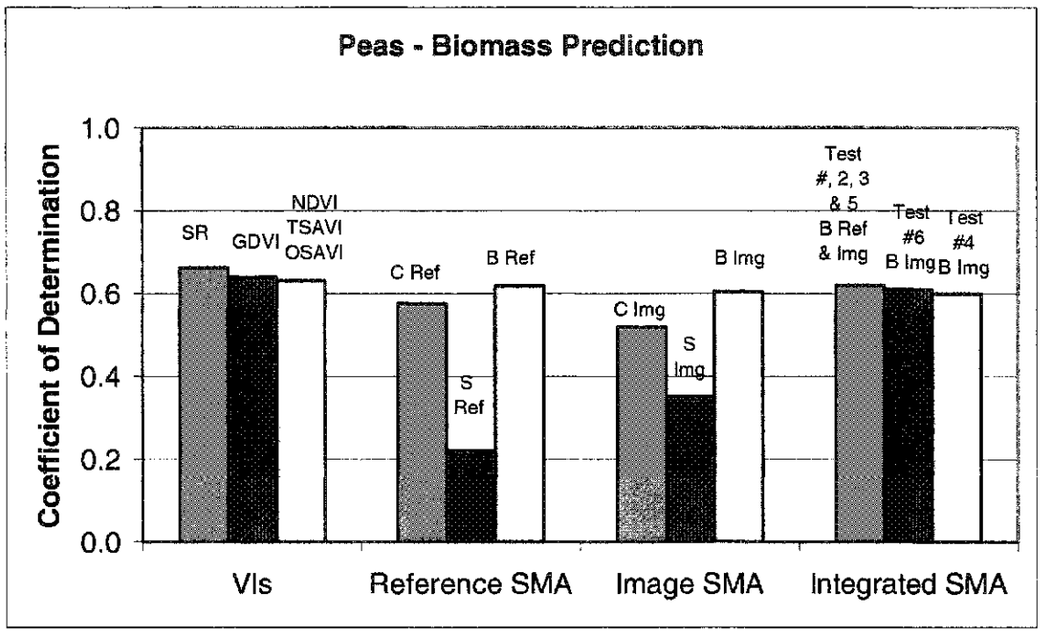

Figure 5-11 Summary of results for the prediction of pea biomass using remote sensing.

Figure 5-12 summarizes the performance of all of the remote sensing methods used in this research for the prediction of canola biomass. The highest r^2 value for predicting canola biomass was both the image and reference shadowed crop fractions (r^2 of 0.85) from integrated test one and four. However, the reference or image sunlit crop fraction in all of the SMA tests was also a good predictor of canola biomass (r^2 of 0.80 to 0.81). Comparatively, all of the VIs predicted canola biomass with an r^2 of 0.75 to 0.77. Overall, the shadow fraction provided an improvement in r^2 of 0.08 to 0.10 over all of the conventional VIs used to predict canola biomass. As a result, the integrated endmember approach does offer an advantage because not all of the endmembers are reference (more labour intensive), and some endmembers can be selected from the imagery. In the future, this approach may offer the most flexibility, especially when the development of national reference spectral libraries may be a long and complex task for agriculture.

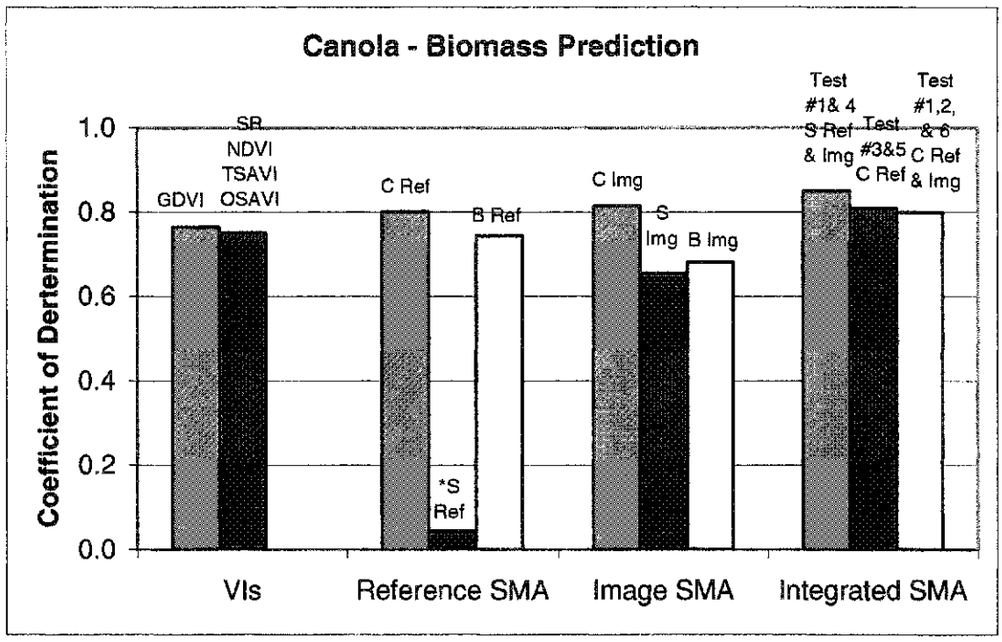

Figure 5-12 Summary of results for the prediction of canola biomass using remote sensing. Note"*" not statistically significant at the 95% confidence level.

In the case of the wheat crop, and biomass prediction, there was no statistically significant relationship to any of the remote sensing methods tested in this research. As discussed previously in section 5.3, this may be due to (i) the architecture of the wheat plant, and / or (ii) the method used to collect the ground based biomass data.

5.5.2 LAI Prediction by Crop Type

Figure 5-13 summarizes the performance of all of the remote sensing methods used in this research for the prediction of pea LAI. The highest r^2 value for predicting pea LAI was the reference and image sunlit crop fraction from all SMA tests (r^2 of 0.57 to 0.58). The highest r^2 value for predicting pea LAI from the VIs was the OSAVI (r^2 of 0.50). The relatively new SMA method provided an improvement in r^2 of 0.07 to 0.08 for pea LAI prediction early in the growing season. This meaningful level of improvement may warrant the implementation of SMA over conventional methods for

pea LAI prediction early in the growing season. These results also indicate that further analysis should be done later in the growing season to understand the full potential of SMA as an improved spatial management tool.

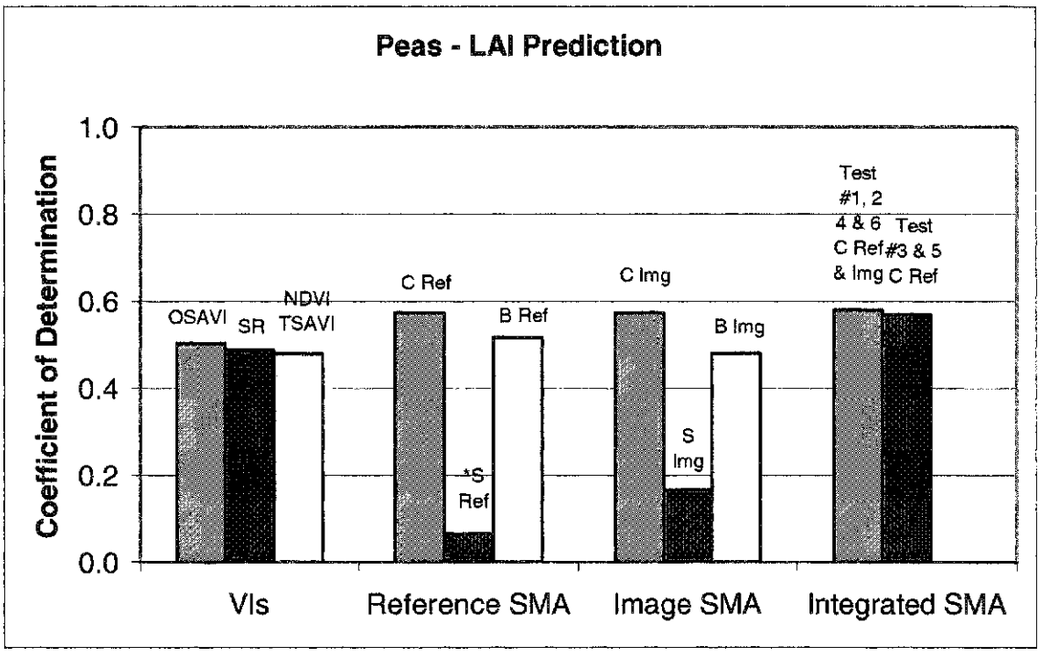

Figure 5-13 Summary of results for the prediction of pea LAI using remote sensing. Note"*" not statistically significant at the 95% confidence level.

Figure 5-14 summarizes the performance of all of the remote sensing methods used in this research for the prediction of canola LAI. The highest r^2 value for predicting canola LAI was the GDVI vegetation index with r^2 of 0.69. In all of the SMA approaches, the highest r^2 values for predicting canola LAI were the reference and image sunlit crop fractions (r^2 of 0.60 to 0.61). In this case, the conventional method was a better predictor of canola LAI. SMA as a predictive tool may not be advantageous for canola early in the growing season unless the objective is to obtain an improved spatial map that shows only the sunlit crop component for crop input management.

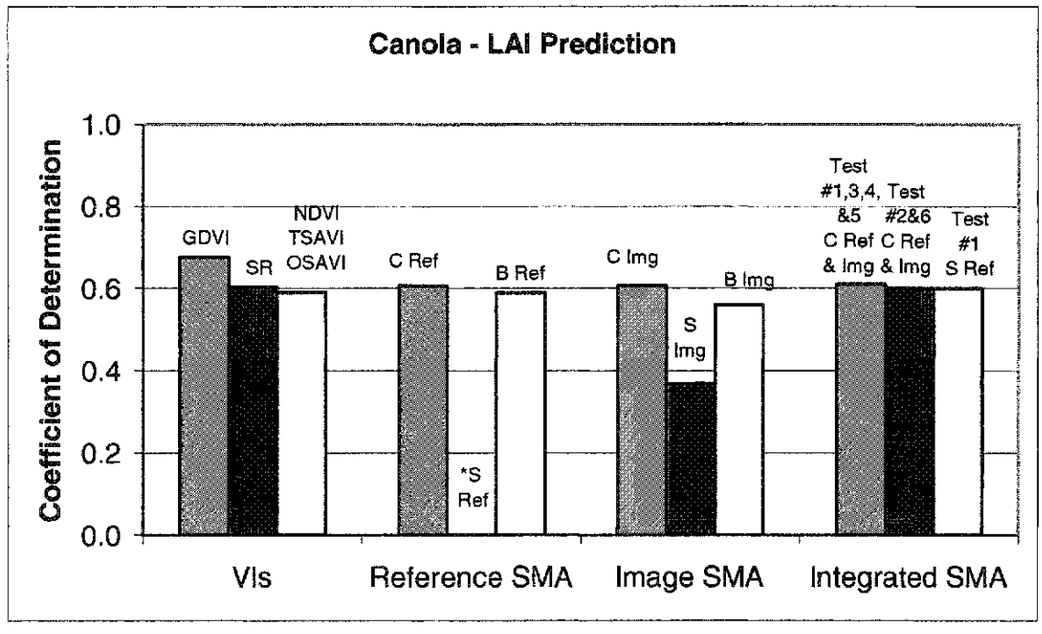

Figure 5-14 Summary of results for the prediction of canola LAI using remote sensing. Note"*" not statistically significant at the 95% confidence level.

Figure 5-15 summarizes the performance of all of the remote sensing methods used in this research for the prediction of wheat LAI. The highest r^2 value for predicting wheat LAI was obtained from both the reference and image sunlit crop fraction (r^2 of 0.71) and these results included three different integrated SMA tests (one, two and six). The highest r^2 value for predicting wheat LAI using VIs was the SR (r^2 of 0.65). Overall, the sunlit crop fraction from SMA provided an improvement in r^2 of 0.06 over the conventional VI approach as a predictor of wheat LAI. These early growing season results indicate that the implementation of SMA as an improved management tool may be advantageous for wheat LAI prediciton. Image endmembers performed adequately in this case and therefore reduces the need for labour intensive reference endmembers and image correction as input into the SMA algorithm.

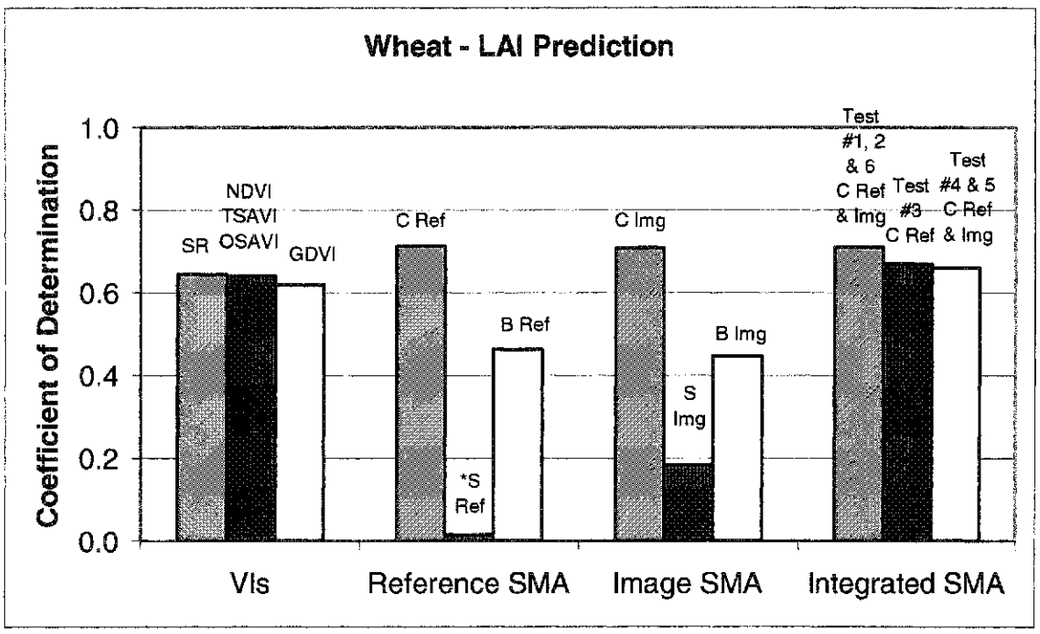

Figure 5-15 Summary of results for the prediction of wheat LAI using remote sensing. Note"*" not statistically significant at the 95% confidence level.

5.5.3 Summary of Results for All Crop Types

Figures 5-16 and 5-17 provide a useful and graphic summary of the best results from each remote sensing method for predicting biomass and LAI for all three crop types. These figures are most useful for deciphering which method (new or conventional) was the most advantageous in predicting crop biophysical parameters. For canola, SMA provided an improved means for biomass prediction, whereas conventional methods appeared to be satisfactory in predicting pea biomass (Figure 5-16). For wheat there was no relationship between any of the remote sensing methods and biomass, but the results show that SMA provided an improved means for predicting wheat LAI (Figure 5-17). The conventional method appeared to be sufficient in predicting canola LAI, whereas SMA provided an improved means for predicting pea LAI.

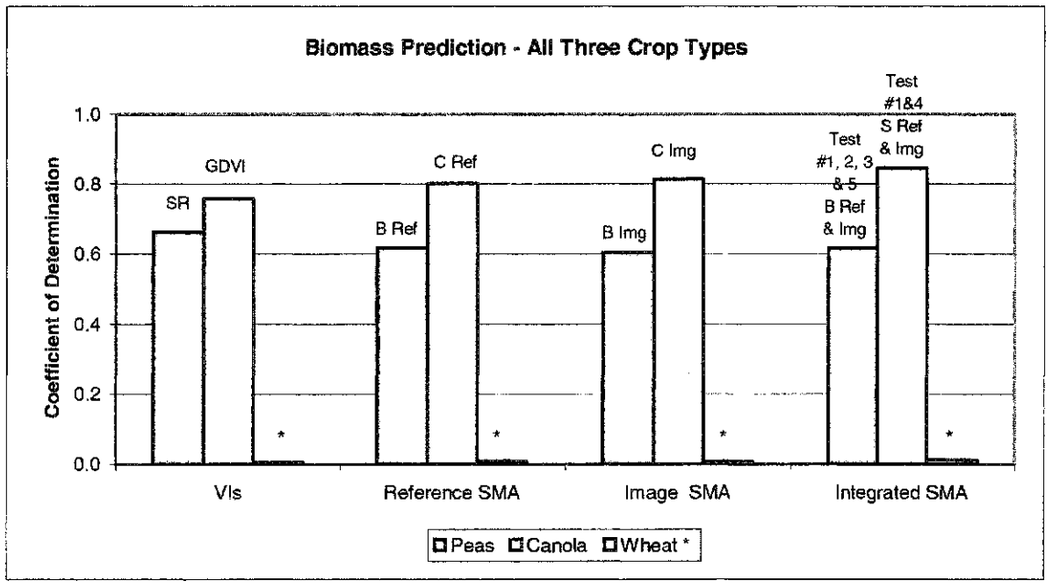

Figure 5-16 Summary of best results obtained in terms of magnitude of the coefficient of determination (r^2) for each remote sensing method tested to predict biomass for each crop type. Note: "*" not statistically significant at the 95% confidence level.

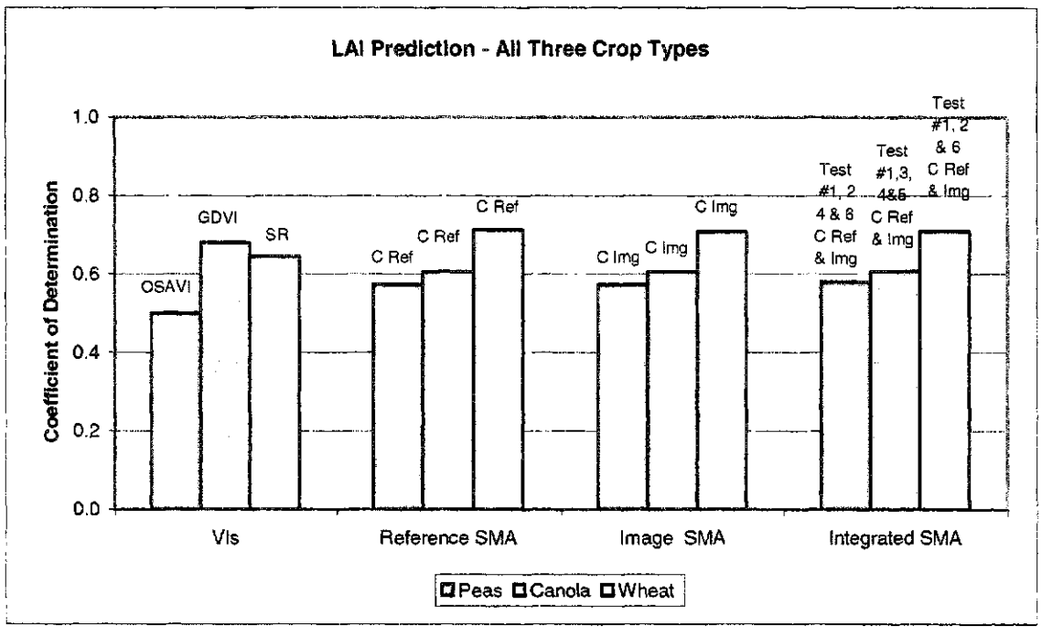

Figure 5-17 Summary of best results obtained in terms of magnitude of the coefficient of determination (r^2) for each remote sensing method tested to predict LAI for each crop type.

5.6 Chapter Summary

In this chapter, remote sensing results from VIs and SMA were presented and discussed for predicting crop biomass and LAI. The ground based biophysical data (i.e. biomass and LAI) for all 98 sample site locations were first summarized for each crop type using descriptive statistics. Several different VIs were tested as predictors of crop biophysical parameters, and then a series of SMA approaches were tested which utilised reference, image and integrated endmembers. The final section of this chapter contained a discussion that was based primarily on practical management considerations that a user should evaluate prior to implementing any of the new or conventional remote sensing methods in site-specific agriculture. In this section, the strongest overall predictors of biomass and LAI from all of the remote sensing methods were presented.

Early in the growing season, the conventional VI method appeared to be sufficient in predicting pea biomass and canola LAI. In all other cases, SMA fractions were slightly better in predicting LAI and biomass early in the growing season. The advantage of implementing one method over the other is highly dependent on the end-users' specification for crop management in site-specific agriculture. Practical considerations for the time, cost and resources required to perform each method may dictate which method is more advantageous for real time agricultural applications. Previous research (Peddle et al., 1999b; Peddle and Smith, 2003) has shown greater improvements from SMA in comparison to VIs in the middle of the growing season. This research only examined three specific crops early in the growing season, however the slight improvements shown in this work warrants further investigation of SMA at other times during the growing season.

Not only was SMA useful in predicting biophysical parameters, but this research also suggests that SMA can provide improved spatial segregation of relevant and irrelevant agronomic information (e.g. isolating the percent crop over a field, while separating the shadow component which would not likely be useful in delineating management zones for crop input application). Overall, the image endmembers were equivalent for predicting crop biophysical parameters to that of the reference endmembers in the SMA. In practical and real-time environments this is a positive result in that labour intensive field work, and image radiometric correction may be reduced or omitted entirely from the SMA pre-processing requirements. In this research, high resolution airborne imagery (5m) was used at a very detailed local scale. Future research would be required to determine if image-based endmembers would perform as well as

reference endmembers for agricultural applications that use coarser resolution imagery (e.g. Landsat 30m, or NOAA's GOES 1km visible or 4km IR) over much larger regional or national areas.

CHAPTER VI

6.0 SUMMARY AND CONCLUSIONS

6.1 Introduction

The ability to predict crop biophysical parameters using remote sensing in site-specific agriculture is important for furthering the development of spatially refined management tools. Remote sensing is a unique technology in that it provides farmers with a non-invasive and broader perspective of their crops throughout the growing season. This technology potentially provides an improved means to achieve sustainable agriculture in farm practices, and to promote basic principles of sustainability such as stewardship of land resources. Understanding and spatially defining crop variability is essential to maximize the use of costly crop inputs such as fertilizer, and pesticides. This type of spatial inventory allows the farmer to apply crop inputs to only areas of the field that require them, and in turn can reduce any negative environmental impacts (e.g. chemical run off and leaching).

This research was conducted on an experimental farm near Indian Head, Saskatchewan, Canada, and was part of a much larger multi-organizational and multi-disciplinary project undertaken at the Indian Head Agricultural Research Foundation (IHARF) to demonstrate the full potential of remote sensing in site-specific agriculture. The IHARF project was led by the Canada Centre for Remote Sensing (CCRS) with contributions from partners including Agri-Food and Agriculture Canada (AAFC) as well as a number of Canadian universities. In this study, three crops were examined early in the growing season; peas, wheat and canola. The objective of the research was to use remote sensing imagery to estimate crop biophysical parameters (LAI and biomass) by

employing a more recently developed image processing method (SMA) and a conventional image processing method (VIs). In this chapter, a summary of the results and findings are provided for the objectives identified (sections 6.2 and 6.3). The last two sections of this chapter describe the contribution of this study to the research community (section 6.4), and future research areas are suggested (section 6.5).

6.2 Summary of the Comparison between VIs and SMA for Predicting Crop Biomass and LAI

In this research, a series of VIs were used to predict biomass and LAI of peas, canola, and wheat. The VIs used were the: simple ratio (SR), green difference vegetation index (GDVI), normalized difference vegetation index (NDVI), transformed soil adjusted vegetation index (TSAVI), and the optimized soil adjusted vegetation index (OSAVI). Three approaches to SMA were implemented by varying endmember inputs, these approaches were: (i) reference, (ii) image, and (iii) integrated. Overall, the VIs performed very similarly in predicting biomass and LAI for all crop types early in the growing season. Similar to results found in forestry applications, it may be that complex interactions between scene components in an agricultural image (e.g. crop, soil, residue, and shadow) may not be differentiated by the relationship typically found in the red-NIR space of VIs (Peddle et al., 2001b). The results of this research suggest that utilizing a number of VIs early in the growing season may be empirically redundant.

In assessing which remote sensing method (SMA or VIs) was most appropriate for predicting biomass and LAI for each crop type several factors were outlined that included considerations for the investment of time and resources, as well deciphering what other advantages SMA may provide beyond biophysical prediction. The highest r^2

value for predicting pea biomass prediction was the SR vegetation index (r^2 of 0.66), whereas the highest r^2 value for predicting pea LAI was both the reference and image sunlit crop fractions from all SMA approaches (r^2 of 0.57 to 0.58). The highest r^2 value for predicting canola biomass was both the image and reference shadowed crop fractions (r^2 of 0.85), and the highest r^2 value for predicting canola LAI was the GDVI (r^2 of 0.69). There was no significant relationship between any of the remote sensing methods and wheat biomass. It is suggested that this may have been due to the architecture of the crop, and issues surrounding how the ground data was collected. However, this research did determine that the strongest predictor of wheat LAI was both the reference and image sunlit crop fractions (r^2 of 0.71) for all of the SMA approaches tested.

In general, all three approaches to SMA (i.e. reference, image and integrated endmembers) provided a slightly improved predictive tool for crop LAI and biomass early in the growing season, except in the case of pea biomass and canola LAI where the conventional VI approach was sufficient. In the reference and image SMA approaches, the sunlit crop fraction was the most consistent predictor of LAI and biomass, except in the case of the pea crop where the sunlit background fraction was a better predictor of biomass. In the integrated endmember approach to SMA, there was an improvement in the predictive capability of the shadowed crop fraction for canola biomass, but in most cases the sunlit crop fraction was consistently the best predictor of LAI and biomass.

Successful adoption of SMA in site-specific agriculture could hinge on such factors as the ability to obtain proper endmember inputs, and to a lesser extent achieving comparable processing time to that of the conventional methods (i.e. VIs). SMA fraction results that only quantify the crop (and not irrelevant contributions to the pixel signal

such as soil and residue) could be used to improve variable rate application strategies for crop inputs (e.g. fertilizers, pesticides including herbicides). In this research, SMA did provide a marginally improved tool for predicting crop LAI and biomass early in the growing season, except in the case of pea biomass and canola LAI. The image endmembers performed very similarly to the more labour intensive and spectrally pure reference endmembers. The satisfactory performance of image endmembers as predictors of crop biophysical parameters means that the complexity of SMA, and the processing time required, would be reduced since field based reference endmember collection and image radiometric correction are not required.

6.3 Conclusions

A number conclusions were made from this research:

- The variety of VIs tested for this research all performed very similarly and this suggests that implementing a series of VIs may be empirically redundant in agriculture, as has been found in forestry.
- The soil-adjusted VIs may not have been required in this research because the background was primarily residue with some bare soil, and vegetation cover was not greater than 50% therefore the sensitivity of the soil-adjusted VIs may have been minimized because there wasn't enough crop present in the imagery to induce a canopy-scattered background-reflected signal.
- Overall the results showed that image endmembers performed similarly to the reference endmembers as input for SMA. The reduction in both complexity and time required to perform SMA using image endmembers suggests this is not a confounding factor in comparison to conventional VIs.

- SMA fraction maps can be produced using all three approaches to SMA. This type of sub-pixel output could provide a more spatially refined management tool for site-specific agriculture compared to the conventional methods.

6.4 Contributions to Research

This research has made several scientific contributions to the research community. The theoretical motivation for this research was to evaluate a relatively new remote sensing method (SMA) against conventional methods to improve on what spatial tools are available for farmers who practice site-specific agriculture. In theory, if a farmer can spatially predict crop biomass and LAI early in the growing season then opportunity exists to try and improve deficient regions of the field. As a result, the farmer could better understand what regions of a particular field are worth investing in economically. If a farmer is making better site-specific decisions on where to place crop inputs (e.g. fertilizers and pesticides) then it is likely that the crop is using those inputs more efficiently. If the crop is using inputs more efficiently then more environmentally sound and sustainable practices are being encouraged on the farm. This thesis research has evaluated improved remote sensing management tools that can further the development of existing site-specific management programs.

Methodological contributions of this research stem from the fact that this work has addressed two important remote sensing issues that have not been explicitly dealt with in the literature: (i) evaluating different inputs to linear SMA for agriculture, and (ii) the use of several spectral bands from airborne hyperspectral imagery in the early part of the growing season. A variety of endmember approaches to SMA were evaluated (e.g. reference, image and integrated) as well as two different software programs. This

research also dealt with several pre-processing issues due to the use of two different ground based sensors in conjunction with the corresponding hyperspectral imagery. The purpose of testing a variety of approaches to the new remote sensing image analysis method was to establish the most advantageous approach for site-specific agricultural applications. It should be noted that this research expanded on previous work done in agriculture by predicting the biophysical parameters of three prominent crop types found in the prairie region of western Canada. However, these crop types were specific to one geographic location, and further tests at other locations would be needed to verify how well these methods work elsewhere.

This research not only evaluated a relatively new image processing method (SMA), but did so in a direct comparison with conventional methods (VIs). In most cases, SMA did provide slight improvements in comparison to conventional VIs for predicting biomass and LAI early in the growing season. Unlike conventional methods, SMA takes advantage of a number of spectral bands that can better characterize the spectral response of specific crop types throughout the entire electromagnetic spectrum. These empirically based findings suggest that SMA is worth investigating not only for biophysical prediction but also at a more simplistic level for spatially separating relevant and irrelevant agronomic information for farmers. SMA provides a sub-pixel analysis tool which can take full advantage of the information provided in both hyperspectral and multispectral remote sensing imagery. The results of this research were from the early part of the growing season, and suggest that further examination of SMA later in the growing season is warranted.

6.5 Future Research

Several areas for future research have been identified in this thesis. First, an evaluation of the full potential of SMA should include a multi-temporal analysis that encompasses the life cycle of the crop (i.e. multiple image acquisitions throughout the growing season). There are well known limitations with the use of VIs later in the growing season because the ratio of red to near infrared approaches limiting values asymptotically as LAI increases (Wiegand and Richardson, 1984). The relationship between VIs and LAI, photosynthetic activity, and yield are not as strong in high LAI conditions (Wiegand and Richardson, 1990), thus SMA may provide a tool for accurately quantifying agricultural image components later in the growing season. Earlier work by Peddle and Smith (2003) showed improvements using SMA in the middle portion of the growing season for potatoes. However, new research should be expanded to include other crop types in a variety of geographic locations.

Secondly, this research utilized a SMA algorithm and software described in Shimabukuro and Smith (1991) that was an accessible and well documented starting point for agricultural applications, however, it did not readily produce fraction maps. Future research should evaluate how fraction maps can be easily transferred into site-specific management strategies (e.g. as input into a GIS) especially for those strategies where the objective is variable rate application of crop inputs such as fertilizer and pesticides. This could involve conventional image classification of fraction maps, or simple thresholding techniques that can provide the analyst with a method of implementing specific intervals. For example, fraction maps could be produced with a legend or look-up table applied that isolates regions of the field with only pixels that have

greater than or less than 50% contribution of sunlit crop. This type of spatial segregation focuses the attention of field managers to discrete regions of the field which require immediate attention (stressed areas with less than 50% crop) and those regions that may not require any further crop inputs (above 50% crop).

Apart from the spatial advantages of SMA, this research only examined a three endmember SMA algorithm, however, it may require modification for specific agricultural applications. This research assumed that the interaction of solar energy within the crop canopy was a linear problem. More comprehensive and additional algorithms may be worth investigating such as the use of more than three endmembers, and possibly more involved non-linear approaches. As highlighted in Chapter 3, there are a variety of SMA algorithms available, as well as methods for the optimization of the endmember selection process.

The development of analysis techniques using hyperspectral data, especially SMA, have emerged out of the field of spectroscopy and therefore focus on the spectral nature of the data (Plaza et al., 2002). In the case of the image endmember approach to SMA, typically the analyst will examine the spectral characteristics of the imagery prior to the selection of endmembers and very little consideration for spatial variability is explored. However, in agriculture there is explicit examination of spatial variability especially with the objective of creating management zones. Plaza et al. (2002) established a method based on mathematical morphology that recognized the selection of endmembers is a non-linear task, and requires a "local-to-global" approach in which the spatial correlation of pixels is examined in addition to spectral purity. The spatial context of the Plaza et al. (2002) work is based on local operators, which use pixel neighborhoods to replace an

anomalous pixel with a value that meets specific conditions (i.e. in the endmember case this is criteria for spectral purity). This approach is based on image endmember selection that in this research proved to be more than adequate. In site-specific agriculture, one of the main objectives is to produce or use existing 'management zone maps' which can be implemented and customized over time to treat the crop according to production limitations. Spatial considerations for endmember selection could be provided in agricultural applications of SMA by using management zones as input into this selection process.

Another suggestion for the future of SMA in agricultural research is modelling. Prospective models may ingest SMA results or at a minimum help in modelling more effective SMA inputs such as endmembers. Modelling could take the form of deriving endmembers in n-dimensional space from image-based spectral inputs for deriving more spectrally pure endmembers that are also known in the literature as virtual endmembers (Tompkins et al., 1997). Another related area of research may involve canopy reflectance models and associated model inversions (e.g. SAIL, PROSPECT, and NADI). These models can use endmember inputs to model canopy reflectance, and can be inverted to obtain canopy level biochemical and biophysical parameters of the crop such as chlorophyll content and LAI (Jaquemoud et al., 2000).

Geometric-optical reflectance models may provide a mechanism for defining agricultural regions more effectively. Geometric-optical models have been used primarily in forestry, but may have promise in other vegetation applications such as agriculture where the interaction of scene components is somewhat similar. For example, crops are much smaller than trees but on a micro-scale have complex backgrounds with

similar sun-surface-sensor geometry that can be modeled. Geometric-optical models can be used to study the effects of solar zenith angle on mixture fractions (Peddle et al., 1999a). Modelling of this nature may be useful for multi-temporal studies in agriculture where imagery is obtained at different times in the growing season, and at different times of the day, and therefore require correction for bi-directional reflectance factors (BDRF). More advanced geometric-optical models such as the Multiple Forward Mode 5-Scale approach could provide agriculture with structural (e.g. crop height and density) and biophysical information (e.g. LAI) that is obtained explicitly from the model and avoids the necessity for empirically driven relationships (Peddle 2003a,b,c).

REFERENCES CITED

Adams, J.B. and M.O. Smith, 1986. Spectral Mixture modeling: A new analysis of rock and soil types at the Viking Lander 1 Site. Journal of Geophysical Research, 91(B8): 8098-8112.

Adams, J.B. M.O. Smith, A. R. Gillespie. 1993. Imaging spectroscopy interpretation based on spectral mixture analysis. *In* Remote Geochemical Analysis: Chapter 7 Elements and Mineralogical Composition. C.M. Peters and P. Englert, editors. LPI and Cambridge University Press, Cambridge, pp 145-166.

Agriculture and Agri-Food Canada, 1976. Regina research station and Indian Head Experimental Farm Research Highlights. Unpublished document.

Analytical Spectral Devices (ASD) Inc., 2001. FieldSpec® Pro Technical Guide. Boulder, Colorado. Variously Paged.

Analytical Spectral Devices (ASD) Inc., 2003. Product Description. Retrieved January, 2003. WWW: http://www.asdi.com/asdi_t2_pr_sp_fsp.html

Asner, G.P., and D.B. Lobell, 2000. A biogeophysical approach for automated SWIR unmixing of soils and vegetation. Remote Sensing of Environment, 74: 99-112.

Bannari, A., D. Morin, and F. Bonn, 1995. A review of vegetation indices. Remote Sensing Reviews, 13:95-120.

Baret, F., G. Guyot, and D. J. Major, 1989. TSAVI: A vegetation index which minmizes soil brightness effects on LAI and APAR estimation. In proceedings of 12th Canadian Symposium on Remote Sensing, Ottawa, Canada, pp 1355-1358.

Baret and Guyot, 1991. Potentials and limits of vegetation indices for LAI and PAR assessment. Remote Sensing of Environment, 35:161-173.

Bateson, C.A., G.P. Asner, and C.A. Wessman, 2000. End member Bundles: A new approach to incorporating end member variability into Spectral Mixture Analysis. IEEE Transactions on Geoscience and Remote Sensing, 38(2):1083-1094.

Batte, M.T., 2000. Factors Influencing the Profitability of Precision Farming Systems. Journal of Soil and Water Conservation. 55(1): 12-18.

Boardman, J.W., 1989. Inversion of Imaging Spectrometry Data Using Singular Value Decomposition. Proceedings, International Geoscience and Remote Sensing Symposium (IGARSS'89) and 12th Canadian Symposium On Remote Sensing, Vancouver, British Columbia, pp. 2069-2072.

Boardman, J.W., 1993. Automating spectral unmixing of AVIRIS data using convex

geometry. In Summaries of 4th Airborne Geoscience Conference (R.O. Green, Ed.) JPL Publication 93-26, Jet Propulsion Laboratory, Pasadena, CA, Vol I: 11-14.

Boardman, J.W., 1995. Analysis, understanding and visualization of hyperspectral data as convex sets in *n*-space. Proceedings, SPIE the International Society for Optical Engineering, Vol 2480: 14-22.

Boardman, J.W., and F.A. Kruse, 1994. Automated Spectral Analysis: A Geological Example using AVIRIS data. North Grapevine Mountains, Nevada. Proceedings, 10th Thematic Conference on Geologic Remote Sensing, May, Vol I: 407-418.

Borel, C.C. and S.A.W. Gerstl, 1986. Nonlinear spectral mixing models for vegetative and soil surfaces. Remote Sensing of Environment, 47: 403-416.

Brisco, B., R.J. Brown, T. Hirose, H. McNairn and K. Staenz, 1998. Precision Agriculture and the Role of Remote Sensing: A Review. Canadian Journal of Remote Sensing. 24(3): 315-327.

Brklacich, M., C.R. Bryant, and B. Smit, 1991. FORUM: Review and Appraisal of Concept of Sustainable Food Production Systems. Environmental Management. 15(1): 1-14.

Brklacich, M., C. Bryant, C., B. Veenhof, and A. Beauchesne, 1998. Implications of global climatic change for Canadian Agriculture: a review and appraisal of research from 1984 to 1997. *In* Responding to Global Climate Change: National Sectoral Issue (eds) G. Koshida and W. Avis, Environment Canada, Canada Country Study: Climate Impacts and Adaptation, v. VII, p. 219-256.

Broge, N.H. and E. Leblanc, 2000. Comparing the prediction power and stability of broadband and hyperspectral vegetation indices for estimation of green leaf area index and canopy chlorophyll density. Remote Sensing of Environment, 76: 156-172.

Bullock, P., B. Brisco, and T. Hirose, 2000. Remote Sensing for Improving Crop Management. Proceedings, First International Conf. on Geospatial Information in Agriculture and Forestry. Lake Buena Vista, Florida, USA. June 1-3/98. ERIM International. Vol II: 487-494.

Buschman, C. and E. Nagel, 1993. In vivo spectroscopy and internal optics of leavses as basis for sensing of vegetation. International Journal of Remote Sensing, 14(4): 711-722.

Campbell, J.B., 1996. Introduction to Remote Sensing. Guilford Press, New York.

Carlson, T.B., and D.A. Ripley, 1997. On the relationship between NDVI, Fractional

Vegetation Cover, and Leaf Area Index. Remote Sensing of Environment, 62:241-252.

Carter, G.A., 1992. Responses of Leaf Spectral Reflectance to Plant Stress. American Journal of Botany. 80(3): 239-143.

Casals-Carrasco, P., S. Kubo, and B.B. Madhavan, 2000. Application of spectral mixture analysis for terrain elevation studies. International Journal of Remote Sensing, 21(16):3039-3055.

CCRS, 2000. SASK2000 Precision Farming Project: Methodology and Objectives. Unpublished document created by Canada Centre for Remote Sensing (CCRS), November 2000.

Chabrillat, S., Goetz, A.F.H, Krosley, L., and H.W. Olsen, 2002. Use of hyperspectral images in the identification and mapping of expansive clay soils and the role of spatial resolution. Remote Sensing of Environment, 82: 431-445.

Champagne, C and H. McNairn, 2003. Personal communication regarding wheat biomass. Feb 17, 2003.

Chang, C.I., 1998. Further results on relationship between Spectral Unmixing and Subspace Projection. IEEE Transactions on Geoscience and Remote Sensing, 36(3): 1030-1032.

Chapin III, F.S., 1991. Integrated responses of plants to stress. Bioscience, 41: 29-36.

Chen, J.M., 1996. Evaluation of vegetation indices and a modified simple ratio for boreal applications. Canadian Journal of Remote Sensing. 22(3):229-242.

Chen, J.M. and J. Cihlar, 1995. Plant canopy gap size anlaysis theory for improving optical measurements of leaf area index. Applied Optics, 34: 6211-6222.

Chen, J.M., and T.A. Black, 1992. Defining leaf area index for non-flat leaves. Plant, Cell and Environment, 15:421-429.

Chen, J.M. and J. Cihlar, 1996. Retrieving leaf area index of boreal conifer forests using Landsat TM Images. Remote Sensing of Environment, 55:153-162.

Chen, J.M., P.M. Rich, S.T. Gower, J.M. Norman and S. Plummer, 1997. Leaf area index of boreal forests: theory, techniques, and measurements. Journal of Geophysical Research. 102(D24): 59,429-29,443.

Chen, J.M., and S.G. Leblanc, 1998. LAI measurements in deciduous and coniferous forests with two optical instruments. Proceedings, Scaling and Modelling in Forestry: Applications in Remote Sensing and GIS. University of Montreal,

Montreal, Quebec, March 19-21, pp119-125.

Cihlar, J., L. St-Laurent, and J.A. Dyer, 1991. Relation between the Normalized Vegetation Indices and Ecological Variables. Remote Sensing of Environment, 35: 279-298.

Cloutis, E.A., 1996. Hyperspectral geological remote sensing: evaluation of analytical techniques. International Journal of Remote Sensing, 17(12): 2215-2242.

Daughtry, C.S.T., 1990. Direct Measurements of Canopy Structure. Remote Sensing Reviews. 5(1): 45-60.

Daughtry, C.S.T., C.L. Walthall, M.S. Kim, E. Brown de colstoun, and J.E. McMurtrey III, 2000. Estimating corn leaf chlorophyll concetration from leaf and canopy reflectance. Remote Sensing of Environment, 74: 229-239.

Davidson, D.P., 2002. Sensitivity of ecosystem net primary productivity models to remotely sensed leaf area in a montane forest environment. Unpublished Master's Thesis, Department of Geography, University of Lethbridge, Lethbridge, Alberta.

Deguise, J.C., M. McGovern, H. McNairn, and K. Staenz, 1998. Spatial High resolution crops measurements with airborne hyperspectral remote sensing. 4th International Conference on Precision Agriculture, Saint Paul, Minnesota, July 19-22, pp. 1603-1608

Deguise, J.C., K. Staenz, and J. Lefebrvre, 1999. Agricultural applications of airborne hyerpspectral data: Weed Detection. Proceedings, 4th International Airborne Remote Sensing Conference and 21st Canadian Symposium on Remote Sensing: Ottawa, Canada, June 20-24, 1999. Vol. II: 352-358.

Dehaan, K.R., G.T. Vessey, D.A. Holmstrom, J.A. MacLeod, J.B. Sanderson, and M.R. Carter, 1999. Relating potato yield to the level of soil degradation using a bulk yield monitor and differential global positioning systems. Computers and Electronics in Agriculture, 23: 133-143.

Doerge, T.A., 1999. Site Specific Agriculture. Journal of Production Agriculture, 12(1): 54-61.

Earth Search Sciences Inc., 2002. About Probe-1. Retrieved January 2003. WWW: http://www.earthsearch.com/technology/frame_about_probe1.html

Elmore, A.J., J.F. Mustard, S.J. Manning, and D.B. Lobell, 2000. Quantifying Vegetation Change in Semiarid Environments: Precision and Accuracy of Spectral Mixture Analysis and the Normalized Difference Vegetation Index. Remote Sensing of Environment, 73: 87-102.

Endsley, N.H., 1995. Spectral unmixing algorithms based on statistical models. Proceedings, SPIE 1995, Vol. 2480, pp. 23-36.

Environment Canada, 1995. National Action Plan on Climate Change. Retrieved January 2003. WWW: http://www.ec.gc.ca/climate/resource/cnapcc/c3part11.html

Environment Canada, 2003. Narrative Descriptions of Terrestrial Ecozones and Ecoregions of Canada. Retrieved January, 2003. WWW: http://www.ec.gc.ca/soer-ree/English/Framework/Nardesc/TOC.cfm

ESRI (Earth Systems Research Institute), 1995. Understanding GIS – The ArcInfo Method (Version 7 for Unix and Open VMS). New York: John Wiley and Sons, pp1-11.

Franklin, J., S.D. Prince, A.H. Stahler, N.P. Hanan, and D.S. Simonett, 1991. Reflectance and transmission properties of West African savanna tress from ground radiometer measurements. International Journal of Remote Sensing, 12(6):1369-1385.

Gates, D.M., H.J. Keegan, J.C. Schleter, and V.R. Weldner, 1965. Spectral Properties of Plants. Applied Optics, 4(1) 11-20.

Geophysical and Environmental Research Corporation, 2003. GER3700™ Product Description. Retrieved January, 2003. WWW: http://www.ger.com/ground.html

Government of Canada, 2002. Canada and the Kyoto Protocol. Retrieved March 2002. WWW: http://www.climatechange.gc.ca/english/whats_new/forests_e.html

Government of Canada, 2003. Climate Change Plan for Canada. Retrieved January 2003. WWW: http://climatechange.gc.ca/plan_for_canada/plan/pdf/full_version.pdf

Goetz, A.F.H., G. Vane, J.E. Solomon, and B.N. Rock, 1985. Imaging Spectrometry for Earth Remote Sensing. Science, 228(4704): 1147-1153.

Hall, F.G., Y.E. Shimabukaro, and K.F. Huemmrich, 1995. Remote Sensing of forest biophysical structure using mixture decomposition and geometric reflectance models. Ecological Applications, 5(4): 993-1013.

Hammond, M.W., 1992. Cost analysis of variable fertility management of phosphorus and potassium for potato production in central Washington. Proceedings, Soil Specific Crop Management, pp. 213-228.

Hatfield, J.L., E.T. Kanemasu, G. Asrar, R.D. Jackson, P.J. Pinter, Jr., R.J. Reginato, and

S.B. Idso, 1985. Leaf-area estimates from spectral measurements over various planting dates of wheat. International Journal of Remote Sensing, 6(1): 167-175.

Horler, D.N.H., M. Dockray, and J. Barber, 1983. The red edge of plant leaf reflectance. International Journal Remote Sensing, 4(2):273-288.

Horwitz, H.M., R.F. Nalepka, P.D. Hyde, and J.P. Morgenstern, 1971. Estimating the proportions of objects within a single resolution element of a multispectral scanner. Proceedings, 7th International Symposium On Remote Sensing of Environment, Ann Arbor, Michigan, May 17-21, pp.1307-20.

Hu, Y.H., H.B. Lee, and F.L. Scarpace, 1999. Optimal Linear Spectral Unmixing. IEEE Transactions on Geoscience and Remote Sensing, 37(1): 639-645.

Huete, A.R., 1988. A Soil-Adjusted Vegetation Index. Remote Sensing of Environment, 25:295-309.

Ilbery, B.W., and I.R. Bowler, 1998. From Agricultural Productivism to Post Productivism. *In* B.W. Ilbery (ed) The Geography of Rural Change. Harlow, Essex, England : Longman, pp. 57-84.

IHARF, 2003. IHARF Precision Farm Website. Retrieved January, 2003. WWW: http://paridss.usask.ca/cgi-bin/p_farm/tour.pl?function=pic&id=12

Jacquemoud, S., C. Bacour, H. Poilve, and J.-P. Frangi, 2000. Comparison of four radiative transfer models to simulate plant canopies reflectance: Direct and Inverse Mode. Remote Sensing of Environment, 74: 471-481.

Johnson, R., 2000. Airborne Remote Sensing of Forest Leaf Area Index in Mountainous Terrain. MSc. Thesis, Department of Geography, University of Lethbridge, Alberta, Canada.

Khush, G.S., 1999. Green Revolution: preparing for the 21st century. Genome, 42(4): 645-655.

Khush, G.S., 2001. Green Revolution: the way forward. Nature Reviews, 2: 815-822.

Knipling, 1970. Physical and Physiological Basis for the Reflectance of Visible and Near-Infrared Radiation from Vegetation. Remote Sensing of Environment, 1(3):155-159.

Kozac, L.M., and G.A. Padbury, 1999. Soils of the IHARF Research Farm. Retrieved January, 2003.
WWW: http://paridss.usask.ca/cgi-bin/p_farm/pari.pl?function=sheet&id=8.

Labsphere, 2002. Spectralon® panel product description. Retrieved January, 2003

WWW: http://www.labsphere.com/products/products.asp?CID=37&PID=378

Leblanc, S., and J.M. Chen, 1998. LAI measurements in deciduous and coniferous forests with two optical instruments. Proceedings, Scaling and Modeling in Forestry: Applications in Remote Sensing and GIS. University of Montreal, Quebec, Canada, March 19-21, pp119-125.

Leblanc, S.G., J.M. Chen, J.R. Miller, and J. Freemantle, 1999. Compact Airborne Spectrographic Imager (CASI) Used for Mapping LAI of Cropland. Proceedings, 4th International Airborne Remote Sensing Conference and Exhibition/21st Canadian Symposium on Remoste Sensing, Ottawa, Ontario, Canada 21-24 June. Vol I.: 297-303.

Lelong, C.C.D., P.C. Pinet, and H. Poilve, 1998. Hyperspectral Imaging and Stress Mapping in Agriculture: A case study on Wheat in Beau (France). Remote Sensing of Environment, 66: 179-191.

LI-COR, 1992. LAI-2000 Plant Canopy Analyzer: Operating Manual. Lincoln, Nebraska, USA.

LI-COR, 2003a. Product Description LI-3100 Area Meter. Retrieved January, 2003. WWW: http://env.licor.com/Products/AreaMeters/3100.htm

LI-COR, 2003b. Product Description LAI-2000. Retrieved January, 2003. WWW: http://env.licor.com/Products/AreaMeters/lai2000/2000.htm

Lillesand, T.M. and R.W. Kiefer, 2000. Remote Sensing and Image Interpretation. 4th Edition, John Wiley and Sons, New York, NY.

Linco Equipment Inc., 2003. Trimble AgGPS 106 Product Description. Retrieved January, 2003. WWW: http://www.linco.com/ag106.htm

Lorenzen, B. and A. Jensen, 1991. Spectral properties of a barley canopy in relation to the spectral properties of single elaves and the soil. Remote Sensing Environment, 37:23-34.

Lu, Yoa-Chi, C. Daughtry, G. Hart and B. Watkins, 1997. The current state of precision farming. Food Reviews International, 13(2): 141-162.

Mack, A.R., R.L. Desjardins, J.I. MacPherson, and P.H. Schuepp, 1990. Relative photosynthetic activity of agricultural lands from airborne and satellite data. International Journal of Remtoe Sensing, 11(2):237-251.

Maas, S.J. and J.R. Dunlap, 1989. Reflectance, Transmittance, and Absorptance of Light by Normal, Etiolated, and Albino Corn Leaves. Agronomy Journal, 81:105-110.

Maas, S.J., 2000. Linear mixture modeling approach for estimating cotton canopy cover using satellite multispectral imagery. Remote Sensing of Environment, 72:304-308.

Macy, T.S., D.L. Thackery and N.C. Macy, 1994. Yield monitoring experiences – 1994. ASAE Paper No. 94-1581. St. Joseph, Mich.:ASAE.

Major, D.J., F. Baret, and G. Guyot, 1990. A ratio index adjusted for soil brightness. International Journal of Remote Sensing, 11(5):727-740.

Mannion, A.M., 1998. Can biotechnology contribute to sustainable agriculture. Journal of Sustainable Agriculture, 11(4):51-75.

Marriotti, M., L. Ercoli, L., and A. Masoni, 1996. Spectral Properties of Iron-Deficient corn and sunflower leaves. Remote Sensing Environment, 58: 282-288.

Masoni, A. L. Ercoli, and M. Mariotti, 1996. Agroclimatology: Spectral properties of leaves deficient in Iron, Sulfur, Magnesium and manganese. Agronomy Journal, 88:937-943.

McNairn, H. and R.J. Brown, 1999. Remote sensing in support of crop management. Proceedings, United Nations/China/European Space Agency (ESA) Conference on Space Applications for Promoting Sustainable Agriculture. Bejiing, China, Sept. 14-17, 7p.

McNairn, H., J.C. Deguise, J.Secker, and J.Shang, 2001a. Development of remote sensing image products for use in precision farming. In Proc. 3rd European Conference on Precision Farming, Montpellier, France, June 18-20, 5p.

McNairn, H., J.C. Deguise, A. Pacheco, J. Shang, and N. Rabe, 2001b. Estimation of Crop Cover and Chlorophyll from Hyperspectral Remote Sensing. 23rd Canadian Remote Sensing Symposium, Sainte-Foy, Quebec, Canada, August 21-24.

McNairn, H., K. Hochheim, and N. Rabe, 2003. Applying Polarimetric Radar Imagery for Mapping the Productivity of Wheat Crops. Canadian Journal of Remote Sensing (in press).

Miller, J.R.,White, H.P., Chen, J.M, Peddle, D.R., McDermid, G., Fournier, R.A., Shepherd, P., Rubinstein, I., Freemantle, J., Soffer, R., and E. LeDrew, 1997. Seasonal change in understory reflectance of boreal forests and influence on canopy vegetation indices. Journal of Geophysical Research, 102(D24): 29475-29482.

Milton, N.M., B.A. Eiswerth, and C.M. Ager, 1991. Effect of Phosphorus Deficiency on Spectral Reflectance and Morphology of Soybean Plants. Remote Sensing Environement, 36:121-127.

Moran, M.S., Y. Inoue, and E.M. Barnes, 1997. Opportunities and limitations for image based remote sensing in precision crop management. Remote Sensing of Environment. 61: 319-346.

Mulla, D.J., 1991. Using geostatistics and GIS to manage spatial patterson in soil fertility. *In* Automated Agriculture for the 21st Century. Proc. of the 1991 Symp., 336-345. St. Joseph, Mich.:ASAE.

Mustard and Pieters,1987. Quantitative abundance estimates from bi-directional reflectance measurements. Proceedings, 7th Lunar and Planetary Conference, Part 2 Journal of geophysical Research, 92(B4): E617-E626.

Natural Resources Canada, 2002. Climate Change Impacts and Adaptation: A Canadian Perspective – Agriculture. Climate Change Impacts and Adaptation Directorate, pp 1-18.

Nielson, A.A., 2001. Spectral Mixture Analysis: Linear and Semi-parametric Full and Iterated Partial Unmixing in Multi- and Hyperspectral Image Data. Journal of Mathematical Imaging and Vision. 15 (1-2): 17-37.

Norman, J.M. and G.S. Campbell. 1989. Canopy Stucture. In: R.W. Pearcy, J. Ehleringer, H.A. Mooney, and P.W. Rundel. Plant Physiological Ecology: Field Methods and Instrumentation. Chapman and Hall. London. pp 301-326.

Pacheco A., A. Bannari, J-C. Deguise , H. McNairn, and K. Staenz, 2001a. Application of Hyperspectral Remote Sensing for LAI Estimation in Precision Farming. Proceedings of the 23rd Canadian Symposium on Remote Sensing, Ste-Foy, Québec, August 20-24 , 2001 , pp. 281 – 287

Pacheco, A., A. Bannari, K. Staenz, and H. McNairn, 2001b. LAI Measurements in White Beans and Corn Canopies with Two Optical Instruments. Proceedings of 8th International Symposium of Physical Measurements & Signatures in Remote Sensing, Aussois, France January 8-12. pp. 374-379.

Peddle, D.R., 1998. Field Spectroradiometer Data Acquisition and Processing for Spectral Mixture Analysis in Forestry and Agriculture. First International Conference on Geospatial Information in Agriculture and Forestry. Lake Buena Vista, Florida, USA. June 1-3/98. ERIM International. Vol 2, p. 645 - 652.

Peddle, D.R. and A.M. Smith, 2003. Spectral Mixture Analysis of Agricultural Crops: Endmember Validation and Biophysical Estimation in Potato Plots. International Journal of Remote Sensing. (submitted).

Peddle, D.R. and R.L Johnson, 2000. Spectral mixture analysis of airborne remote

sensing imagery for improved leaf area index in mountainous terrain, Kananaskis Alberta. Canadian Journal of Remote Sensing. 26(3):176-187.

Peddle, D.R., A.M. Smith, C. Ivie, M. Bullock, and S. Russell, 1999b. Spectral mixture analysis of agricultural crops under different irrigation regimes: scene fraction validation in potato plots. Proceedings, 4th International Airborne Remote Sensing Conference and 21st Canadian Symposium on Remote Sensing, Ottawa, Canada, June. Vol. II, pp. 275-282.

Peddle, D.R., E.F. LeDrew, and H.M. Holden, 1995. Spectral mixture analysis of coral reef abundance from satellite imagery and in-situ ocean spectra, Savusavu Bay, Fiji. Proceedings, 3rd Thematic Conference on Remote Sensing for Marine and Coastal Environments, Seattle, Washington, USA, Sept. Vol II, p. 563-575.

Peddle, D.R., F.G. Hall and E.F. LeDrew, 1999a. Spectral Mixture Analysis and Geometric-Optical Reflectance Modeling of Boreal Forest Biophysical Structure. Remote Sensing of Environment, 67: 288-297.

Peddle, D.R., H. P. White, R.J. Soffer J.R. Miller and E.F. LeDrew, 2001a. Reflectance processing of remote sensing spectroradiometer data. Computers and Geosciences, 27: 203-213.

Peddle, D.R., R.L. Johnson, J. Cihlar, S.G. Leblanc and J.M. Chen, 2003a. MFM-5-Scale: A Physically-Based Inversion Modeling Approach for Unsupervised Cluster Labeling and Independent Forest Landcover Classification. Canadian Journal of Remote Sensing (accepted).

Peddle, D.R., R.L. Johnson, J. Cihlar and R. Latifovic, 2003b. Large Area Forest Classification and Biophysical Parameter Estimation using the 5-Scale Canopy Reflectance Model in Multiple-Forward Mode. Remote Sensing of Environment BOREAS Special Issue (in press).

Peddle, D.R., S.E. Franklin, R.L. Johnson, M.A. Lavigne and M.A. Wulder, 2003c. Structural Change Detection in a Disturbed Conifer Forest Using a Geometric Optical Reflectance Model in Multiple-Forward Mode. IEEE Transactions on Geoscience and Remote Sensing 41(1): 163-166.

Peddle, D.R., S.P. Brunke, and F.G. Hall, 2001b. A comparison of Spectral Mixture Analysis and Ten Vegetation Indices for Estimating Boreal Forest Biophysical Information from Airborne Data. Canadian Journal of Remote Sensing, 27(6): 627-637.

Perez-Munoz, F. and T.S. Colvin, 1996. Continuous Grain Yield Monitoring. Transactions of the ASAE, 39(3): 775-783.

Petrou, M. and P.G. Foschi, 1999. Confidence in Linear Spectral Unmixing of Single

Pixels. IEEE Transactions on Geoscience and Remote Sensing, 37(1): 624-626.

Petrzelka, P., S. Padgitt, and K. Connelly, 1997. Crop Management - Teaching old dogs survival tricks: A case study in promoting integrated crop management. Journal of Production Agriculture, 10(4): 596-602.

Pierce, F.J. and P.Nowak, 1999. Aspects of Precision Agriculture. Advances in Agronomy, 67: 1-85.

Piwowar, J.M., D.R. Peddle, and E.F. LeDrew, 1998. Temporal Mixture Analysis of Arctic Sea Ice Imagery: A New Approach for Monitoring Environmental Change. Remote Sensing of Environment. 63:195-207.

Price, J.C., 1993. Estimating Leaf Area Index from Satellite Data. IEEE Transaction on Geoscience and Remote Sensing, 31(3): 727-734.

Plaza, A., P. Martinez, R. Perez, and J. Plaza, 2002. Spatial/S[ectral Endmember Extraction by multidimensional morphological operations. IEEE Transactions on Geoscience and Remote Sensing, 40(9): 2025-2041.

Porter, J.R. and M. Gawith, 1999. Temperatures and the growth and development of wheat: a review. European Journal of Agronomy 10 (1999) 23–36.

Purevdorj, T., R. Tateishi, T. Ishiyama, and Y. Honda., 1998. Relationships between percent vegetation cover and vegetation indices. International Journal of Remote Sensing. 19(18): 3519-3535.

Quarmby, N.A., 1992. Towards continental scale crop area estimation. International Journal of Remote Sensing, 13(5): 981-989.

Quarmby, N.A., J.R.G. Townshend, J.J. Settle, K.H. White, M. Milnes, T.L. Hindle, and N. Silleos, 1992. Linear Mixture Modelling applied to AVHRR data for crop area estimation. International Journal of Remote Sensing, 13(3): 415-425.

Radelhoff, V.C, D.J. Mladenhoff, and M.S. Boyce, 1999. Detecting Jack Pine Budworm Defoliation using Spectral Mixture Analysis: Separating Effects from Determinants. Remote Sensing of Environment, 69: 156-169.

Rahman, A. F., Gamon, J.A., Sims, D.A. and M. Schmidts, 2003. Optimum pixel size for hyperspectral studies of ecosystem function in southern California chaparral and grassland. Remote Sensing of Environment, 84 (2): 192-207.

Ray, T.W. and B.C. Murray, 1996. Nonlinear spectral mixing in desert vegetation. Remote Sensing of Environment, 55:59-64.

Rigby, D., Woodhouse, P., Young, T., and M. Burton, 2001. Constructing a farm level

indicator of sustainable agricultural practice. Ecoclogical Economics, 29: 463-478.

Roberts, D.A., M. Gardner, R. Church, S. Ustin, G. Scheer, and R.O. Green, 1998. Mapping Chaparral in the Santa Monica Mountains using Multiple Endmember spectral mixture models. Remote Sensing of Environment, 65:267-279.

Rondeaux, G, 1995. Vegetation Monitoring by Remote Sensing: A review of Biophyscial Indices. Photo-Interpretation, 3:197-213.

Rondeaux,G., M. Steven, and F. Baret, 1996. Optimization of Soil-Adjusted Vegetation Indices. Remote Sensing Environment, 55:95-107.

RSI (Research Systems Inc.), 2001. ENVI Technical Support Personal Communication, October 19, 2001. WWW: http://www.rsinc.com/envi/

Sabol, D.E., J.B. Adams, and M.O. Smith, 1992. Quantitative sub-pixel spectral detection of targets in multispectral images. Journal of Geophysical Research, 97:2659-2672.

Saghri, J.A., A.G. Tescher, F. Jaradi, and M. Omran, 2000. A viable end member selection scheme for spectral unmxing of multispectral satellite imagery data. Journal of Imaging Science and Technology, 44(3): 196-203.

Schilfgaarde, J.V., 1999. Is precision agriculture sustainable? American Journal of Alternative Agriculture. 14(1): 43-46.

Secker, J, K. Staenz, K., Gauthier, R.P., and P. Budkewitsch, 2001. Vicarious calibration of airborne hyperspectral sensors in operational environments. Remote Sensing of Environment, 76: 81-92.

Secker J., K. Staenz, P. Budkewitsch, and R.A. Neville, 1999. A Vicarious Calibration of the Probe-1 Hyperspectral Sensor. Proceedings, 4th International Airborne Remote Sensing Conference and Exhibition/21st Canadian Symposium on Remote Sensing, Ottawa, Ontario, Canada, Vol. II: 75-82.

Shimabukuro, Y.E. and J.A. Smith, 1991. The Least-Squares Mixing Models to generate fraction images derived from remote sensing multispectral data. IEEE Transactions on Geoscience and Remote Sensing, 29(1): 16-20.

Sivakumar, M.V.K., Gommes, R., and W. Baier, 2000. Agrometerology and sustainable agriculture. Agricultural and Forest Meteorology, 103: 11-26.

Small, C., 2001. Estimation of urban vegetation abundance by spectral mixture analysis. International Journal of Remote Sensing, 22(7):1305-1334.

Smith, A.M., D.R. Peddle, and T.C. Foster, 1999. Detection of Moisture Stress in Potatoes using multispectral remote sensing. Proceedings, 4th International Airborne Remote Sensing Conference and 21st Canadian Symposium on Remote Sensing, Ottawa, Canada, June. Vol. II, pp. 283-289.

Space Imaging, 2003. IKONOS Spectral Band Characteristics. Retrieved March 9, 2003. WWW: http://www.spaceimaging.com/products/ikonos/spectral.htm

Staenz, K and D.J. Williams, 1997. Retrieval of surface reflectance from hyperspectral data using a look-up table approach. Canadian Journal of Remote Sensing, 23(4): 354-367.

Staenz, K., T. Szeredi, R.J. Brown, H. McNairn, amd R. Van Acker, 1997a. Hyperspectral Information Extraction Techniques Applied to Agricultural CASI Data for Detection of Within-Field Variations; International Symposium, Geomatics in the Era of RADARSAT (GER'97), Ottawa, Canada, May 25-30 .

Staenz, K, J.C. Deguise, J. Schwarz, and R. Brown, 1997b. Overview of ISDAS Hyperspectral Information Extraction Techniques with focus on Agricultural Applications. Proceedings, International Symposium on Spectral Sensing Research, San Diego, CA, 7pp.

Staenz K. , J.C. Deguise, J.M., Chen, H., McNairn, T., Szeredi, and M. McGovern, 1998a. The Use of Hyperspectral Data for Precision Farming. ISPRS Commission VII Symposium, Budapest, Hungary, September 1-4, pp. 38-42

Staenz, K., T. Szeredi, and J. Swarz, 1998b. ISDAS – A System for Processing/Analyzing Hyperspectral Data. Canadian Journal of Remote Sensing, 24(2): 99-113.

Staenz, K., J.C. Deguise, J.M. Chen, H. McNairn, and T. Szeredi, 1999. Estimation of Leaf Area Index (LAI) from Crop Fraction Using Hyperspectral Data, Commission VII, Working Group I, 31pp.

Stafford, J.V., B. Ambler and M.P. Smith, 1991. Sensing and mapping grain yield variation. In Automated Agriculture for the 21st century. Proc. Of the 1991 Symp., 356-365. St. Joseph, Mich.: ASAE.

Stafford, J.V., 2000. Implementing Precision Agriculture in the 21st Century. Journal of Agriculture Engineering Research. 76:267-275.

Steven, M.D., 1998. The sensitivity of the OSAVI Vegetation Index to Observational Parameters. Remote Sensing of Environment. 63:49-60.

Stoskopf, N.C., 1981. Leaf area and plant architecture. *In*: Stoskopf, N.C. Understanding Crop Production, Reston Publishing Company inc., Reston, Virginia. pp 93-111.

Szeredi, T., K. Staenz, and R.A. Neville, 1999. Automatic End member Selection: Part 1 Theory. Preprint submitted to Elsevier Science. Feb 13, 1999. pp.1-21.

Thenkabail, P.S., A.D. Ward, and J.G. Lyon, 1994. Landsat-5 Thematic Mapper models of soybean and corn crop characteristics. International Journal of Remote Sensing, 15(1) 49-61.

Thenkabail PS, Smith RB, De Pauw E, 2000. Hyperspectral vegetation indices and their relationships with agricultural crop characteristics. Remote Sensing of Environment, 71(2): 158-182.

Thomas, J.R. and H.W. Gausman, 1977. Leaf Reflectance vs. Leaf Chlorophyll and Cartonoid Concentration for Eight Crops. Agronomy Journal, 69: 799-802.

Todd, S.W. and R.M. Hoffer, 1998. Responses of spectral indices to variations in vegetation cover and soil background. Photogrammetric Engineering and Remote Sensing, 64(9): 915-921.

Tompkins, S., J.F. Mustard, C.M. Pieters, and D.W. Forsyth, 1997. Optimization of Endmembers for Spectral Mixture Analysis. Remote Sensing of Environment, 59:472-489.

Trietz, P.M. and P.J. Howarth, 1999. Hyperspectral remote sensing for estimating biophysical parameters of forest ecosystems. Progress in Physical Geography 23 (3): 359-390.

Tromp, M., and G.F. Epema, 1999. Spectral Mixture analysis for mapping land degradation in semi-arid areas. Geologie en Mihnbouw, 77:153-160.

Turner, D.P., W.B. Cohen, R.E. Kennedy, K.S. Fassnacht, and J.M Briggs, 1999. Relationships between Leaf Are Index and Landsat TM Spectral Vegetation Indices across Three Temperate Zone Sites. Remote Sensing of Environment, 70:52-68.

Tyler, D.A., D.W. Roberts and G.A. Nielson, 1997. Location and Guidence for Site Specific Management. *In* The State of Site Specific Management for Agriculture, F.J. Pierce and E.J. Sadler (Eds.), Madison, WI, Amercian Society of Agronomy, pp161-181.

Ungar, S.G. and E. Bryant, 1981. Fanning: A classification algorithm for mixture landscapes applied to Landsat data of Maine forests. Proceedings, 15th International Symposium on Remote Sensing of Environment, Ann Arbor, Michigan, USA, May. pp. 1113-1120.

USGS, 2003. Reference Spectral Libraries for Minerals and Vegetation. USGS

Spectroscopy Lab. Retrieved June 2, 2003. WWW:http://speclab.cr.usgs.gov/

VanLeeuwen, W.J.D., A.R. Huete, C.L. Walthall, S.D. Prince, A. Begue, and J.L. Roujean, 1997. Deconvolution of remotely sensed spectral mixtures for retrieval of LAI, fAPAR, and soil brightness. Journal of Hydrology, 188-189: 627-724.

Walter-Shea, E.A., J.M. Norman, B.L. Blad, and B.F. Robinson, 1991. Leaf Reflectance and Transmittance in Soybean and Corn. Agronomy Journal, 83:631-636.

Welles, J.M., 1990. Some Indirect Methods of Estimating Canopy Structure. Remote Sensing Reviews, 5(1):31-43.

Welles, J.M. and J.M. Norman, 1991. Instrument for Indirect Measurement of Canopy Arichitecture. Agronomy Journal, 83: 818-825.

Wessman, C.A., C.A. Bateson, and T.L. Benning, 1997. Detecting fires and grazing patterns in tall grass prairie using Spectral Mixture Analysis. Ecological Applications, 7(2): 493-511.

White, H.P., 2002. LAI 2000 agriculture protocol. Personal Communication Dr. Peter White, August 14, 2002.

Wiegand, C.L. and A.J. Richardson, 1977. Distinguishing Vegetation from Soil Background Information. Photogrammetric Engineering and Remote Sensing, 43(12):1541-1552.

Wiegand, C.L. and A.J. Richardson, 1984. Leaf area, light interception, and yield estimates from spectral components analysis. Agronomy Journal, 76: 543-548.

Wiegand, C.L. and A.J. Richardson, 1990. Use of spectral vegetation indices to infer leaf area, evapotranspiration and yield: I. Rationale. Agronomy Journal, 82: 623-629.

Wiegand, C.L., A.J. Richardson, D.E. Escobar, and A.H. Gerbermann, 1991. Vegetation Indices in crop assessments. Remote Sensing of Environment, 35: 105-119.

Wolley, J.T., 1971. Relfectance and transmittance of light by leaves. Plant Physiology, 47: 656-662.

Wollenhaupt, N.C. and D.D. Buchholz, 1992. Profitability of farming by soils. Proceedings, Soil Specific Crop Management, pp. 199-211.

World Commission on Environment and Development, 1987. Our common Future. New York : Oxford University Press, 1987

Yoder, B.J., and R.E. Pettigrew-Crosby, 1995. Predicting nitrogen and chlorophyll

content and concentrations from reflectance spectra (400-2500nm) at leaf and canopy scales. Remote Sensing Environment, 53: 199-211.

Zarco-Tejada, P.J., J.R Miller, G.H. Mohammed, and T.L. Noland, 2000. Chlorophyll Fluorescence Effects on vegetation reflectance: I. Leaf-Level measurements and model simulation. Remote Sensing of Environment, 74:582-595.

Appendix A - Probe-1 Bands and Gains

Probe-1 Band	Center Wavelength (nm)	Band Width	Minimum Wavelength (nm)	Maximum Wavelength (nm)	ESSI Gains	CCRS – Vicarious Calibration Gains
1	435.7	15.0	428.20	443.20	0.1543373	0.177052
2	446.2	15.3	438.55	453.85	0.0391416	0.042215
3	460.4	17.1	451.85	468.95	0.0248649	0.026552
4	476.5	16.6	468.20	484.80	0.018852	0.019539
5	491.0	16.0	483.00	499.00	0.0146456	0.015059
6	506.8	15.7	498.95	514.65	0.0121300	0.012597
7	521.6	16.3	513.45	529.75	0.0110068	0.011295
8	537.5	16.9	529.05	545.95	0.0105144	0.010662
9	552.8	15.7	544.95	560.65	0.0092656	0.009395
10	567.5	15.5	559.75	575.25	0.0090569	0.009239
11	582.1	20.0	572.10	592.10	0.0122845	0.012531
12	599.0	14.0	592.00	606.00	0.0094949	0.009705
13	613.7	15.2	606.10	621.30	0.0086864	0.008932
14	627.8	14.4	620.60	635.00	0.0109377	0.011224
15	645.9	14.7	638.55	653.25	0.0113623	0.011683
16	660.1	16.5	651.85	668.35	0.0088306	0.008972
17	675.7	16.4	667.50	683.90	0.0090487	0.009231
18	690.9	15.9	682.95	698.85	0.0096394	0.009658
19	705.2	16.4	697.00	713.40	0.0128806	0.012548
20	721.6	15.3	713.95	729.25	0.0116502	0.011168
21	735.8	16.0	727.80	743.80	0.0095932	0.008870
22	750.9	16.5	742.65	759.15	0.0094918	0.008936
23	765.9	15.9	757.95	773.85	0.0100221	0.008742
24	780.7	18.7	771.35	790.05	0.0126871	0.011336
25	796.9	16.2	788.80	805.00	0.0110071	0.010177
26	812.1	16.9	803.65	820.55	0.0105378	0.010041
27	827.6	16.8	819.20	836.00	0.0106492	0.010026
28	843.1	17.0	834.60	851.60	0.0118954	0.010954
29	857.2	16.8	848.80	865.60	0.0159936	0.014348
30	874.7	15.8	866.80	882.60	0.0170974	0.015619
31	888.5	16.9	880.05	896.95	0.016836	0.015787
32	903.0	16.1	894.95	911.05	0.0238442	0.021957
33	895.2	15.8	887.30	903.10	0.0148945	0.000165
34	908.7	12.9	902.25	915.15	0.0146048	0.000157
35	929.0	13.8	922.10	935.90	0.0102206	0.010384
36	943.0	15.7	935.15	950.85	0.0059243	0.006007
37	958.9	15.2	951.30	966.50	0.0052679	0.005215
38	972.9	19.1	963.35	982.45	0.0082198	0.007434
39	991.7	14.4	984.50	998.90	0.0057196	0.005342
40	1006.2	15.5	998.45	1013.95	0.0043127	0.003869
41	1021.4	15.4	1013.7	1029.10	0.0044344	0.003860

Probe-1 Band	Center Wavelength (nm)	Band Width	Minimum Wavelength (nm)	Maximum Wavelength (nm)	ESSI Gains	CCRS – Vicarious Calibration Gains
42	1036.0	19.7	1026.15	1045.85	0.0066560	0.005782
43	1053.7	14.2	1046.60	1060.80	0.0043655	0.003964
44	1067.7	15.8	1059.80	1075.60	0.0032962	0.002993
45	1082.8	15.6	1075.00	1090.60	0.0031843	0.00295
46	1097.5	16.0	1089.50	1105.50	0.003556	0.003375
47	1113.0	16.2	1104.90	1121.10	0.0035504	0.003494
48	1127.9	15.9	1119.95	1135.85	0.0029810	0.003065
49	1142.5	15.3	1134.85	1150.15	0.0027851	0.002939
50	1157.0	15.6	1149.20	1164.80	0.0028301	0.002802
51	1171.5	16.0	1163.50	1179.50	0.0031104	0.003042
52	1186.4	16.2	1178.30	1194.50	0.0030937	0.003081
53	1200.8	15.4	1193.10	1208.50	0.0030545	0.003055
54	1215.0	15.6	1207.20	1222.80	0.0032295	0.003184
55	1229.3	16.0	1221.30	1237.30	0.0034878	0.003398
56	1243.7	15.8	1235.80	1251.60	0.0034135	0.003339
57	1258.0	15.5	1250.25	1265.75	0.0033913	0.003480
58	1271.9	15.4	1264.20	1279.60	0.0035512	0.003695
59	1286.2	16.2	1278.10	1294.30	0.0037672	0.003752
60	1300.4	15.5	1292.65	1308.15	0.0037155	0.003716
61	1314.3	15.5	1306.55	1322.05	0.0037690	0.003938
62	1328.1	15.3	1320.45	1335.75	0.0039934	0.004273
63	1341.3	14.3	1334.15	1348.45	0.0047860	0.004834
64	1353.7	14.6	1346.40	1361.00	0.0086448	0.008645
65	1396.7	16.0	1388.70	1404.70	0.0022702	0.002270
66	1410.2	17.0	1401.70	1418.70	0.0019774	0.001977
67	1424.6	17.6	1415.80	1433.40	0.0020577	0.002058
68	1440.0	17.3	1431.35	1448.65	0.0019664	0.001966
69	1454.7	16.2	1446.60	1462.80	0.0016230	0.001623
70	1468.4	15.9	1460.45	1476.35	0.0014044	0.001643
71	1482.3	15.8	1474.40	1490.20	0.0013066	0.001563
72	1496.2	15.9	1488.25	1504.15	0.0012881	0.001454
73	1510.0	15.3	1502.35	1517.65	0.0012772	0.001372
74	1523.6	15.3	1515.95	1531.25	0.0013521	0.001413
75	1537.3	15.5	1529.55	1545.05	0.0014252	0.001451
76	1551.0	15.5	1543.25	1558.75	0.0014526	0.001461
77	1564.6	15.1	1557.05	1572.15	0.0014018	0.001413
78	1577.7	14.9	1570.25	1585.15	0.0013439	0.001379
79	1590.8	15.2	1583.20	1598.40	0.0013326	0.001370
80	1604.0	15.1	1596.45	1611.55	0.0013601	0.001382
81	1617.1	14.8	1609.70	1624.50	0.0014010	0.001415
82	1630.0	14.7	1622.65	1637.35	0.0014388	0.001433
83	1642.9	15.0	1635.40	1650.40	0.0014563	0.001448

Probe-1 Band	Center Wavelength (nm)	Band Width	Minimum Wavelength (nm)	Maximum Wavelength (nm)	ESSI Gains	CCRS – Vicarious Calibration Gains
84	1655.8	14.6	1648.50	1663.10	0.0014565	0.001454
85	1668.4	14.5	1661.15	1675.65	0.0014956	0.001502
86	1681.0	14.4	1673.80	1688.20	0.0015328	0.001548
87	1693.7	14.9	1686.25	1701.15	0.0015808	0.001606
88	1706.3	14.3	1699.15	1713.45	0.0016134	0.001649
89	1718.7	14.2	1711.60	1725.80	0.0015943	0.001643
90	1731.0	14.0	1724.00	1738.00	0.0016011	0.001669
91	1743.3	14.2	1736.20	1750.40	0.0016025	0.001684
92	1755.5	14.0	1748.50	1762.50	0.0016608	0.001735
93	1767.7	13.8	1760.80	1774.60	0.0017374	0.001804
94	1779.7	13.7	1772.85	1786.55	0.0018449	0.001931
95	1791.8	14.0	1784.80	1798.80	0.0020216	0.002022
96	1803.8	13.5	1797.05	1810.55	0.002217	0.002217
97	1979.2	21.1	1968.65	1989.75	0.0006373	0.000637
98	1998.0	21.2	1987.40	2008.60	0.0006068	0.000607
99	2016.7	21.4	2006.00	2027.40	0.0005959	0.000733
100	2035.7	21.6	2024.90	2046.50	0.0005789	0.000641
101	2054.7	21.3	2044.05	2065.35	0.0005716	0.000600
102	2073.3	20.9	2062.85	2083.75	0.0005623	0.000637
103	2091.5	20.2	2081.40	2101.60	0.0005499	0.000612
104	2109.7	20.1	2099.65	2119.75	0.0005303	0.000587
105	2127.6	20.3	2117.45	2137.75	0.0005165	0.000569
106	2145.8	20.4	2135.60	2156.00	0.0005084	0.000555
107	2163.8	20.1	2153.75	2173.85	0.0005060	0.000556
108	2181.4	19.1	2171.85	2190.95	0.0005174	0.000569
109	2198.1	19.4	2188.40	2207.80	0.0005334	0.000597
110	2216.5	19.1	2206.95	2226.05	0.0005576	0.000635
111	2234.1	18.8	2224.70	2243.50	0.0005804	0.000635
112	2251.5	19.4	2241.80	2261.20	0.0006032	0.000640
113	2268.9	18.6	2259.60	2278.20	0.0006317	0.000672
114	2286.1	18.5	2276.85	2295.35	0.0006558	0.000703
115	2303.0	17.9	2294.05	2311.95	0.0006865	0.000736
116	2319.6	17.4	2310.90	2328.30	0.0007116	0.000754
117	2336.2	18.0	2327.20	2345.20	0.0007102	0.000758

Appendix B - Comparison of SMA Programs

In order to demonstrate that SMA can be performed in a commercially available software package, the Shimabukuro and Smith (1991) SMA program and the ENVI Linear Spectral Unmixing (LSU) results were directly compared for the wheat crop using the reference endmembers as input. As mentioned in Chapter 4, the Shimabukuro and Smith (1991) SMA program was limited to seven bands (Table 4-9) and to ensure a good comparison with the ENVI LSU tools the same seven bands were utilized. For research purposes the Fortran program created by Shimabukuro and Smith (1991) allowed for much more flexibility in this research in terms of access to the algorithm and its parameters. Each respective program is based on the unconstrained algorithm where underflow and overflow fraction values can result, but the total of each fraction must sum to unity. The advantage of ENVI in comparison to the Shimabukuro and Smith (1991) program is that ENVI produces fraction maps for each individual scene component, as well as an overall RMS error map. The RMS error map is useful in identifying regions of the study area where the endmember input was not sufficient, and provides the analyst with a visual method to investigate why this may have occurred.

Figure B-1 shows the minimum, maximum, and mean absolute fraction values for each scene component and all sample site locations (n=34) of the wheat crop. The minimum, maximum, and mean absolute fraction values were identical between the two programs for the reference sunlit crop. The reference shadowed crop maximum fraction values were identical for both programs (0.57), whereas the minimum fraction value for Shimabukuro and Smith (1991) was slightly lower (0.27) then the ENVI LSU minimum fraction value (0.34). There were slight differences in the reference sunlit background

fraction results in that the Shimabukuro and Smith (1991) program produced minimum and maximum fraction values that were slightly higher (0.12 versus 0.08, and 0.60 versus 0.55) than the ENVI LSU minimum and maximum fraction values. Overall, the mean value for all absolute fractions from both SMA programs varied +/- 0.05. In conclusion, it would be feasible to use the commercial program in operational environments to produce very similar fractions results as were found in this research for using the Shimabukuro and Smith (1991) software.

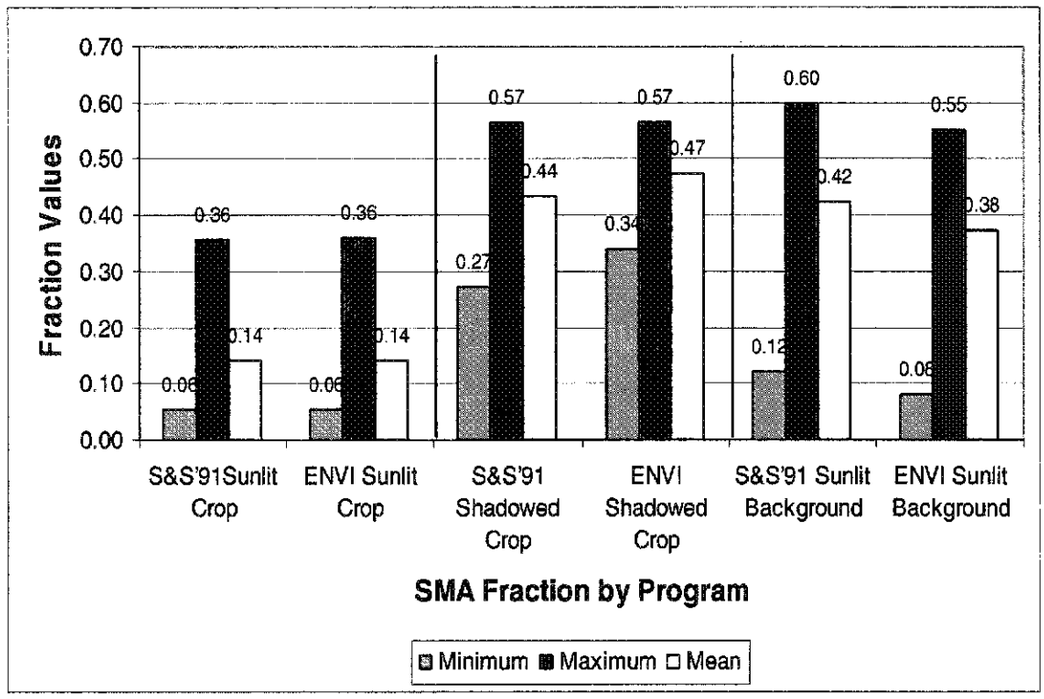

Figure B-1 Shimabukaro and Smith (1991) SMA (S&S'91) and the ENVI LSU fraction results using only the reference endmembers for SMA of the wheat crop (n=34). Each fraction result labeled with minimum, maximum and mean absolute fraction values.

Appendix C: Linear Regression Analysis for the Prediction of Biomass and LAI using Vegetation Indices

Figure C-1: Linear regression analysis results for vegetation index prediction of pea LAI and biomass.

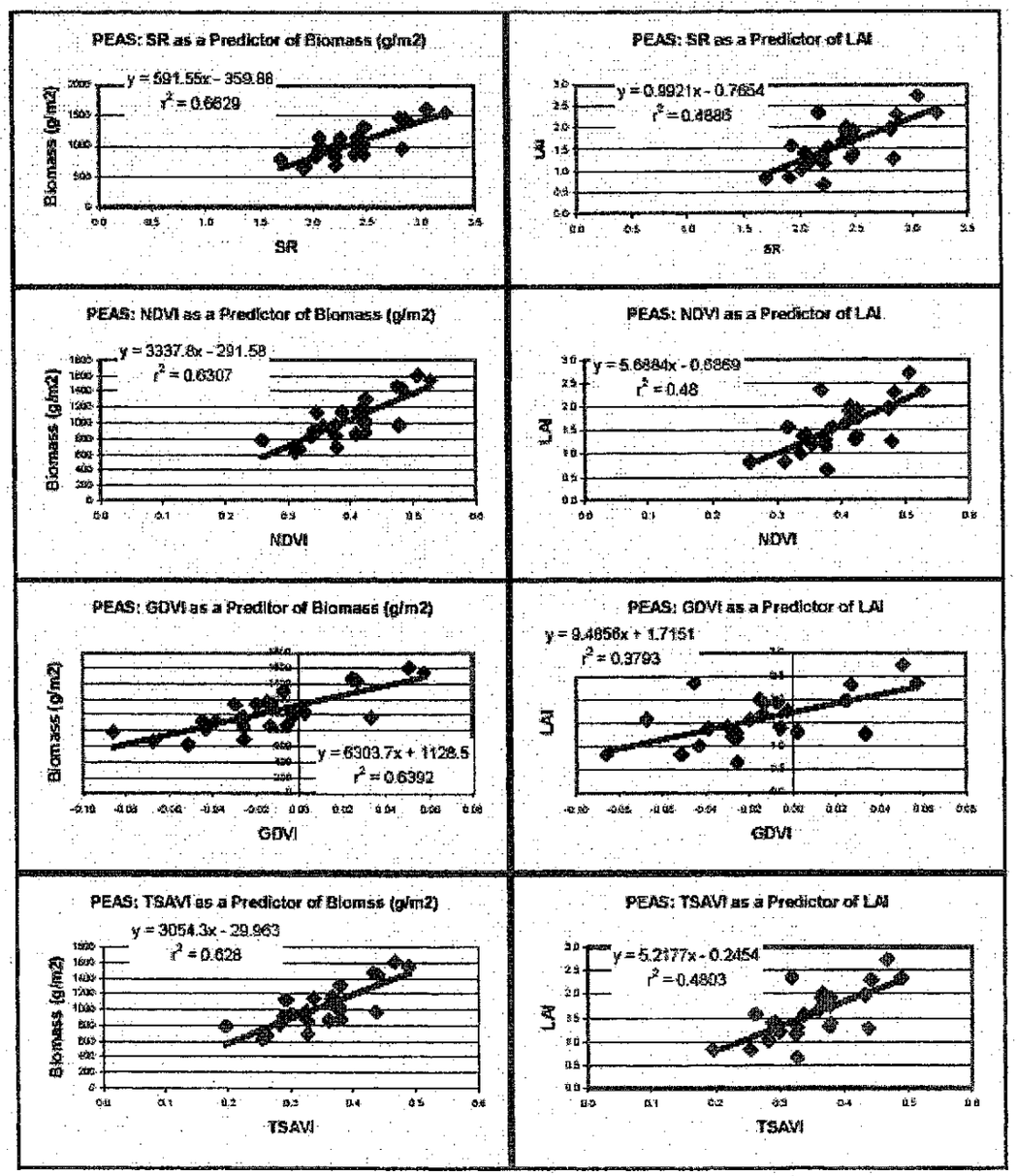

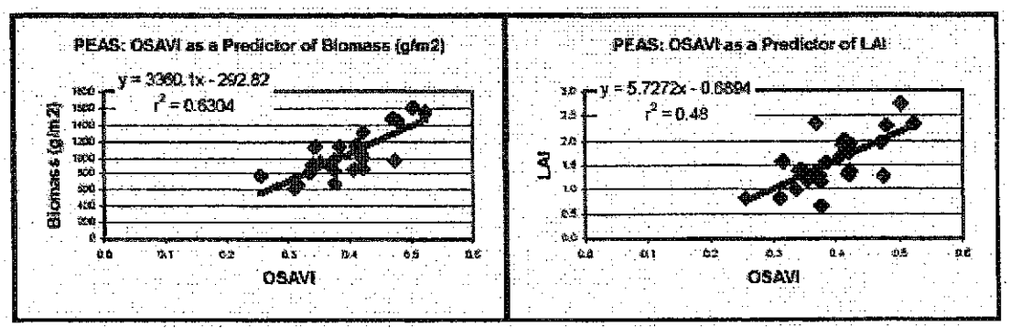

Figure C-2: Linear regression analysis results for vegetation index prediction of canola LAI and biomass.

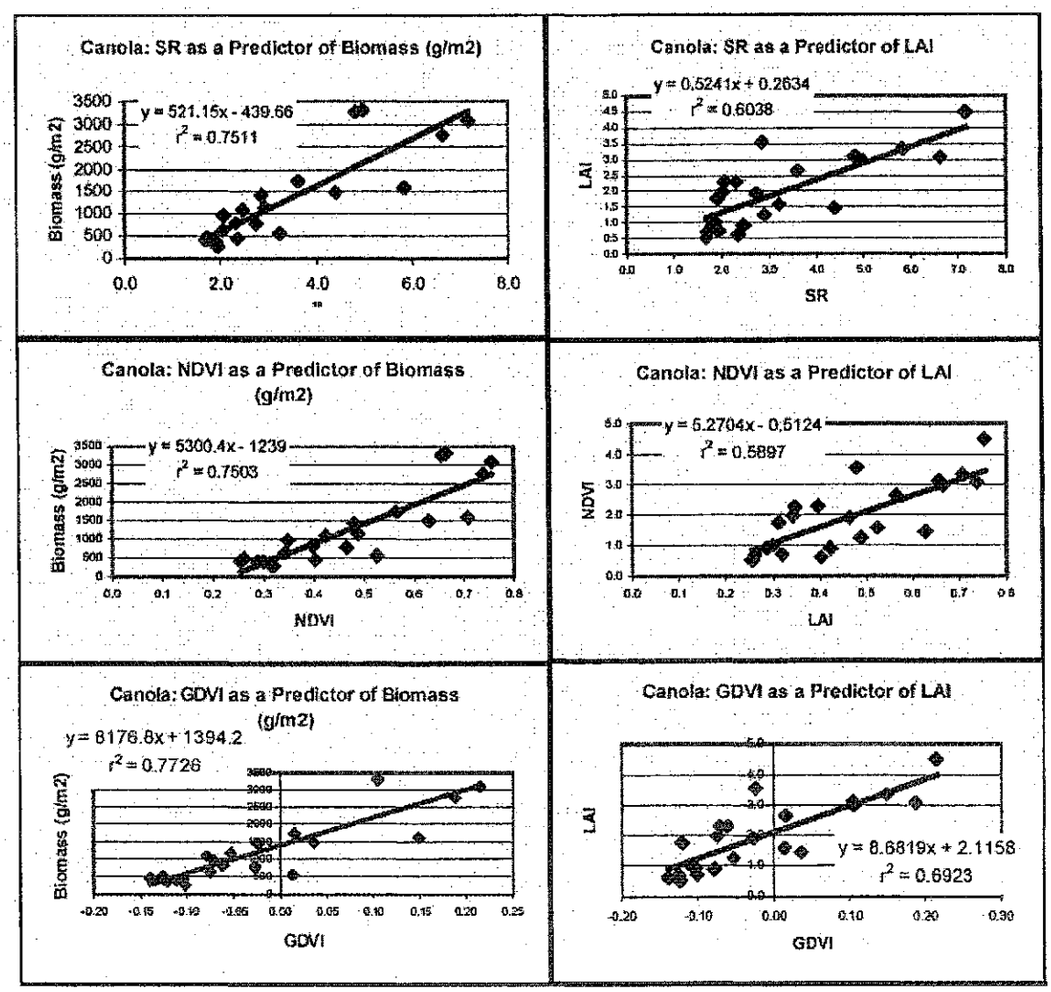

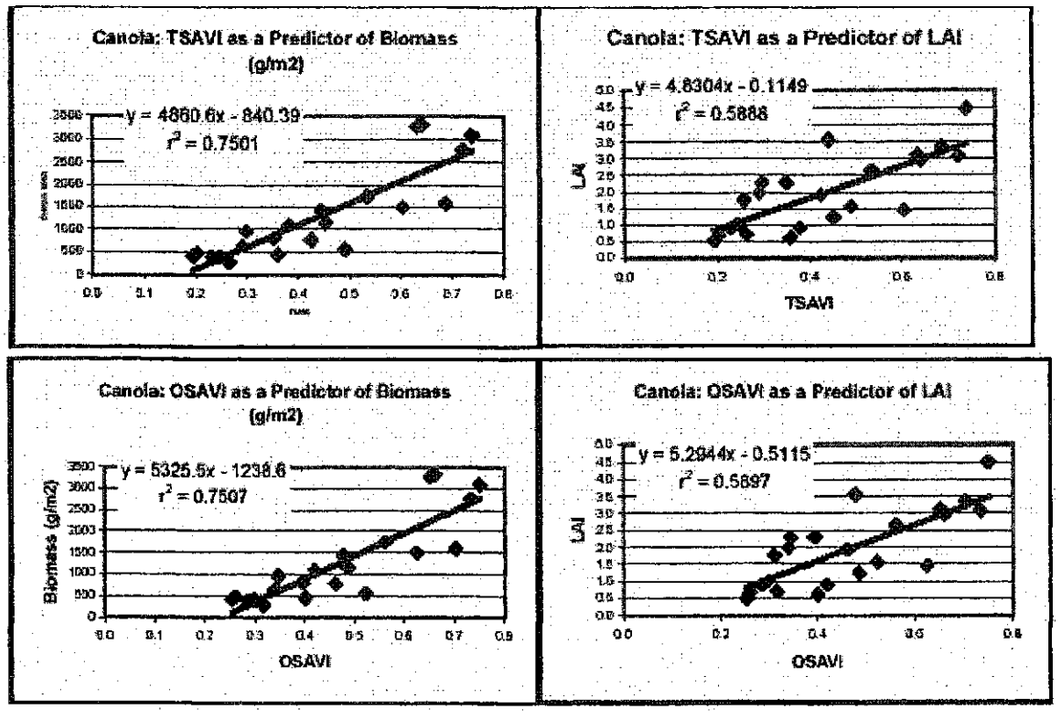

Figure C-3: Linear regression analysis results for vegetation index prediction of wheat LAI and biomass.

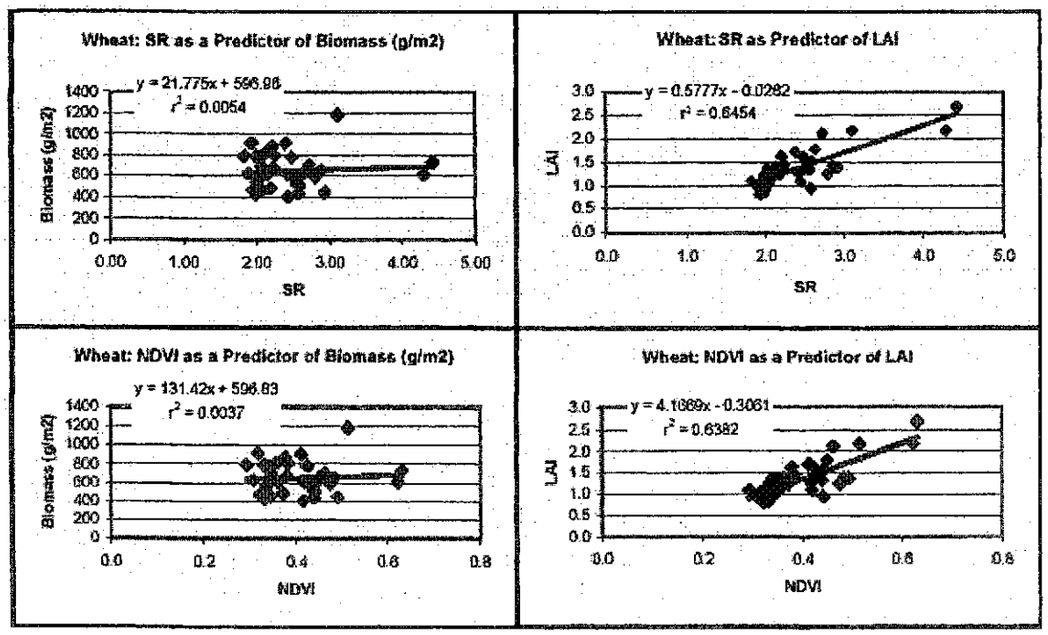

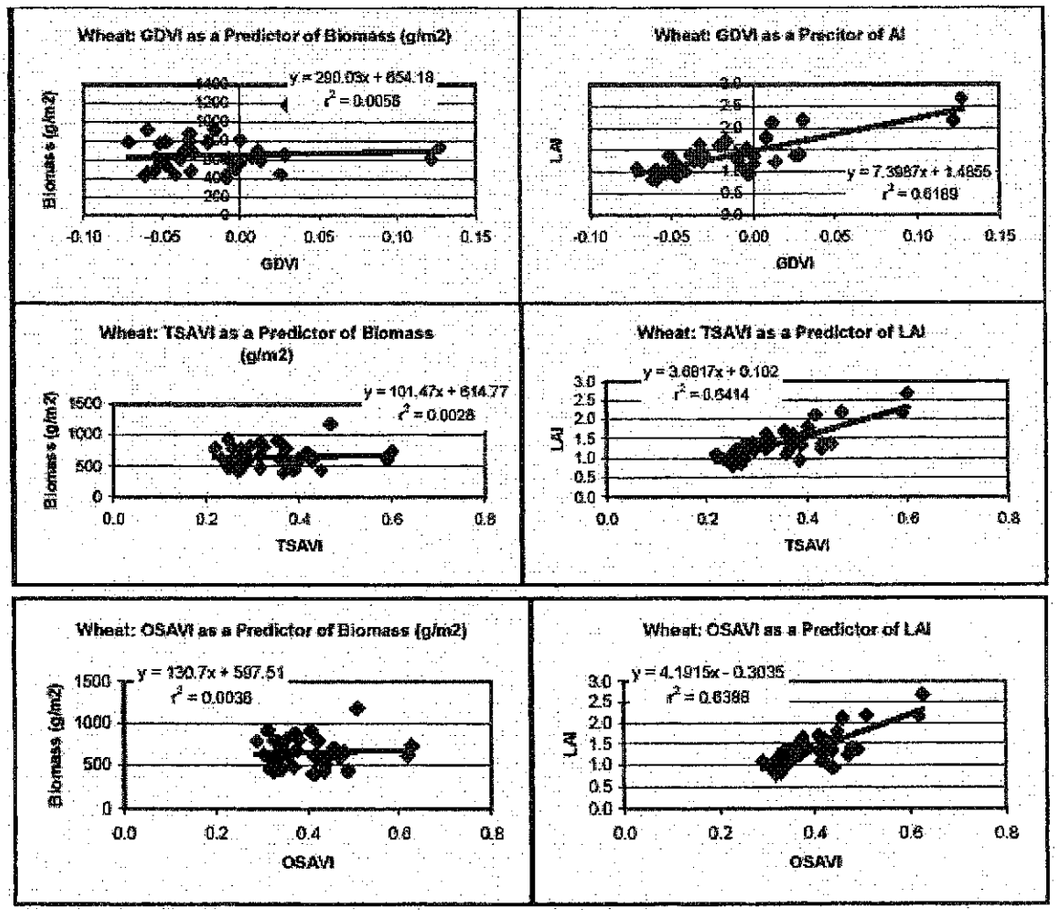
Wheat: GDVI as a Predictor of Biomass (g/m2)
y = 290.03x + 654.18
r² = 0.0058
Biomass (g/m2)
GDVI
Wheat: GDVI as a Precitor of AI
y = 7.3987x + 1.4855
r² = 0.6189
LAI
GDVI
Wheat: TSAVI as a Predictor of Biomass (g/m2)
y = 101.47x + 614.77
r² = 0.0028
Biomass (g/m2)
TSAVI
Wheat: TSAVI as a Predictor of LAI
y = 3.6817x + 0.102
r² = 0.6414
LAI
TSAVI
Wheat: OSAVI as a Predictor of Biomass (g/m2)
y = 130.7x + 597.51
r² = 0.0036
Biomass (g/m2)
OSAVI
Wheat: OSAVI as a Predictor of LAI
y = 4.1915x - 0.3035
r² = 0.6388
LAI
OSAVI

Appendix D: Linear Regression Analysis for the Prediction of Biomass and LAI using SMA

Figure D-1: Linear regression analysis results for SMA using reference endmembers to predict of pea biomass and LAI.

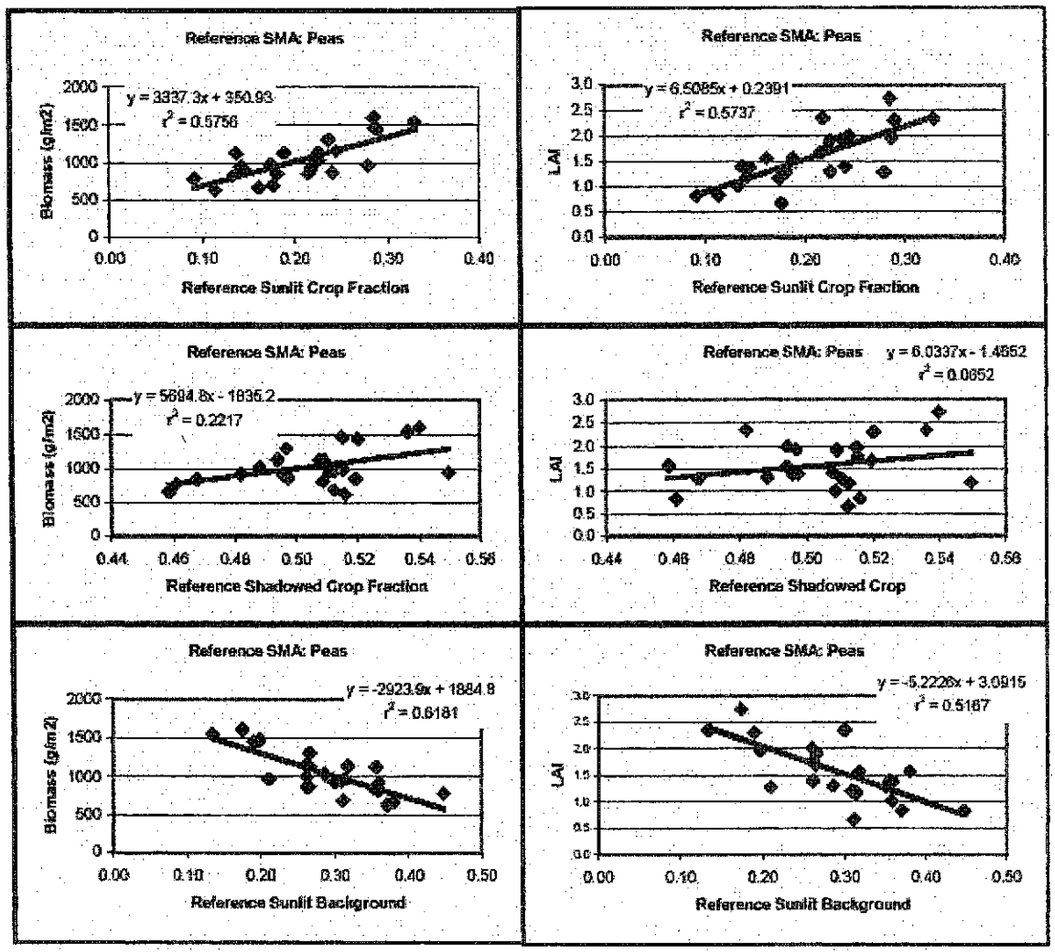

Figure D-2: Linear regression analysis results for SMA using image endmembers to predict of pea biomass and LAI.

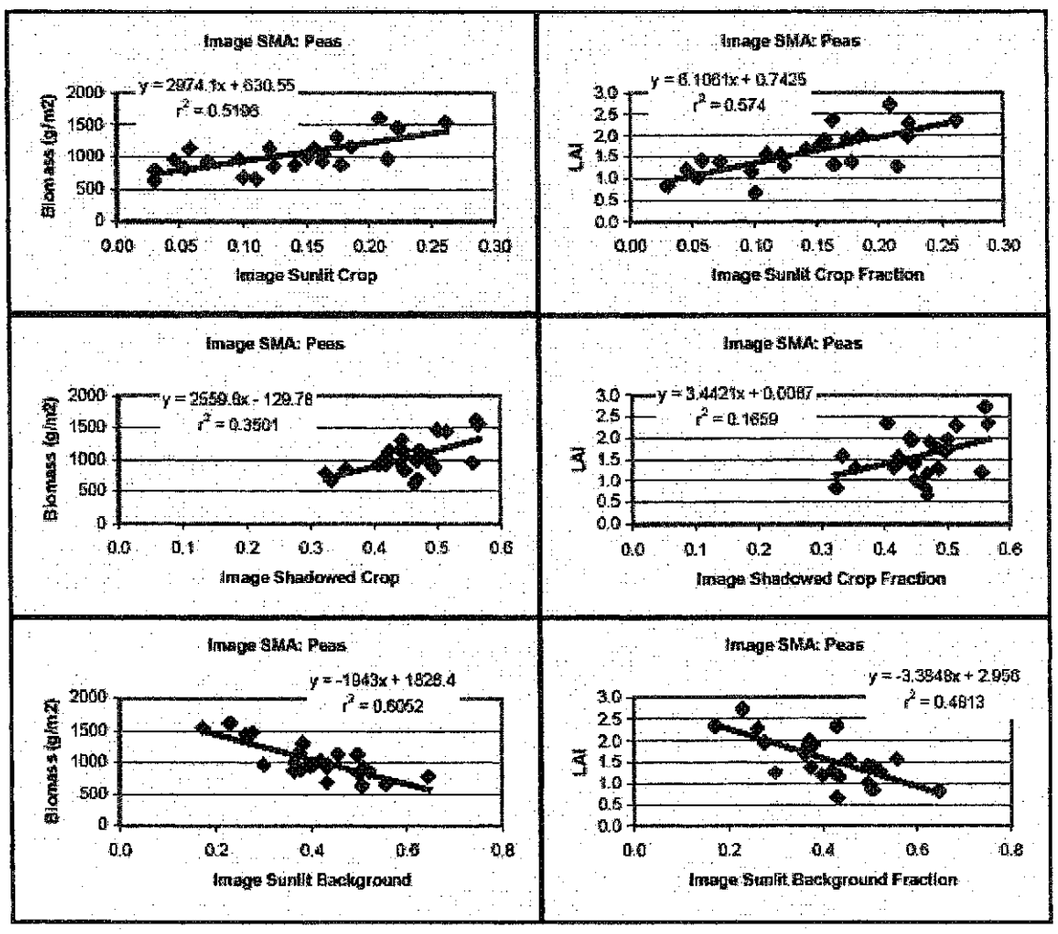

Figure D-3: Linear regression analysis results for SMA using reference endmemebrs to predict canola biomass and LAI.

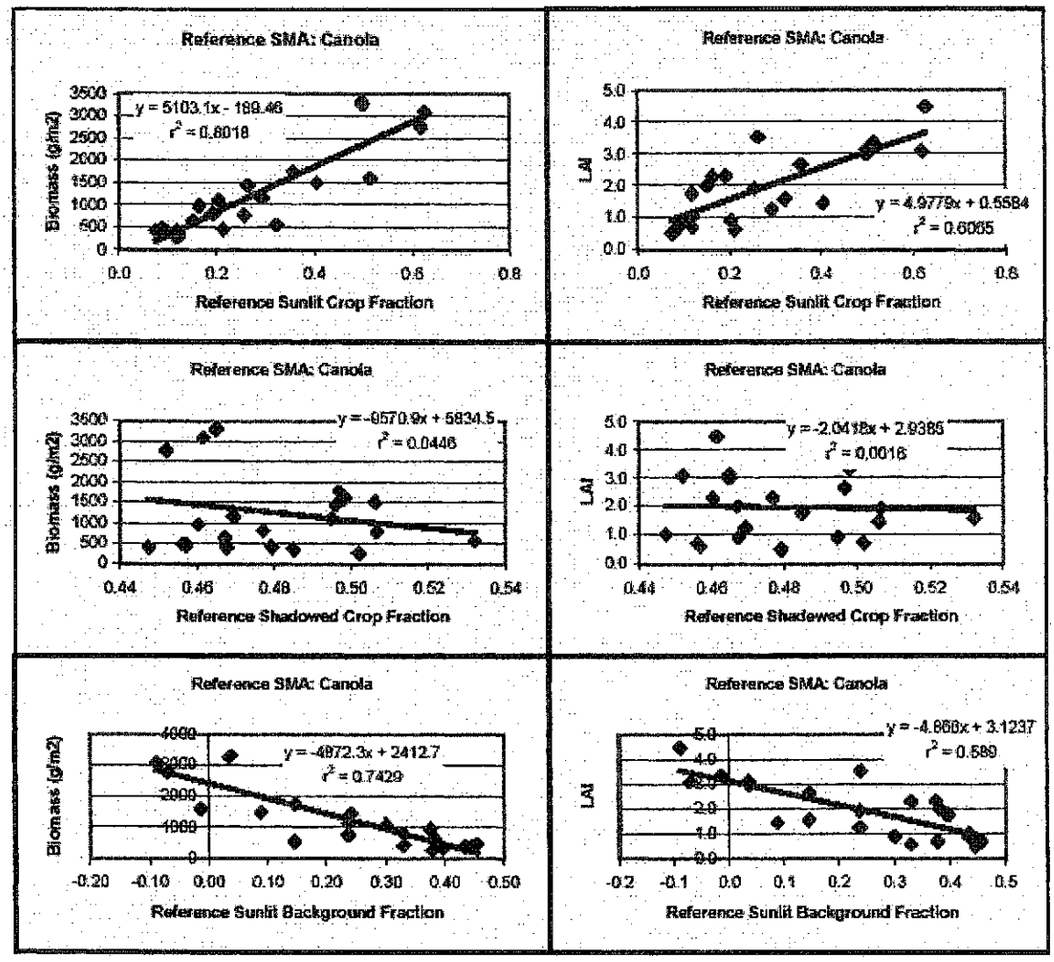

Figure D-4: Linear regression analysis results for SMA using image endmembers to predict canola biomass and LAI.

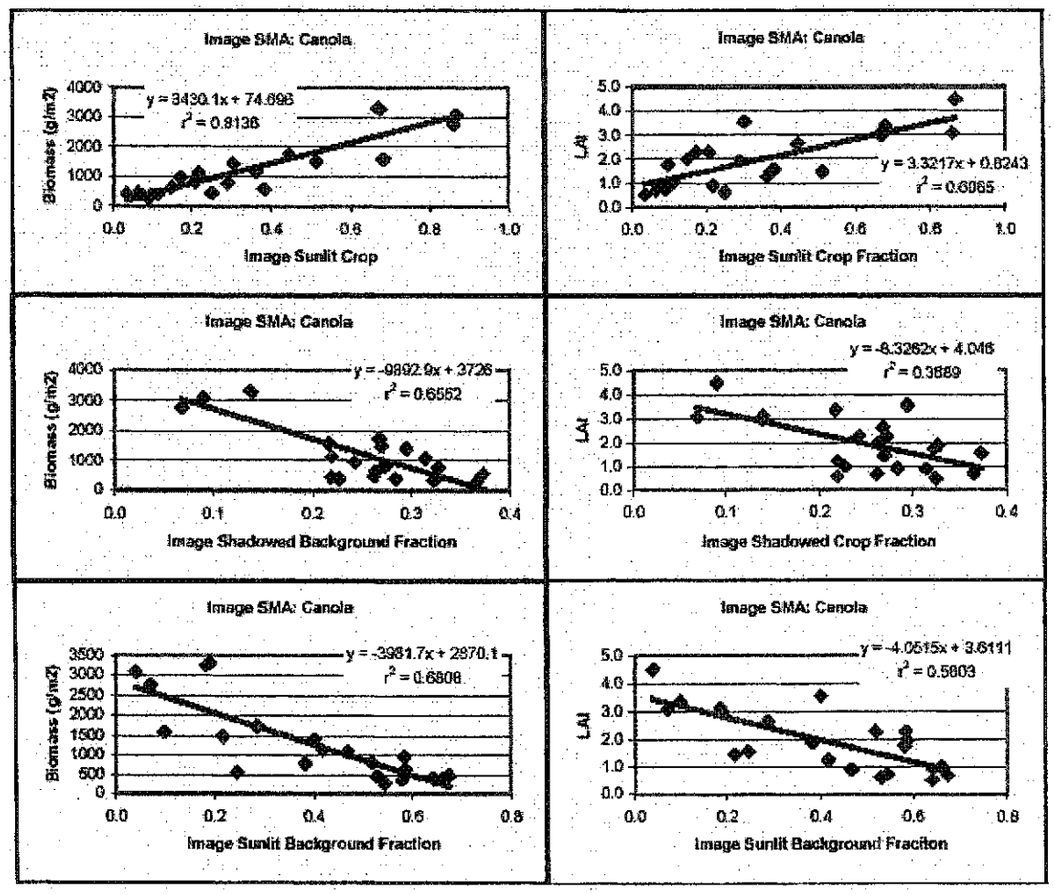

Figure D-5: Linear regression analysis results for SMA using reference endmembers to predict wheat biomass and LAI.

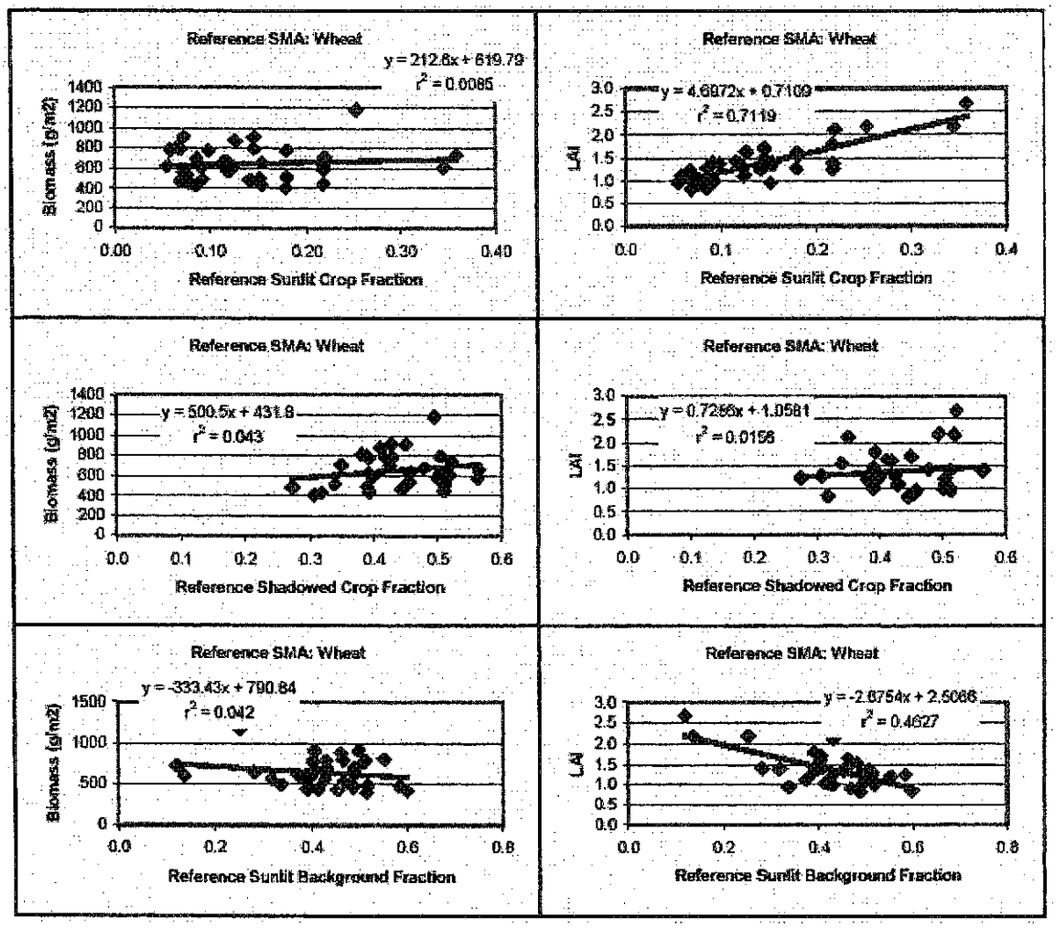

Figure D-6: Linear regression analysis results for SMA using image endmembers to predict wheat biomass and LAI.

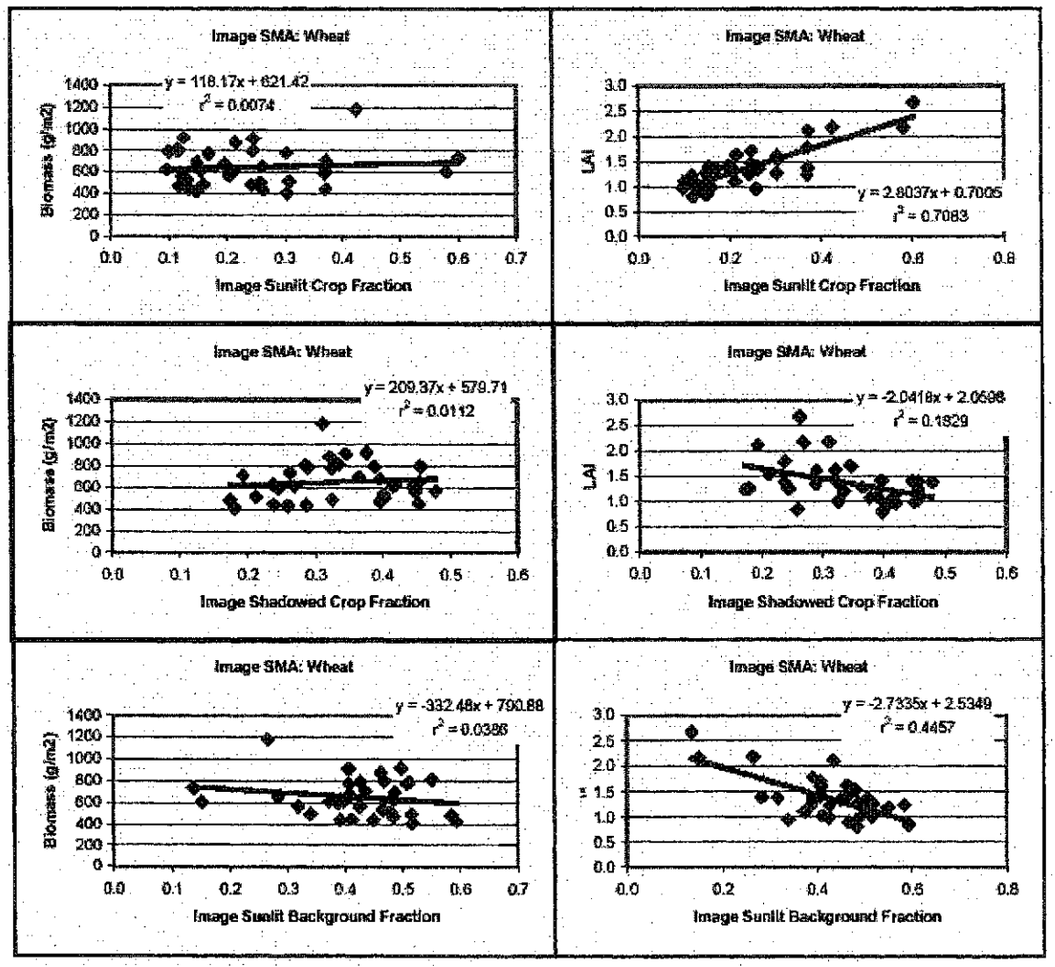

Appendix E: Linear Regression Analysis of ground-based Biomass and LAI data for each crop type.

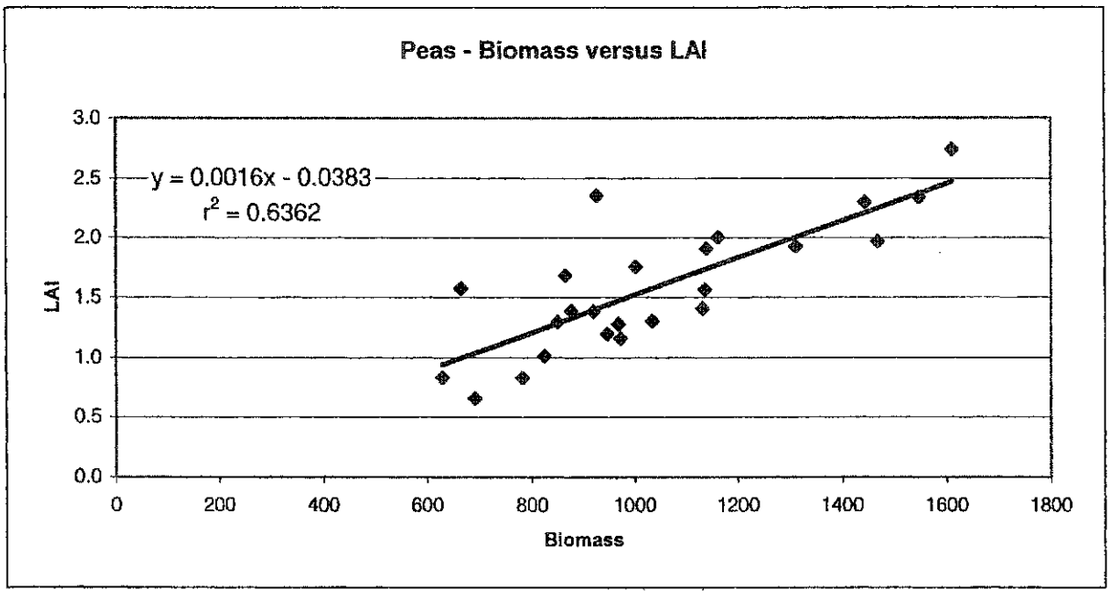

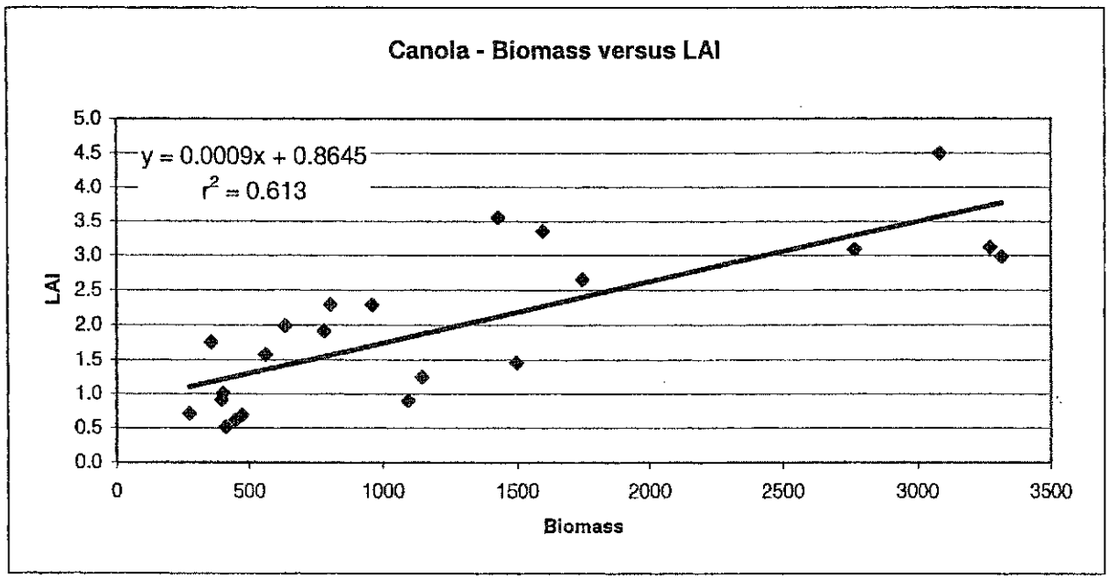

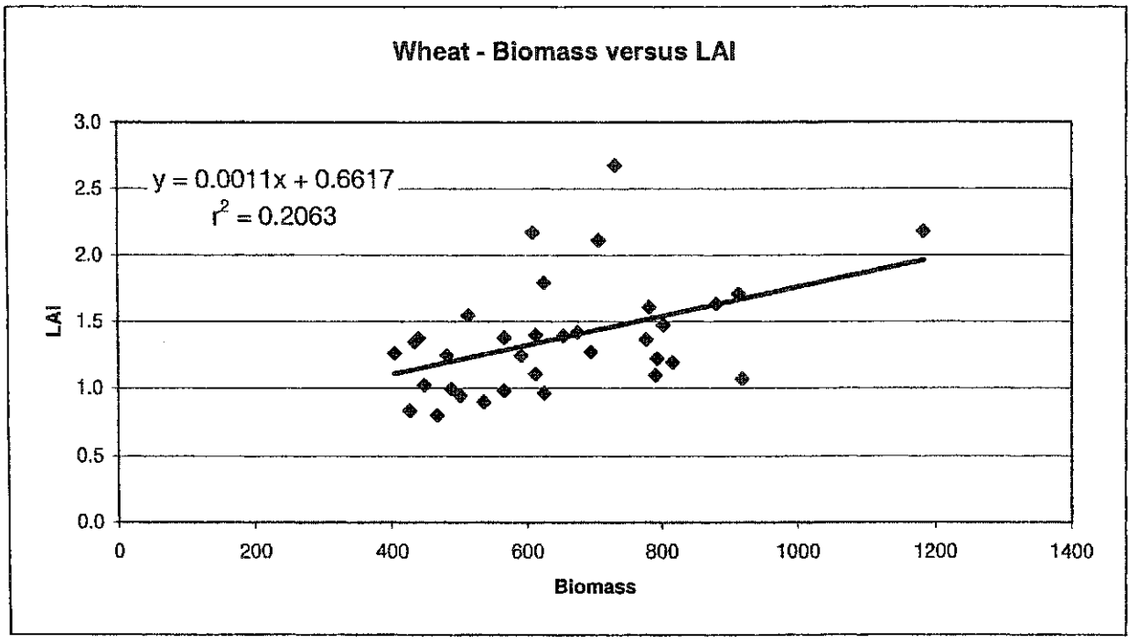
Wheat - Biomass versus LAI
y = 0.0011x + 0.6617
r2 = 0.2063
LAI
Biomass
3.0
2.5
2.0
1.5
1.0
0.5
0.0
0
200
400
600
800
1000
1200
1400